DE-FC07-01ID13980

METALLIC REINFORCEMENT OF DIRECT SQUEEZE DIE CASTING ALUMINUM ALLOYS FOR IMPROVED STRENGTH AND FRACTURE RESISTANCE

Final Report

David Schwam
John F. Wallace
Yulong Zhu
Jun-Wan Ki

Case Western Reserve University

October 2004

Work Performed Under Contract DE-FC07-01ID13980

For

U.S Department of Energy
Assistant Secretary for
Energy Efficiency and Renewable Energy
Washington D.C.

TABLE OF CONTENTS

TABLE OF CONTENTS ……..…….…….……...……i

LIST OF TABLES …….……...……...……iv

LIST OF FIGURES …..……...……..……. v

ABSTRACT …….…….….. x

PART 1: EVALUATION OF REINFORCEMENT MATERIALS AND COATINGS

1.0 INTRODUCTION ..……...……...1

1.1 Multimaterial Technology ..……..……1

1.1.1 The Purpose of This Work …….……..…….2

1.2 Interactions and Bonding at the Interface of Dissimilar Materials …...6

1.2.1 Metallurgical Phenomena ……...7

1.2.2 Chemical Bonding ……..……...……8

1.2.2.1 Wetting …….……11

1.2.2.2 Diffusion and Chemical Reactions ...……..15

1.2.3 Residual Stresses and Mechanical Bonding ...……..19

1.3 Diffusion and Reaction between Fe and Al-Si Alloy ...……..21

1.3.1 Effect of Alloying Elements ...……..25

1.4 Toughening Mechanisms of Composites ...……...…..28

1.4.1 Toughening Mechanisms of

Continuous Fiber Composites ..……28

1.4.2 Toughening Mechanisms of Crack Arrester Type Laminated Metal Composites (LMC) ..……28

1.5 Role of Electroplated Coating ..…….……31

2.0 EXPERIMENTS ...……32

2.1 Materials ...……...32

2.1.1 A354 Aluminum cast Alloy ..……...32

2.1.2 Strengthening Materials and Preparation ..……...32

2.1.2.1 Surface Treatments and Coatings ...……36

2.1.2.2 Preparation ..……...36

2.1.3 Meshes and Preparation ..…….39

2.2 Molds ...……...42

2.2.1 Molds for Strengthening ..……42

2.2.2 Molds for Meshes ...……..45

2.3 Melting and Casting ..…….45

3.0 RESULT AND DISCUSSION ..……...47

3.1 Analysis of Aluminum Bronze Inserts in the Aluminum Casting 47

3.1.1 Dissolution of Aluminum Bronze ..……..47

3.1.2 Metallurgical Analysis of Interface ...……...48

3.2 Analysis of Cast Iron Inserts in the Aluminum Casting ..……..57

3.2.1 Metallurgical Analysis of Interface ...……...57

3.2.1.1 Role of Surface Treatments and Coatings ...……...58

3.2.2 Thermal Expansion Coefficient, Residual Stresses and

Failure of Bonding ..……..……..59

3.2.2.1 Effect of Electroplated Coatings ……59

3.2.3 Effect of Heat Treatment ……..……60

3.3 Analysis of Ni-Resist Inserts in the Aluminum Casting ..……..73

3.3.1 Metallurgical Analysis of Interface ...……...73

3.3.2 Effect of Heat Treatment on Bonding Strength ...…….73

3.4 Analysis of Mesh Reinforced Aluminum Casting ...……...77

3.4.1 Metallurgical Analysis of Interface ...……...77

3.4.2 Results of Charpy Impact Test ..……..….77

4.0 CONCLUSIONS ..……91

PART 2: REINFORCEMENT OF SQUEEZE CAST ALUMINUM

5.1 PROCEDURE AND EXPERIMENTS……92

5.2 RESULTS AND DISCUSSION……..94

5.3 CONCLUSIONS……98

BIBLIOGRAPHY ……..…….99

LIST OF TABLES

Table 1 – Fe-Al System Phases ……..….22

Table 2 – Fe-Al-Si Phases ……...……23

Table 3 – Density ρ and Molar Volume M_v Values of Important Phases in Fe-Si-Al System ……24

Table 4 - Impurity/Alloying Effect on the Interatomic Interaction of Al and Fe Atoms in $Fe_{0.95}(Al_{1-n}X_n)_{0.05}$ Ternary System and the Change in Thickness of the Aluminized Diffusion Layer at T=800□ for 1 at.% Concentration of X Element ……....27

Table 5 – The Dimension of Discs ……34

Table 6 – Thermal Expansion Coefficients of Materials ……...…….35

Table 7 – Surface Treatments and Coatings of Discs ……37

Table 8 – Data of Stainless Steel Wire Meshes ……..40

Table 9 – Shear Test Results of Ni-resist Insert in the Small Casting ……76

Table 10 – Data on Meshes and Impact Energy ……..……...84

Table 11 – Impact Test Results ……...88

LIST OF FIGURES

Figure 1 – A squeeze cast piston with Ni-resist insert (a) ……..…..4
– The groove area with Ni-resist insert (b) ……..……4

Figure 2 – Pictures of casting with stainless steel wire mesh …….……..5

Figure 3 – Phase diagram showing complete miscibility in the solid state (a) ……9
– Phase diagram showing limited solid solubility (b) ……9
– Schematic illustration of a binary alloy system with the formation of intermetallic compounds (c) ……10

Figure 4 – Interface zone between dissimilar metals showing solid solution and intermetallic compound formation ……10

Figure 5 – Configuration of a liquid sessile drop on a solid substrate ……...….14

Figure 6 – Schematic diagrams to illustrate the growth of the A_pB_q layer between the elements A and B ……..18

Figure 7 – The methods to set discs in the mold ……...……..38

Figure 8 – Sketch of multi-layer meshes (a) ……..…..41
– Picture of multi-layer meshes (b) ……..……41

Figure 9 – The schematic feature of mold and position of disc-inserts (a) ……..…43
– The picture of mold with discs (b) ……...….43

Figure 10 – Mold for small casting (a), (b), (c), (d) …….……..44

Figure 11 – Sketch of mold and dimension of casting (a), (b) …….……..46

Figure 12 – Casting with metallic inserts and cutting line ……...…50

Figure 13 – Cross section of aluminum bronze insert (a) ……...50
– Cross section of aluminum bronze insert with Cu electroplating (b) …..…51
– Cross section of aluminum bronze insert with heavy Ni electroplating(c) ……..51
– Cross section of aluminum bronze insert with Cu/Ni electroplating (d) ….52
– Cross section of aluminum bronze insert with Zn electroplating (e) ……..52

Figure 14 – Cross section of cast iron insert ……...…53

Figure 15 – Phase diagram of Al-Cu binary system (a) ……..54

– Phase diagram of Fe-Al binary system (b) ……..54

Figure 16 – Optical microscope picture of interface between Al bronze and aluminum alloy (a) ……...55
– Optical microscope picture of interface between intermediate layer and aluminum alloy (b) ……56
– Optical microscope picture of interface between Al bronze and intermediate layer (c) ……..……56

Figure 17 – Cross section of cast iron insert ……...61

Figure 18 – Optical microscope picture of the interface between cast iron and Al alloy ……61

Figure 19 – Result of micro hardness test across the interface between Al alloy and cast iron insert with Zn coating (a) ……62
– Micro hardness across the interface between Al alloy and cast iron insert (b) ……...62

Figure 20 – SEM picture of interface between A354 Al alloy and cast iron with Cu coating (a) ……...63
– Compositional profile across the interface between A354 Al alloy and cast iron with Cu coating (b) ……...64

Figure 21 – Phase diagram of Al-Si binary system ……65

Figure 22 – Interface of A354 aluminum cast alloy and cast iron with carbon nitriding ……66

Figure 23 – Interface of A354 Al alloy and cast iron after aluminizing (a) ……...66
– Interface of A354 Al alloy and cast iron with electroplated Cu coating (b) ……..67
– Interface of A354 Al alloy and cast iron with electroplated Cu/Ni coating (c) ……67
– Interface of A354 Al alloy and cast iron with electroplated Ni/Cr coating (d) ……..68
– Interface of A354 Al alloy and cast iron with electroplated Zn coating (e) ……...68

Figure 24 – The thickness of intermediate layer of aluminum alloy and cast iron interface ……..69

Figure 25 – Interface between A354 Al alloy and cast iron after Kolene process with Cu coating (a) ……..70
– Interface between A354 Al alloy and cast iron after Kolene process with

Cu/Ni coating (b) ……70

Figure 26 – Cast iron insert utilized in the aluminum casting (a) ……..71
– Degrading of the interface by different thermal contraction of A354 Al alloy and cast iron insert (b) ……..71

Figure 27 – Crack in the intermediate layer (a) ……..72
– Crack in the Al alloy (b) ……72

Figure 28 - Interface between A354 and cast iron with Cu/Ni coating after heat treatment (a) ……..73
– Interface between A354 and cast iron with Zn coating after heat treatment (b) ……73

Figure 29 – The interface between A354 Al alloy and Ni-resist insert ……..74

Figure 30 – The interface between A354 Al alloy and Ni-resist insert with Al coating ……74

Figure 31 – Small casting with Ni-resist insert (a) ……..75
– Shear test specimens (b) ……..75

Figure 32 – Optical microscope picture of stainless steel wire (a) ……80
– Optical microscope picture of stainless steel wire mesh (b) ……...80

Figure 33 – SEM micrograph of intermediate layer (a) ……..81
– EDS result of the intermediate layer (b) ……..81

Figure 34 – Stainless steel wire with Zn coating after heat treatment (a) ……...82
– Stainless steel wire without coating after heat treatment (b) ……...82

Figure 35 – Impact energy of A354 Aluminum alloy and casting reinforced by galvanized steel wire mesh ……83

Figure 36 – Area fraction with varying mesh count ……...85

Figure 37 – Impact energy with varying mesh count ……86

Figure 38 – Effect of area fraction of wire on impact energy ……87

Figure 39 – Effect of number of layer ……89

Figure 40 – Effect of heat treatment ……...90

Figure 41a – Ejector insert for metal reinforced aluminum dome casting…….99

Figure 41b – Cover insert for metal reinforced aluminum dome casting…… ……...100

Figure 43a – AISI 304 Stainless wire mesh and punched sheet …….....101

Figure 43b – Unalloyed 1020 steel wire mesh ……..…....101

Figure 44 – Dome performs of 304 stainless, 1020 unalloyed wire mesh and punched 304 stainless steel sheet…….102

Figure 45 – Weight of the reinforced material in aluminum dome castings ……103

Figure 46 – Weight of the castings made of aluminum with and w/o reinforcement 103

Figure 47 – X-Ray picture of castings with and w/o reinforcement ……....104

Figure 48 – Setup for water pressure testing ……....104

Figure 49 - Failure mode of castings in water pressure testing……..105

Figure 50 – Setup for piston pressure testing of the hemispheric casting…….106

Figure 51 – Effect of reinforcement on impact resistance…….107

Figure 52 – Effect of SS304 wire reinforcement (casting produced at 7,600 psi)…..108

Figure 53 – Typical load-deformation plot of castings made with 17,000 psi pressure with and w/o reinforcement (as-cast) ……..109

Figure 54 – Effect of SS304 wire reinforcement on failure energy (Load*Dispacement) at 7,600 psi (as-cast)……..110

Figure 55 – Effect of reinforcement on failure energy (Load*Dispacement) at 17,000 psi (as-cast)..……..110

Figure 56 – Failure mode of castings tested with piston pressure……..111

Figure 57 – Effect of mesh are afraction in cross-sections of stainless mesh reinforced A354 on CVN impact strength…….……..112

ACKNOWLEDGEMENTS

This research investigation was supported by the Department of Energy, Office of Industrial Technology through the Cast Metal Coalition program. The Research and Development Committee of the North American Die Casting Association provided guidance for this work. The efforts of Mr. Steve Udvardy, Director of Research and Education at NADCA and the members of the committee are gratefully acknowledged.

This publication was prepared with the support of the U.S. Department of Energy (DOE), Award No. DE-FC07-01ID13980. However, any opinions, findings, conclusions or recommendations expressed herein are those of the authors and do not necessarily reflect the views of the DOE.

ABSTRACT

The utilization of aluminum die casting as enclosures where internal equipment is rotating inside of the casting and could fracture requires a strong housing to restrain the fractured parts. A typical example would be a supercharger. In case of a failure, unless adequately contained, fractured parts could injure people operating the equipment. A number of potential reinforcement materials were investigated. The initial work was conducted in sand molds to create experimental conditions that promote prolonged contact of the reinforcing material with molten aluminum. Bonding of Aluminum bronze, Cast iron, and Ni-resist inserts with various electroplated coatings and surface treatments were analyzed. Also toughening of A354 aluminum cast alloy by steel and stainless steel wire mesh with various conditions was analyzed.

A practical approach to reinforcement of die cast aluminum components is to use a reinforcing steel preform. Such performs can be fabricated from steel wire mesh or perforated metal sheet by stamping or deep drawing. A hemispherical, dome shaped casting was selected in this investigation. A deep drawing die was used to fabricate the reinforcing performs. The tendency of aluminum cast enclosures to fracture could be significantly reduced by installing a wire mesh of austenitic stainless steel or a punched austenitic stainless steel sheet within the casting. The use of reinforcements made of austenitic stainless steel wire mesh or punched austenitic stainless steel sheet provided marked improvement in reducing the fragmentation of the casting. The best strengthening was obtained with austenitic stainless steel wire and with a punched stainless steel sheet without annealing this material. Somewhat lower results were obtained with the annealed punched stainless steel sheet. When the annealed 1020 steel wire mesh was used, the results were only slightly improved because of the lower mechanical properties of this unalloyed steel. The lowest results were obtained with unreinforced 356 aluminum casting.

Good strength can be obtained with a sound die casting without any defects produced by squeeze casting. The use of higher pressure to produce the squeeze casting

has been shown to increase the strength of a hemispherical dome casting. This dome shape casting has been produced both with and without reinforcement and tested to determine its pressure resistance under internal pressure of water. Only a slight improvement in strength could be determined because of water leaks at the seal between hemispherical dome and its flat supporting side. However, when the ability of the casting was tested under the compressive force of a plunger, the strengthening effect of wire mesh or sheet was evident. Higher loads to failure were obtained because of the reinforcement of the stainless steel wire and punched sheet. Rather than a sudden failure occurring, the reinforcement of the stainless steel wire or the punched hard stainless steel sheet held the material together and prevented any loss of the fractured casting to the surroundings. Unalloyed steel did not have the required strength or mechanical properties to increase the properties of the casting.

PART 1: EVALUATION OF REINFORCEMENT MATERIALS AND COATINGS

1.0 INTRODUCTION

1.1 Multimaterial Technology

Many high performance products and engineering structures are required to operate under demanding condition without premature failure. Often, such severe operating condition are localized to a certain part of a component. Local reinforcement can provide industry with the ability to increase resistance against localized stresses, or with various functional capabilities. Similarily, efficient combinations of conventional materials in those places where they are most useful and economic can provide cost effective solutions to engineering problems. Multimaterial technology is becoming more widespread and provides promising solutions for the design and fabrication of many high performance products and engineering structures.

The reasons for using multimaterial combinations for a single product are based on several considerations [1]. Firstly, the multimaterial combination has to meet the technical requirements of the product. The combination has to satisfy mechanical requirements, such as a combinations of strength and rigidity for static and fatigue loading, reduced weight, local wear and corrosion resistance, and high temperatures

resistance. Also the multimaterial combination has to satisfy functional requirements, such as electric or magnetic activity, damping and kinematic behavior. Secondly, multimaterial assemblies provide designers and manufacturers with more flexibility and degrees of freedom. In order to take full advantage of the properties of various materials, it is necessary for designers to use the most suitable materials for each part of a given structure. The use of multimaterial techniques can combine the various properties of each component and fully utilize their individual advantages to fulfill the special requirements of the product. Thirdly, the fabrication of multimaterial products can yield economic benefits, because the materials properties of each part can be utilized more efficiently. Multimaterial technology can result in use of less expensive materials and reduces the cost of products. The use of a novel, high performance material in critical parts of a structure can extend the life cycle of the product.

1.1.1 The Purpose of This Work

The purpose of this work is to employ multimaterial technology in casting processes. An example of a particular applications of multimaterial technology in casting processes is a diesel engine piston with a nickel containing cast iron, called Ni-resist, in the groove area of the pistons to provide wear resistance (Fig. 1). This piston is produced

by squeeze casting process. The present work addresses two related subjects: reinforcing aluminum castings with dissimilar material inserts with or without coating; and reinforcing cast aluminum housings with stainless steel wire meshes to improve the impact strength (Fig 2).



Figure 1(a): A squeeze cast piston with Ni-resist insert

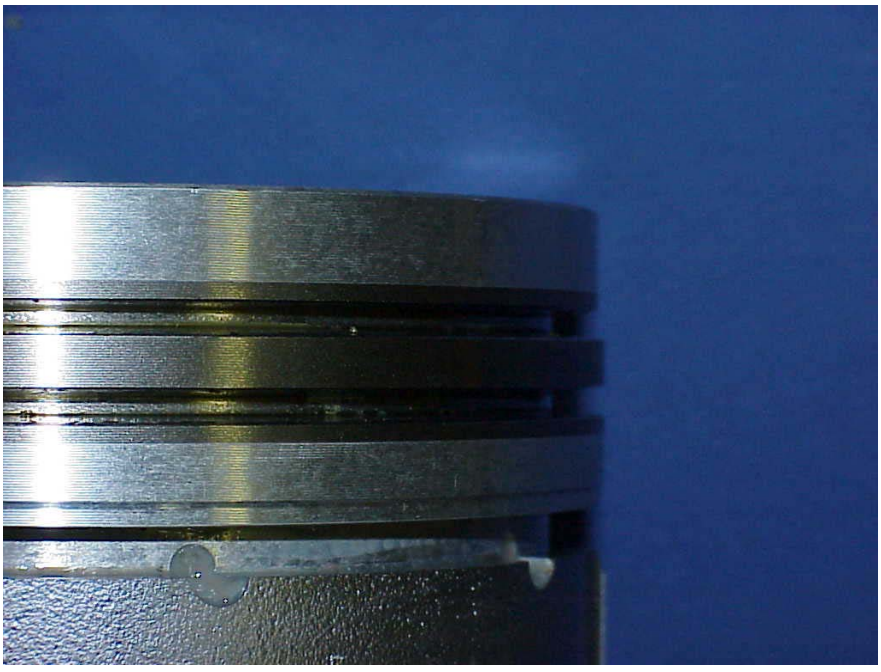
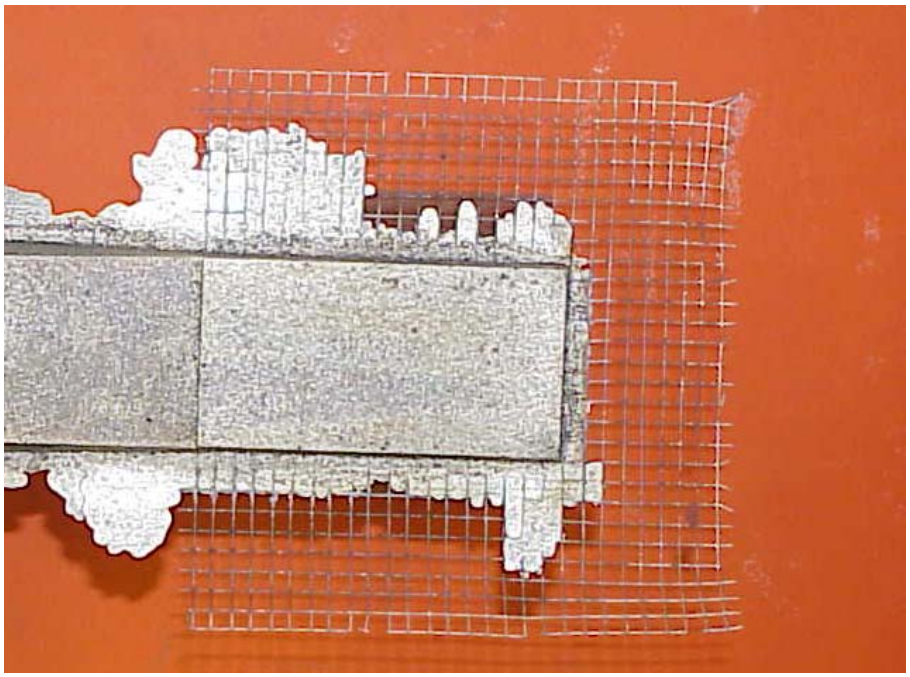


Figure 1(b): The groove area with Ni-resist insert



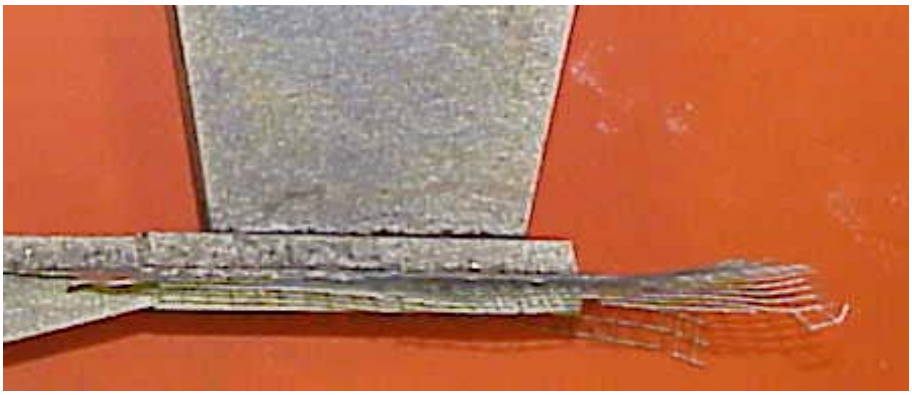


Figure 2: Pictures of casting reinforced with stainless steel wire mesh.

1.2 Interactions and Bonding at the Interface of Dissimilar Materials

Various materials can be joined to produce multimaterial products. The physical and mechanical properties of these materials vary significantly. These differences in properties between various materials provide a broad range of materials available for special operating conditions and environments. However, these large differences in material properties also lead to difficulties in joining them together. Physical and chemical mismatches can result in incompatibility. Physical mismatches such as differences in melting temperature, thermal expansion coefficients and thermal conductivity can create joining problems. Chemical mismatches can result in the formation of brittle compounds. Diffusion of elements can sometimes result in the degrading of the dissimilar joint properties.

The type of interfacial bonding can be classified as mechanical bonding and/or chemical bonding. When one material is surrounded by another material, any contraction of the surrounding material can result in a “gripping” effect. This effect can lead to a considerable degree of mechanical bonding. Also dissolution, wetting, and reaction can cause chemical bonding at the interface.

1.2.1 Metallurgical Phenomena

Phase diagrams are useful tools for understanding the bonding of dissimilar metals. It should be noted that casting processes normally produce relatively high heating and cooling rates, which lead to the formation of structures different from the equilibrium. Some elementary forms of binary phase diagrams illustrate a simple example [1].

The first example is a binary system (Fig.3 (a)) in which two metals are mutually soluble in all proportions and in both the liquid and solid states. In this case, they can normally form a bonding with a tough solid solution with low cracking sensitivity. The bonding normally exhibits good metallurgical and mechanical properties. If the heating and cooling rates are not too slow, bonding dissimilar metals of this type does not present serious problems. In case of slow heating and cooling rate can cause a dissolution problem. Copper-nickel and gold-platinum alloy systems belong to this category.

A binary eutectic system is the second category (Fig. 3(b)). In this type of system, the liquid is completely miscible, but miscibility in the solid state is limited. In this case, the quality of the joints depends on the properties of the eutectic. Normally the

eutectic is harder and more brittle than the primary crystals A and B [2]. Therefore, the eutectic phase can impair their behavior during service. Thus, it is more difficult to join materials belonging to this system. Examples of this system include silver-copper, lead-tin and aluminum-silicon alloys.

The third type of system is one in which the intermediate phase exists in the form of an intermetallic compound (Fig.3 (c)). Intermediate phases show hard and brittle behavior. If they form an intermetallic composition, fusion techniques are difficult to apply in bonding. This difficulty arises from the fact that these brittle components will result in lower ductility and increased crack-sensitivity. Therefore, the combination of elements belonging to this type of system should be employed with caaution. Although it is difficult to bond dissimilar alloy systems forming intermetallic phases, a few solutions are readily available to minimize the problems. For instance, it is possible to use a filler material, which does not form intermetallic compounds with either of the two base metals.

1.2.2 Chemical Bonding

Dissimilar materials can be chemically bonded by dissolution, wetting, and reaction at the interface. The planar interface, which is initially formed at the interface of

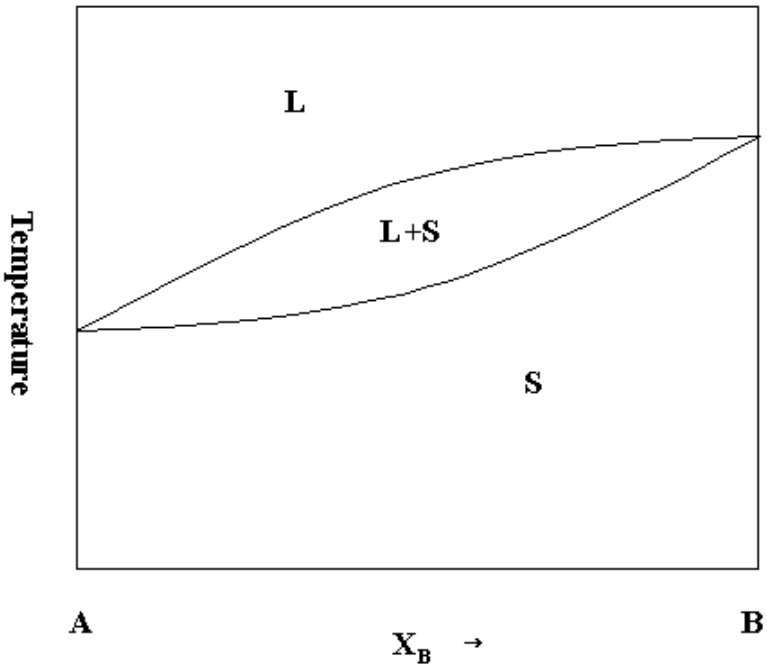


Figure 3(a): Phase diagram showing complete miscibility in the solid state

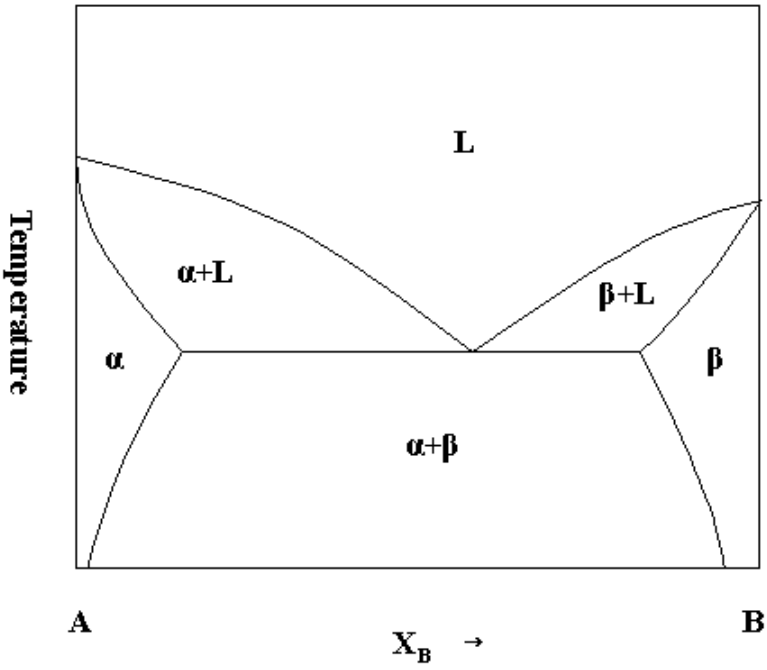


Figure 3(b) Phase diagram showing limited solid solubility

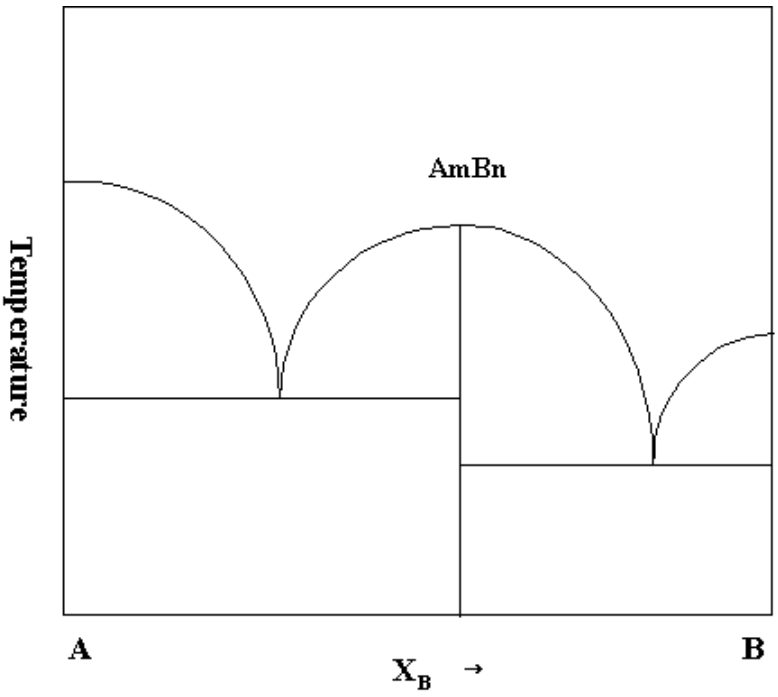


Figure 3(c): Schematic illustration of a binary alloy system with the formation of intermetallic compounds

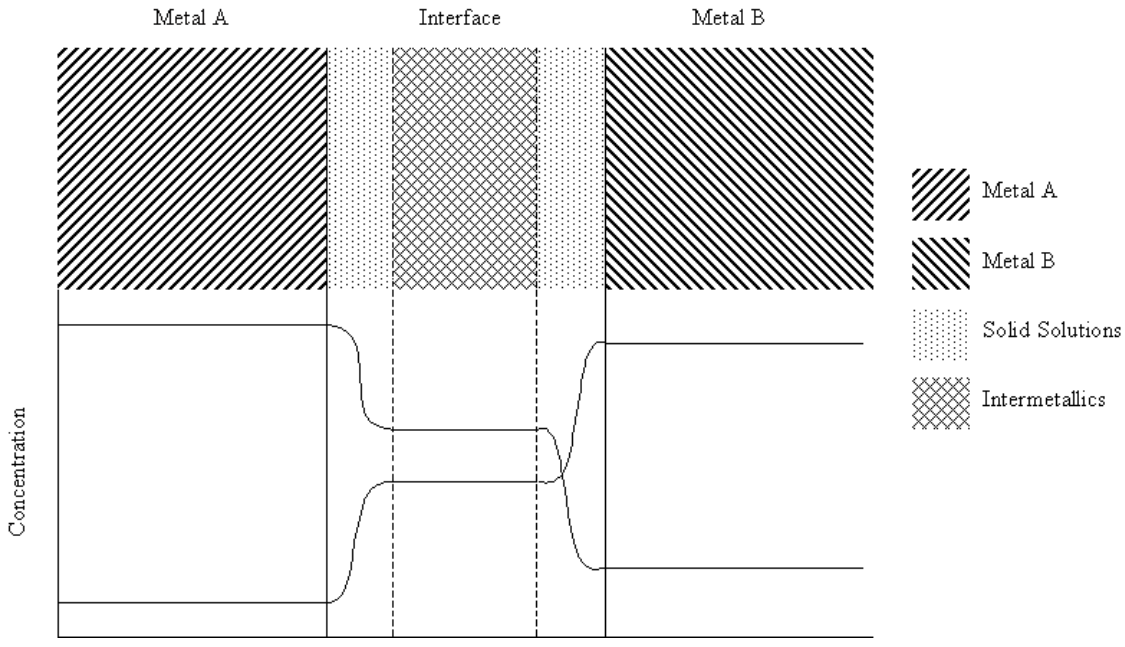


Figure 4 Interface zone between dissimilar metals showing solid solution and intermetallic compound formation

dissimilar metals, becomes an interfacial zone having multiple interfaces, which include intermetallic compounds, solid solutions, and so on (Fig. 4). In such a case, not only the compositional parameter and processing parameters (time and temperature), but also other parameters (microstructure and mechanical, physical, chemical, and thermal characteristics of different phases present in the interfacial zone) are needed to characterize the interfacial zone. Some controlled amount of reaction at the interface may be desirable for obtaining strong bonding between dissimilar materials. The intermetallic compound layer forms a metallurgical bond between both materials. However too thick an interaction zone will adversely affect the bonding properties. Therefore the control of formation and evolution of an intermediate layers in bonding two different materials is metallurgically very important. The successful application of dissimilar materials depends on the physical and mechanical properties of the intermetallic compounds formed at the interface

1.2.2.1 Wetting

Wetting is one of the most important phenomena in joining process. The mechanical strength of the bond after solidification can be approximately evaluated from W_a in liquid state [3]. Wetting phenomena depends on temperature and the chemical

composition of the phases. Wetting becomes more pronounced with increased temperature.

Figure 5 illustrates a drop of liquid placed on the surfaces of a solid. The relationship between the contact angle and the interfacial energies at interfaces is expressed by Equation 1.

$$\cos\theta = (\gamma_{SV} - \gamma_{SL}) / \gamma_{LV} \qquad (1)$$

Where γ_{LV}, γ_{SV}, and γ_{SL} are the liquid-vapor, solid-vapor, and solid-liquid interfacial energy, respectively. The interfacial energy γ_{LV} and contact angle θ determine the energy needed to form a new interface from the two surfaces, known as the work of adhesion (W_a) defined as $W_a = \gamma_{SV} + \gamma_{LV} - \gamma_{SL}$. Their relationship is described by Equation 2 (Young-Dupre equation):

$$W_a = \gamma_{LV}(1 + \cos\theta) \qquad (2)$$

The contact angle influences the magnitude of the interfacial bonding. For example, as the contact angle decreases the work of adhesion increases resulting in increasing bond strength. This is often achieved with increasing temperature.

Generally the boundary between wetting and non-wetting is $\theta = 90^{\circ}$. Theoretically, $\theta < 90^{\circ}$ represents conditions of wetting. In practice, good wetting can be obtained with a much smaller angle, e.g. $\theta < 15^{\circ}$.

It should be noted that the Equation 1 and Equation 2 are valid for weakly reacting systems. However in reactive systems chemical reactions occur at the interfaces, and may greatly influence wetting. The driving force for wetting is provided by the sum of the contribution of the reactions between the substrate and liquid and the contribution of the surface energies. Therefore Equation 2 has to be modified so it takes into account the reaction as expressed in Equation 3 [4].

$$W_a = \gamma_{LV}(1+\cos\theta) + \gamma_R - C\Delta G^{\circ} \qquad (3)$$

Where γ_R is the interfacial energy between the solid and the reacting interfacial layer, ΔG° is the Gibbs free energy of the formation of the new interfacial compound, and C is a constant. The driving force for wetting comes from the contribution of the reaction and the contribution of the surface energies.

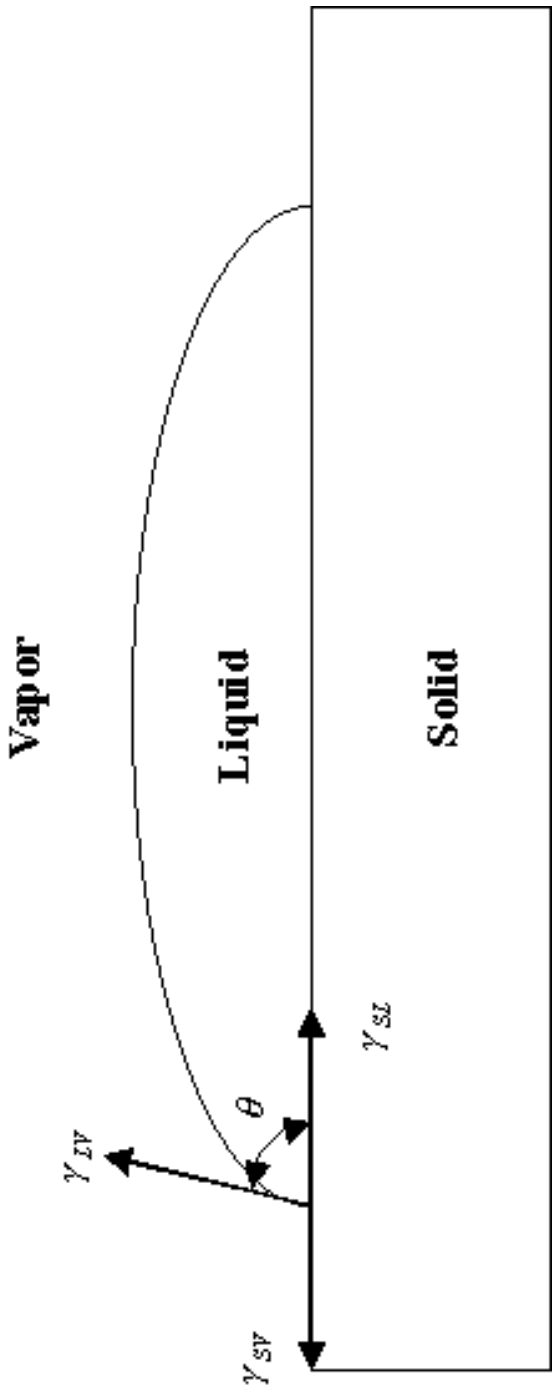


Figure 5 Configuration of a liquid sessile drop on a solid substrate

1.2.2.2 Diffusion and Chemical Reactions

The formation and growth characteristics of the diffusion layer depend on several factors such as the crystal structure, the range of solid solubility, the magnitude and sign of interatomic interaction potentials between the atoms of mutually interacting elements and also their interdiffusion coefficient. However, the observed kinetics can be governed either by the rate of diffusion across the product phase(s), diffusion control, or by the process(es) taking place at the interfaces, interface or reaction control, or more generally by a combination of both [5].

The characteristics of diffusion with chemical reactions are different from that of non-reactive diffusion. There are number of discrepancies between conventional diffusion theory and the experimental data. Therefore "diffusion" theory is not necessarily valid for reaction diffusion. The main discrepancies are the following [6]:

1. According to the "diffusion" theory, there is no restriction on the number of compound layers growing simultaneously in a given couple. However no reports show the simultaneous growth of five or six compound layers between the couples in

which up to ten compounds exist in a certain range of temperatures. The usual number of layers has been reported are one to three and rarely four [7, 8].

2. The layer growth is often non-parabolic, especially in those cases where two or more compound layers grow simultaneously. In the initial stage the process is always non-parabolic, the layer thickness time relationship being linear [7,8,9].
3. According to the "diffusion" theory once formed a layer cannot disappear since the smaller the thickness the greater is the layer growth rate. [7,10, 11]. However experimental data do not prove this case.

The neglect of a chemical reaction appears to be the main source of discrepancies between the theory and experiment.

Dybkov[6] proposed the physicochemical theory of heterogeneous kinetics in binary systems. Evans'equation[12] and Arkharov's concept of the reaction diffusion[13,14] reveal the role of diffusion and that of chemical reactions in determining the compound layer-growth kinetics. The theory is based on the following assumptions:

1. The concentrations of components A and B in the layer at boundaries 1 and 2 are equal to the limits of the ApBq homogeneity range;

2. A change in concentration with distance within the ApBq layer is linear;

3. During growth, both boundary concentrations behave as a linear concentration distribution that remains almost unchanged.

In case of a single layer of the chemical compound ApBq, p and q being positive integers, grows between the elements A and B as illustrated in Fig. 6. A general equation describing the A_pB_q layer growth between the A and B phases is expressed by Equation 4.

$$\frac{dx}{dt} = \frac{k_{0B1}}{1 + (k_{0B1}x / k_{1B1})} + \frac{k_{0A2}}{1 + (k_{0A2}x / k_{1A2})} \qquad (4)$$

where x is the thickness of the A_pB_q layer; t the time; k_{0B1}, k_{1B1}, k_{0A2}, and k_{1A2} the rate constants of the layer growth under conditions of reaction control. The three digits in the subscript indicates regime of the layer growth, 0 and 1 indicate reaction and diffusional regime of the layer growth, atoms which diffuse towards the reaction site, and the interface where chemical reactions take place. If the contributions of both components to the layer growth are equal ($k_{0B1}=k_{0A2}$ and $k_{1B1}=k_{1A2}$) then

$$\frac{dx}{dt} = \frac{2k_{0B1}}{1 + (k_{0B1}x / k_{1B1})} \qquad (5)$$

and

$$t = \frac{x^2}{4k_{1B1}} + \frac{x}{2k_{0B1}} \qquad (6)$$

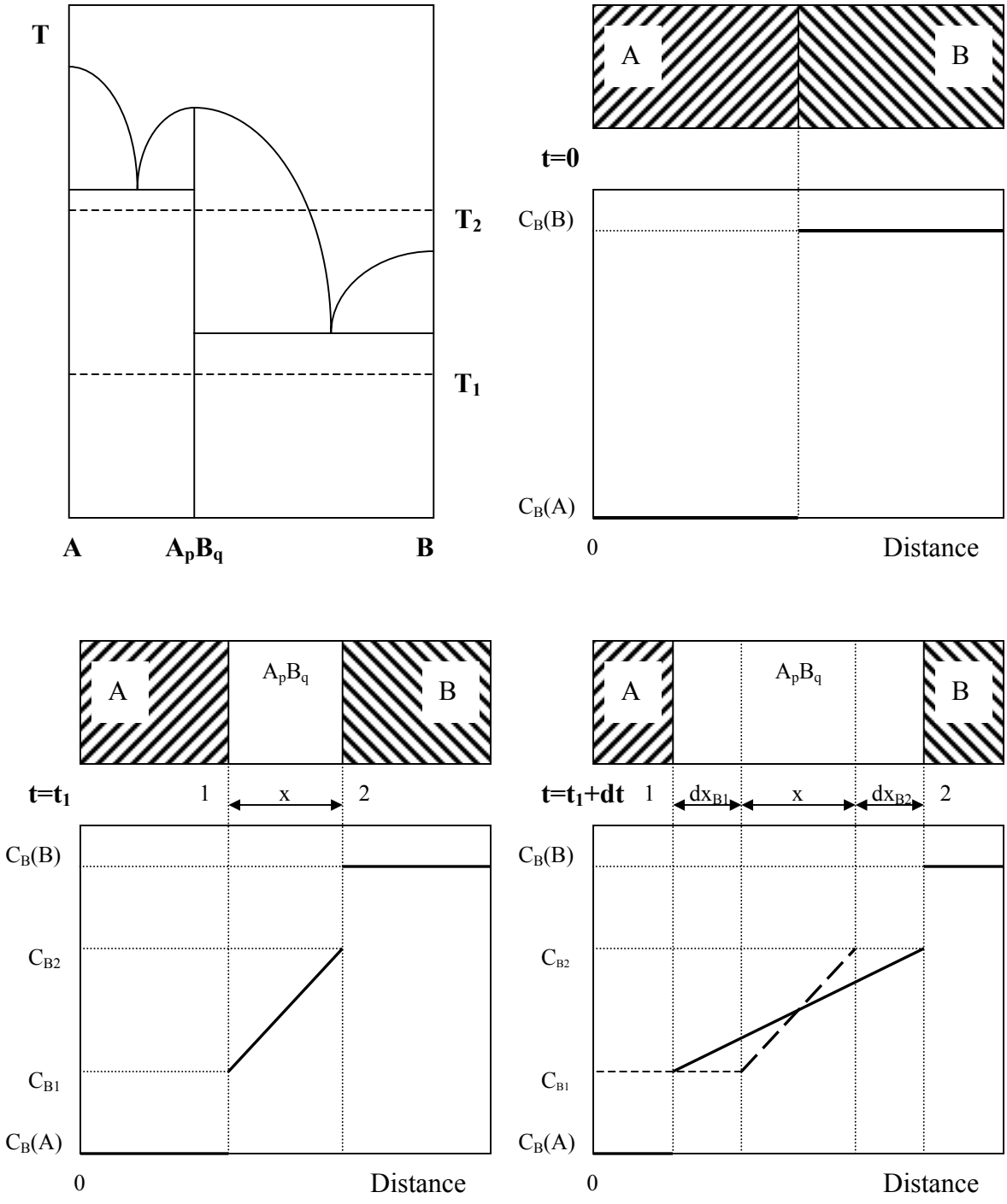


Figure 6: Schematic diagrams to illustrate the growth of the A_pB_q layer between the elements A and B

For small x,

$$x = 2k_{0B1}t\,, \tag{7}$$

whereas for large x

$$x^2 = 4k_{1B1}t\,. \tag{8}$$

1.2.3 Residual Stresses and Mechanical Bonding

Normally, dissimilar materials have different thermal expansion coefficients. When joined, cooling dissimilar materials from high temperature can result in increased residual stress at the interface. These residual stresses affect the quality and integrity of the bonding. In particular, tensile residual stresses have an adverse effect on bonding. Controlling residual stress is therefore very important. Generally, the use of suitable filler materials can be expected to produce a joint area with a thermal expansion coefficient between the two base materials that is sufficient to provide plastic deformation capabilities [1].

Residual stresses do not always effect the bonding adversely. An example is the mechanical gripping that occurs when one material is surrounded by another material with higher thermal expansion coefficient at the high temperature. After cooling, the

different thermal contraction results in gripping of the inside material by the surrounding material. Residual stresses can therefore provide a strong mechanical bonding.

1.3 Diffusion and Reactions between Fe and Al-Si Alloy

The reaction between aluminum and iron is extremely rapid and accompanied by a diffusion process leading to formation of a continuous layer of Fe-Al intermetallic compounds, which are hard and brittle [15-19]. The growth of the intermetallic layers would be diffusion controlled and diffusion is the rate-limiting step for the growth of the interfacial reaction products [20, 21].

Table 1[22] and Table 2[23] show phases in Fe-Al and Fe-Al-Si system, respectively. Also Table 3 shows density and molar volume of Al, Fe, Si and some Fe-Al and Fe-Al-Si intermetallic compounds. Base on this data, the formation of intermetallic compounds leads to negative volume change. Not only do these volume change but also the brittle characteristics of intermetallic compounds make it harder to have a good bonding at the Fe-Al interface.

$Fe + 3Al = FeAl_3$ $\Delta V = -1.98\ cm^3/mol$

$2Fe + 5Al = Fe_2Al_5$ $\Delta V = -4.19\ cm^3/mol$

$2Fe + Si + 8Al = Fe_2SiAl_8$ $\Delta V = -8.01\ cm^3/mol$

Table 1 Fe-Al System Phases

Phase	Stoichiometry	Crystal structure
α-FeAl		bcc
β_1	Fe_3Al	Cubic
β	FeAl	Disordered, bcc
β_2	FeAl	Ordered, bcc
ζ	$FeAl_2$	Monoclinic
	(47%-50wt %)	
η	Fe_2Al_5	Orthorhombic
	(52-54 wt %)	
θ	$FeAl_3$	Monoclinic
	(57-62 wt %)	
Al-Fe		Fcc
Solubility of Fe in Al 700ºC ~ 2.5 wt % 600ºC~ 0.1 wt %		

Table 2 Fe-Al-Si Phases

Nomenclature	Stoichiometry	Crystal structure	Composition, wt %		
			Fe	Al	Si
α	Fe_2SiAl_8	Hexagonal	30-33	55-65	6-12
β	$FeSiAl_5$	Monoclinic	20-30	55-68	12-15
δ	$FeSi_2Al_4$	Tetragonal	25.4	25.5	49.1
γ	$FeSiAl_3$	c-face centered Monoclinic	33.9	49.2	16.9
Unnamed	Fe_2SiAl_9		27-35	6-8	57-67

Table 3 Density ρ and Molar Volume M_v Values of Important Phases in Fe-Si-Al System

Phase	ρ, gcm^{-3}	M_v, cm^3mol^{-1}
θ-$FeAl_3$	3.90	35.11
η-Fe_2Al_5	4.11	59.99
α-Fe_2SiAl_8	3.62	98.23
Al	2.70	10.00
Fe	7.87	7.09
Si	2.33	12.06

1.3.1.1 Effect of Alloying Elements

Time and temperature are the two main parameters of reaction diffusion. However, alloying element additions may affect the rate of diffusion and the characteristics of the chemical reaction. An alloying element reduces the diffusion rate of iron or that of aluminum by formation of solid solutions or new phases. The thickness of the alloy layer can be reduced [21,24-26]. For example, addition of silicon results in the formation of a layer of $Fe_xSi_yAl_z$, which acts as a diffusion barrier and restricts the Fe-Al compounds formation. Oxygen and nitrogen may reduce the thickness of the alloying layer by the formation of a ceramic oxy-nitride phase, which acts as a diffusion barrier [27]. A copper addition reduces the thickness by reducing the rate of nucleation of the intermetallic compounds [28]. On the other hand, Mg addition, which has high diffusional mobility, results in the rapid growth of intermetallic phases [29].

Akdaniz et al. [30] proposed that alloying elements affect the activity coefficients of the diffusing species in the intermetallic layers, which can be determined from the Eq. 9 and Eq. 10 [31].

$$\mu_i^{excess} = RT \ln \gamma_i \quad (9)$$

$$\ln \gamma_i = \ln \gamma_i^{o} + \Sigma \varepsilon_i^{(j)} c_j \quad (10)$$

Where $\ln \gamma_i^{o}$ is a constant which is independent of concentration of constituent elements in the intermetallic layers, γ_i is the activity coefficient of element i, $\varepsilon_i^{(j)}$ is the interatomic interaction parameters of the element i due to the element j, and c_j is the concentration of the element j in the intermetallic layers. Table 4[30] shows impurity/alloying effect on the interatomic interaction of Al and Fe atoms in $Fe_{0.95}(Al_{1-n}X_n)_{0.05}$ ternary system and the change in thickness of the aluminized diffusion layer at T=800°C for 1 at.% concentration of X element. Based upon these data, alloying elements can be classified into two groups [30]:

(1) I-group : X_I=Si, Ti, Ge, Sb, Mg, Cu, Ca, Ag, Cd or Cr, these impurites decrease the activity coefficient of Al atoms in α-Fe so as to reduce the thickness of intermetallic layer at the interface.

(2) II-group : X_{II}=Co, Zn, Mn, Ni, Pb or Bi. The addition of these impurities tends to increase the activity coefficient, which leads to thickening of the aluminized diffusion layer at the Fe-Al interface.

Table 4 Impurity/Alloying Effect on the Interatomic Interaction of Al and Fe Atoms in $Fe_{0.95}(Al_{1-n}X_n)_{0.05}$ Ternary System and the Change in Thickness of the Aluminized Diffusion Layer at T=800□ for 1 at.% Concentration of X Element.

Impurities	$\gamma_{Al}/\gamma^{\circ}_{Al}$	Thickness change (Experiment)
Si	↓	↓
Ti	↓	↓
Ge	↓	↓
Sb	↓	↓
Mg	↓	↓
Cu	↓	↓
Ca	↓	↓
Ag	↓	↓
Cd	↓	↓
Cr	↓	↓
Co	↑	↑
Zn	↑	↑
Mn	↑	↑
Ni	↑	↑
Bi	↑	↑
Pb	↑	↑

1.4 Toughening Mechanisms of Composites

1.4.1 Toughening Mechanisms of Continuous Fiber Composites

In ductile metal matrix composites cracks initiate in the fiber/matrix interface, which is a brittle reaction layer. In brittle matrix composites, the critical flaw size is usually smaller than the fiber spacing, and cracks initiate in the matrix. Toughening of these composites involves increasing the energy absorbed in crack growth.

Composite toughening mechanisms are based on microcrack branching in the matrix and on debonding at the fiber/matrix interface [32]. The interface strength, frictional load transfer, and fiber pull-out stresses should not be too high. Fibers provide crack bridging behind the crack front either by pull-out or by ductile deformation [33,34]. Ductile fibers are used to toughen a brittle matrix. It has been suggested that for ceramic matrix composites, a dual fiber coating is required with an inner coating controlling the fiber/matrix debonding and an outer coating controlling the matrix interactions.

1.4.2 Toughening Mechanisms of Crack Arrester Type Laminated Metal Composites (LMC)

- Crack deflection

In many laminate systems, layer delamination can occur ahead of an advancing crack or as the result of a crack encountering an interface. These local delaminations can result in crack deflection, which can significantly reduce the mode component of the local stress intensity because of the large deviations in crack path.

- Crack blunting

When the advancing crack encounters the ductile layer, the crack is deflected and blunted. It is important that the crack deflection and blunting mechanisms are independent of volume fraction, which implies that the fracture toughness should be independent of volume fraction.

- Crack bridging

Unbroken individual layers span the wake of a crack. Growth of the crack requires stretching of these bridging ligaments. It is important to recognize that for crack bridging to occur, the bridging ligaments must have sufficient ductility to avoid fracture

at or ahead of the advancing crack tip. Thus crack bridging occurs when ductility or toughness differences exist between the component layers.

- Stress redistribution

Delamination can provide toughening by reducing the stresses in the layers ahead of the advancing crack. delamination was found to be more effective than slip in reducing the stress ahead of the crack.

1.5 Role of Electroplated Coating

Electroplated coatings play an important role in metal joining processes such as soldering, brazing and welding. Yardy[35] classifies coating for brazing and welding applications into three main types:

1) Active coatings melt and then wet surfaces prior to joining components together on solidification.
2) Passive coatings are pressed out of the joint on melting, expose and clean the surface, thus allowing solid state bonding reactions to occur.
3) Barrier coatings neither melt nor are pressed out of the joint clearance. These coatings form a physical barrier, which protects the substrate from combining with molten solder or brazing alloy.

Electroplated coatings can be justified in the present investigation with two different arguments: first, electroplated coatings can improve wetting characteristics at the interface between metal insert and molten metal. Also, electroplated coatings can protect inserts or act as a barrier to restrict the reaction between\n insert and molten metal.

2.0 EXPERIMENTS

2.1 Materials

2.1.1 A354 Aluminum Alloy

The initial work on potential strengthening materials for aluminum casting used A354 aluminum alloy. A354 aluminum alloy contains 1.6 to 2% Cu, 0.4 to 0.6 % Mg, less than 0.10% Mn, 8.6 to 9.5% Si, less than 2% Fe, less than 0.1% Zn and 0.l05% other elements with balanced Al. A354 was originally used for permanent mold castings that required high strengths and heat treatability. The coefficient of linear thermal expansion is 11.6×10^{-6} in./in.·° F

2.1.2 Strengthening Materials and Preparation

Aluminum bronze, cast iron and Ni-Resist were evaluated as strengthening material to reinforce aluminum.

Aluminum bronzes contain 9~14% Al, 0.75~4% Fe to refine grain structure and increase strength, and lesser amount of manganese or nickel. Aluminum bronzes have higher yield strength (450~900 MPa) and good corrosion and wear resistance.

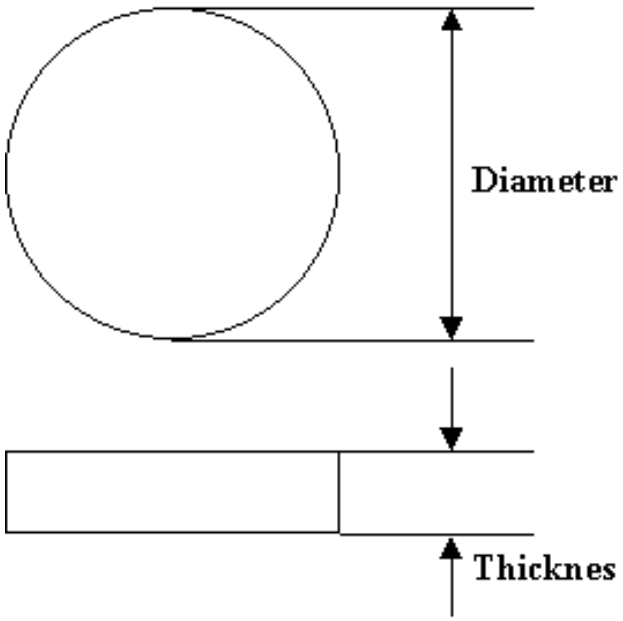
Cast irons are multi-component ferrous alloy which solidifies with an eutectic.

They contain major (iron, carbon, silicon), minor (< 0.1%) and often alloying (>0.1%) elements. Cast iron has higher carbon and silicon contents than steel. Because of the higher carbon content, the structure of cast iron exhibits a rich carbon phase. The coefficient of thermal expansion range $4\sim10.7\times10^{-6}$ in./in.·°F

Ni-Resist is an austenitic cast iron containing 18~36% Ni, up to 7% Cu and 1.75~4% Cr. Ni-resist is used for heat-resistant and corrosion resistant applications. Austenitic irons have the advantage of high toughness and thermal shock resistance. Mechanical properties of Ni-resist are tensile strength of 400 ~ 470 MPa (58~68ksi), yield strengths of 205~275MPa(30~40ksi), and elongations of 10~40%.

The strengthening materials use in this part of the investigation were disc-shape. The dimensions of each discs are listed on the Table 5 and the thermal expansion coefficients of A354 aluminum alloy, cast iron and Ni resist are listed on the Table 6.

Table 5: The Dimension of Discs



Material	Diameter, in	Thickness, in
Al Bronze	1.9	0.25
Cast Iron	2.3	0.25
Ni-Resist	2.0	0.27

Table 6: Thermal Expansion Coefficients of Materials

Material	Temperature range °F	Thermal expansion coefficient μin./in.·°F
A354 Al Alloy	68~212	11.6
Cast Iron	68~212	5.6
	68~392	5.9
	68~932	7.2
	68~1112	7.4
Ni-resist	70~400	10.7

2.1.2.1 Surface Treatments and Coatings

Most discs were used without any surface treatment or coating . Some cast iron discs were used after either Dynablue(carbon nitriding) or the Kolene (surface) process.

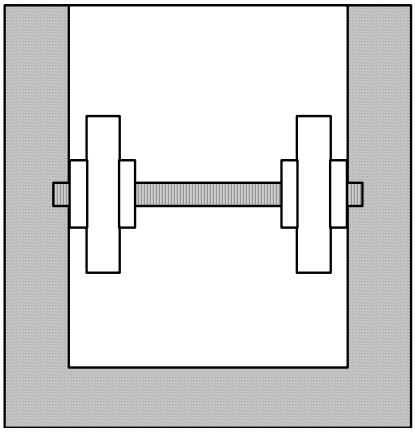
Most discs were electroplated. The types of electroplated coatings were Zn, Cu, and Ni and multi-plated coatings such as Cu / Ni or Ni / Cr. Some discs were used after aluminizing treatment [36] by dipping into molten 380 aluminum alloys. The surface treatments and coatings are listed on the Table 7.

2.1.2.2 Preparation

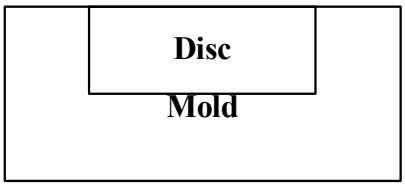
To set these discs in the mold, a hole was made at the center of disc; then these discs were mounted on a ¼ inch threaded rod or set at the bottom of the mold. Figure 7 illustrates how the discs were set in the mold.

Table 7: Surface Treatments and Coatings of Discs

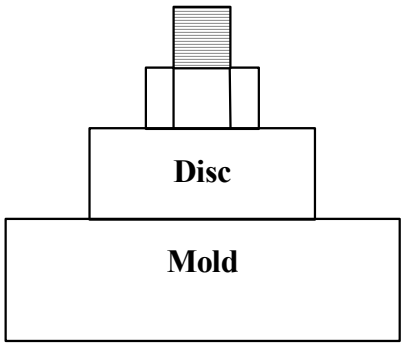
Disc	Surface Treatment	Coating
Al Bronze	None	None
		Cu
		Cu / Ni
		Ni / Cr
		Ni / Ni
		Zn
Cast Iron	DynaBlue	None
	Kolene	Cu
		Cu / Ni
	None	None
		Cu
		Cu / Ni
		Ni / Cr
		Zn
		Aluminizing
Ni-Resist	None	None
		Cu
		Cu / Ni
		Aluminizing



(a)



(b)



(c)

Figure 7: The methods to set discs in the mold

2.1.3 Meshes and Preparation

Galvanized carbon steel wire mesh and 304 type stainless steel wire mesh were used as reinforcement to improve toughness of the compressor housing. The mesh count, diameter of wire and wire spacing are on the Table 8. Stainless steel wire meshes were used as either with electroplated Zn coating or without coating. To introduce multi-layer meshes, meshes were stacked by nuts and bolts (Figure 8).

Table 8: Data of Stainless Steel wire meshes

Mesh Count [No of sq./in^2]	Diameter of wire [in]	Wire Spacing [in]
4X4	0.047	0.25
5X5	0.041	0.2
6X6	0.035	0.166667
10X10	0.025	0.1
12X12	0.023	0.083333
14X14	0.02	0.071429
16X16	0.018	0.0625
18X18	0.017	0.055556
20X20	0.016	0.05
24X24	0.014	0.041667
30X30	0.01	0.033333

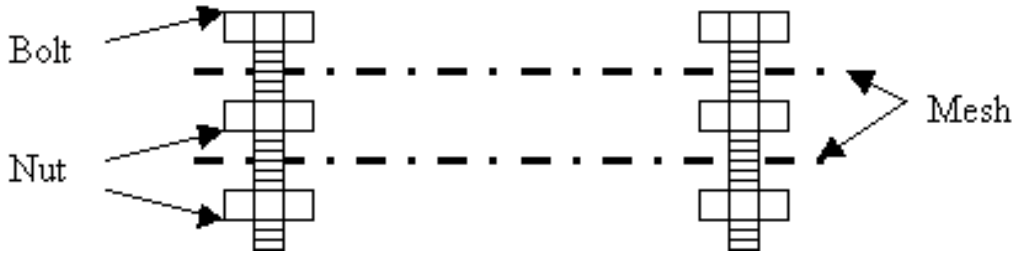


Figure 8(a) Sketch of mutilayer meshes

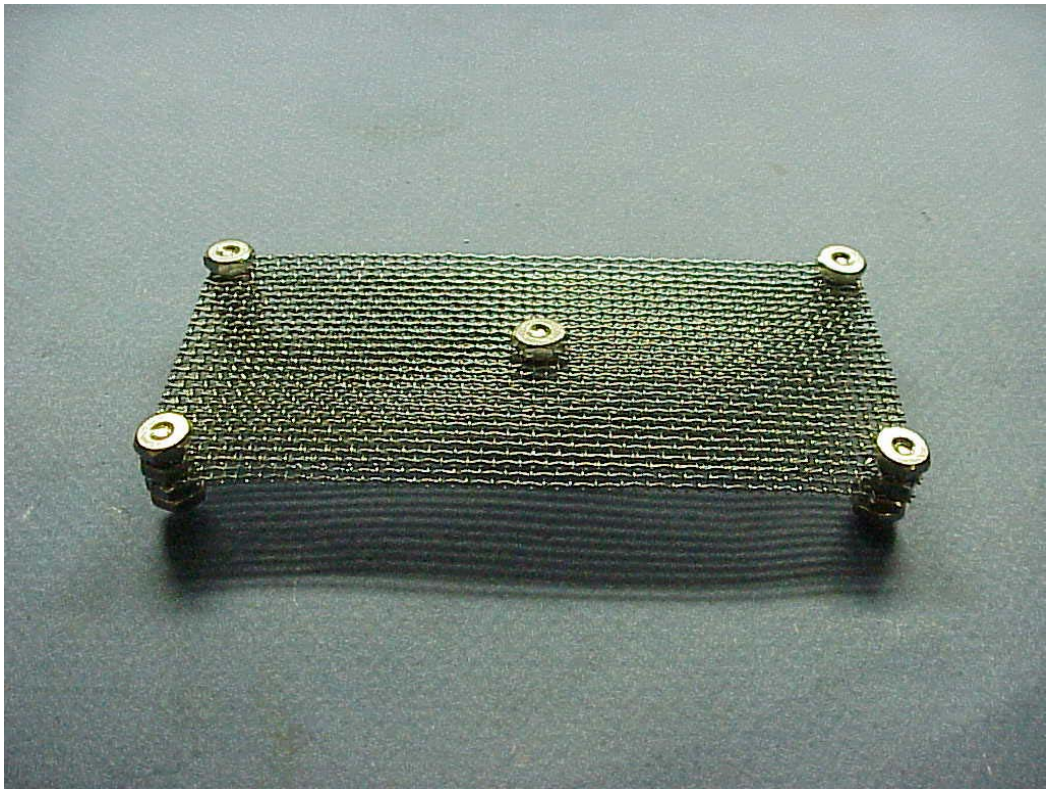


Figure 8(b) Picture of mutilayer meshes

2.2 Molds

No-bake sand molds were used for this part of the project. No bake sand molds were made of silica sand with organic binders, LINO CURE AA-50 and LINO CURE C. The mixing ratio of silica send and binders, LINO CURE AA-50 and LINO CURE C, is 50:0.75:0.15.

2.2.1 Molds for Strengthening

There are nine possible positions for discs in the mold. Six discs are along the wall closest to the gate and furthest from the gate. Three discs are at the bottom of the mold. The schematic of the mold, the position of the disc-inserts and the picture of the mold are shown Figure 9(a) and 9(b). The discs along the walls are mounted on the 1/4" threaded rod and held in place and separated from the wall by nuts (Fig. 7(a)). To set the discs at the bottom, two kinds of method were used. One is making a sink by wood discs when the mold was made (Fig. 7(b)). The other is using threaded rods and nuts after making holes at the bottom of mold (Fig. 7(c)).

Molds with a smaller cavity were made with cores (Fig. 10). The volume of the cavity is about 40% of that of normal mold. The dimension of gating system and raiser is the same as that of normal mold.

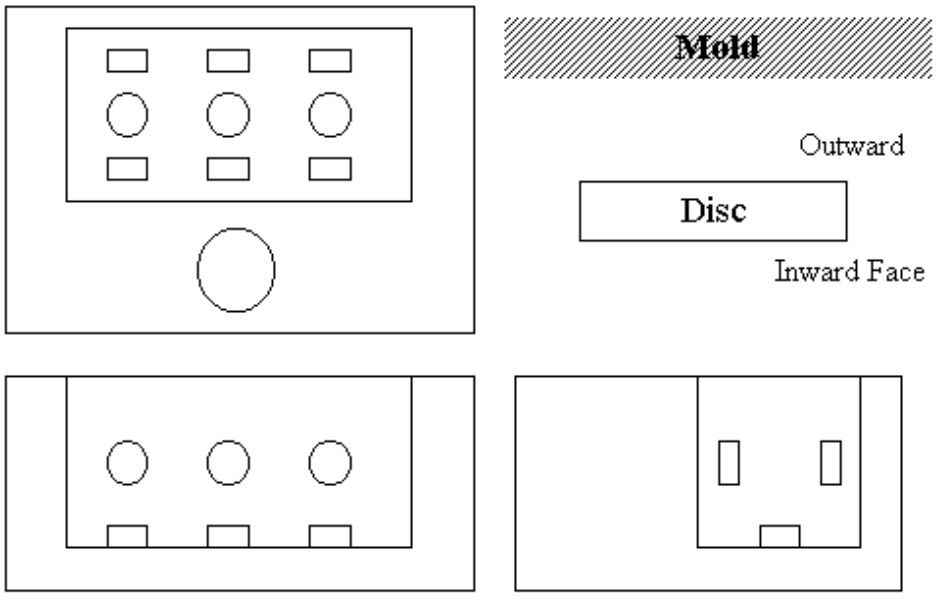


Figure 9(a): The schematic feature of mold and position of disc-inserts

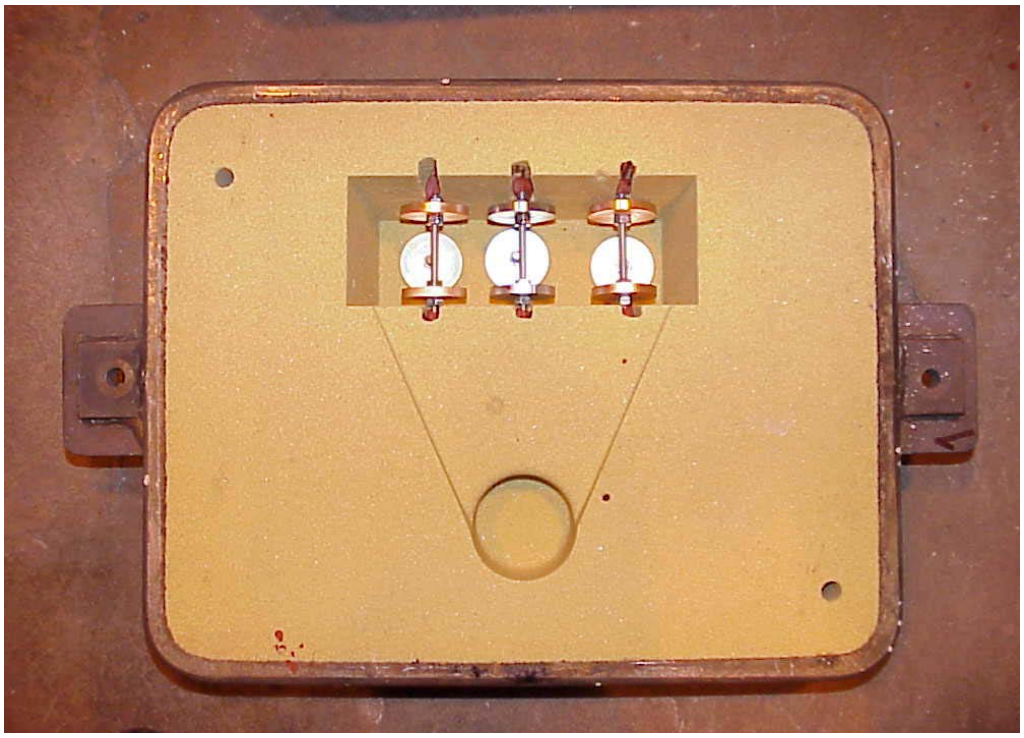


Figure 9(b) The picture of mold with discs

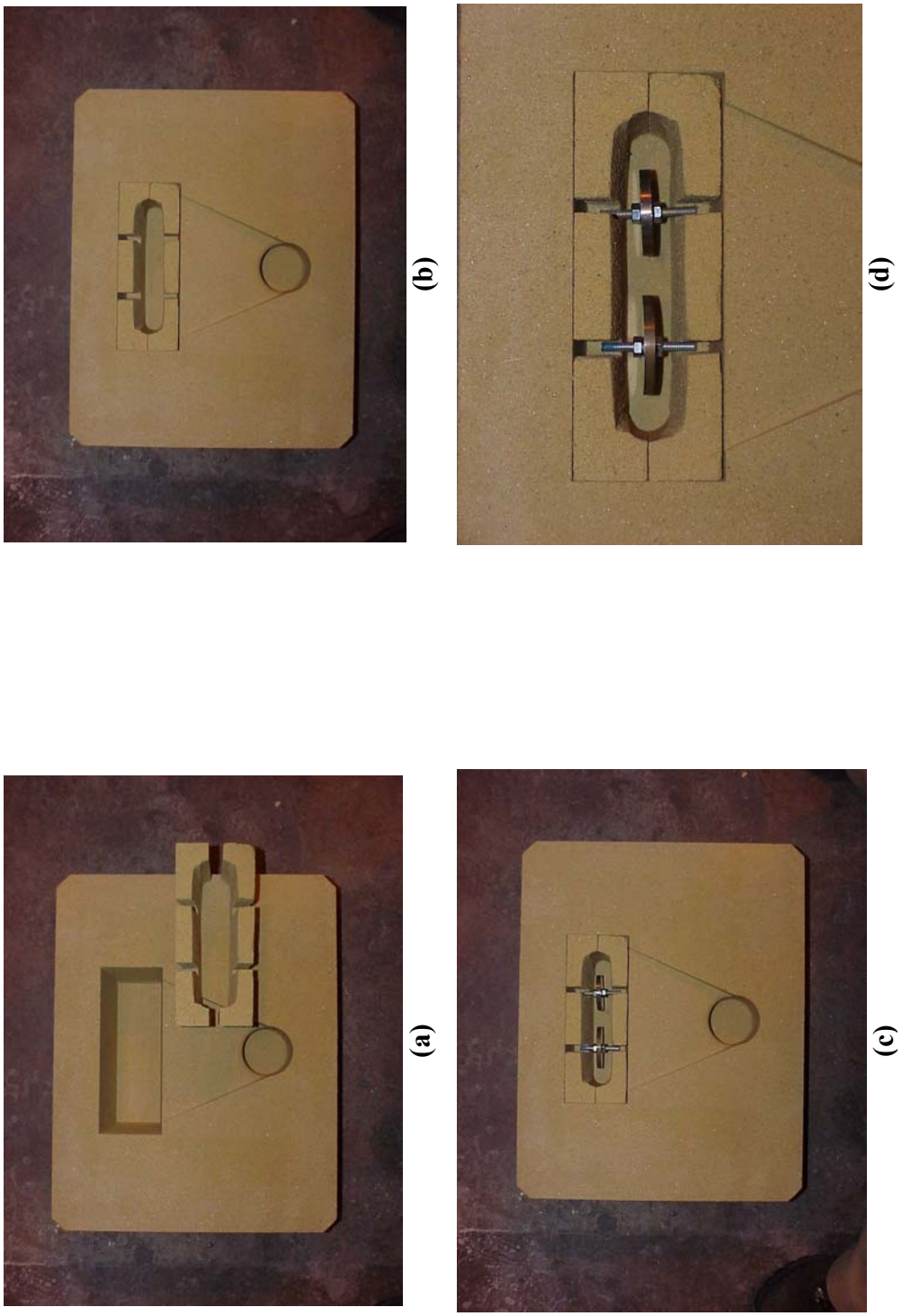


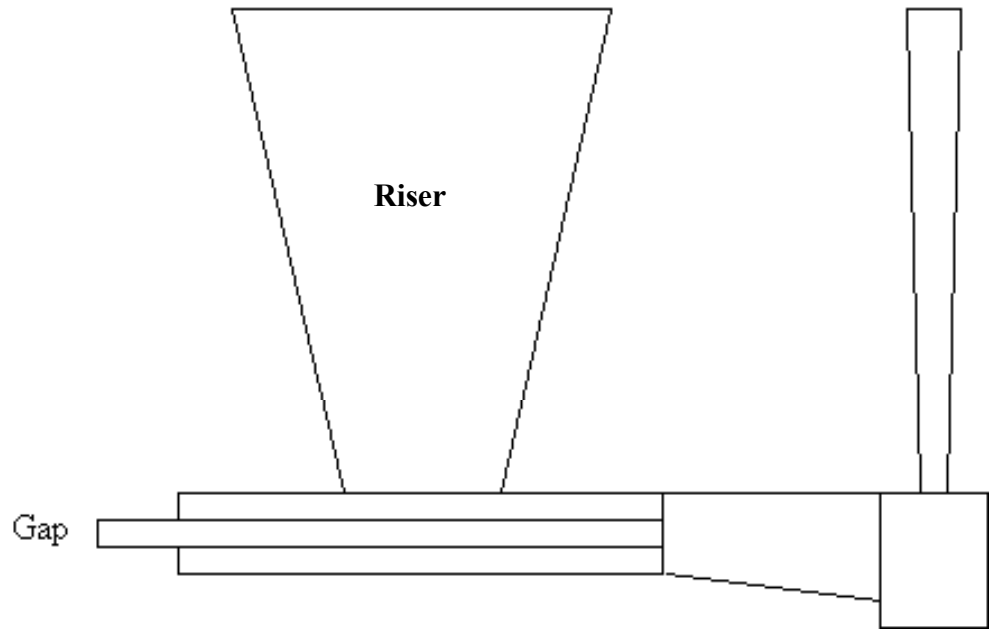
Figure 10 Mold for small casting

2.2.2 Mold for Meshes

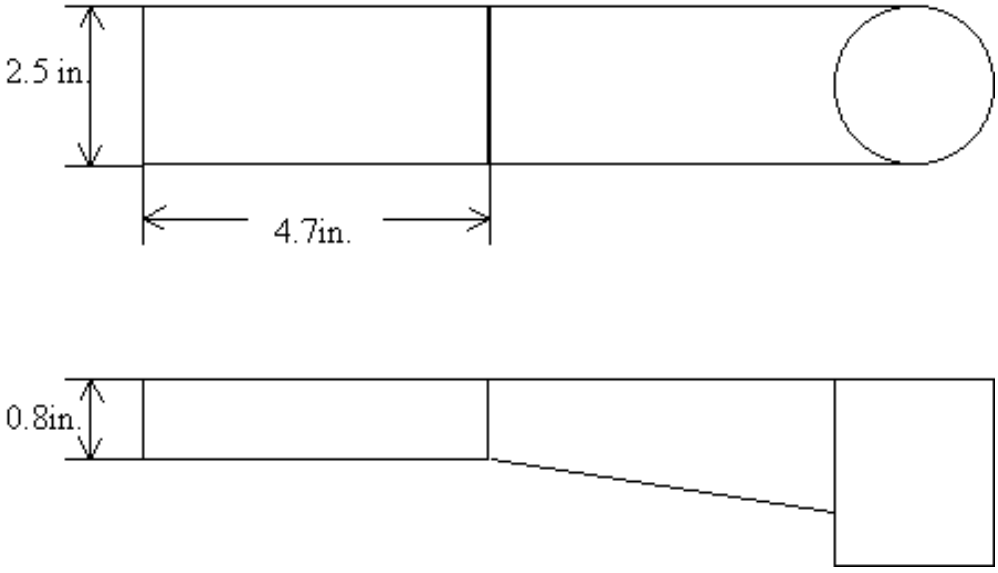
To make Charpy impact test bars, 2.5 in X 4.7 in X 0.8, aluminum slabs with meshes were made. These molds need a gap to allow the mesh to expand. Figure 11 shows a sketch of the mold and the dimensions of the mold for meshes.

2.3 Melting and Casting

The molten metal was prepared by melting commercial 354 aluminum ingots. 354 aluminum ingots were melted in an induction furnace under air atmosphere. Grain refiner and silicon modifier before pouring were not utilized. The target pouring temperature was from 1350 to 1450 □. The molten metal was transferred from the induction furnace to the pouring basin with a silicon carbide ladle.



(a)



(b)

Figure 11: Sketch of mold and dimension of casting

3.0 RESULT AND DISCUSSION

3.1 Analysis of Aluminum Bronze Reinforced Aluminum Casting

Figure 12 is the part of a casting with metallic inserts and shows how the casting was cut. The disc-shape inserts were cut horizontally through the center. Figure 13(a) shows the cross section of the aluminum bronze insert in the casting. The aluminum bronze insert is dissolved and has poor bonding. Figure 13(b) to Figure 13(e) show the pictures of the cross section of aluminum bronze inserts with Cu, Ni, Cu/Ni, and Zn electroplated coatings. None of electroplated coatings can protect the insert from dissolving.

3.1.1 Dissolution of Aluminum Bronze

Dissolution plays one of the important roles in bonding of dissimilar metals. However severe dissolution of inserts could be a problem in cast-in-place reinforcement. Figure 14 shows the cross section of a cast iron insert. The aluminum bronze disc was dissolved more severely than the cast iron disc. Temperature, time, volume of the liquid, and solubility of solid phases in the liquid phase can affect the dissolution of inserts. As the temperature is increased, generally the solubility of solute elements is also increased.

Time is related to the dissolution kinetics. As the time is longer, the quantity of dissolved elements is increased. Higher Cu solubility in liquid Al can explain severe dissolution of aluminum bronze in the aluminum alloy. Figure 14(a) and (b) are phase diagrams of Al-Cu and Fe-Al binary system, respectively. If the temperature of molten aluminum is 660°C (1220°F), the maximum solubility of Cu and Fe in aluminum liquid is about 60 and 2-wt%, respectively.

Figure 13(b) to Figure 13(e) show cross-sections of aluminum bronze inserts with Cu, Ni, Cu/Ni, and Zn electroplated coatings. Even though nickel and copper have higher melting temperature than aluminum, electroplated coatings could not protect the aluminum bronze inserts. During the casting process the electroplated coatings may be dissolved into the molten aluminum. Because the thickness of electroplated coatings is not enough to remain on the surface and protect the inserts, none of coatings could protect the aluminum bronze inserts from dissolving.

3.1.2 Metallurgical Analysis of Interface

Figure 16 shows optical micrographs of the interface between aluminum bronze and the A354 aluminum cast alloy. There is an intermediate layer, which may be formed by dissolution of the aluminum bronze insert, between the aluminum bronze and the

aluminum alloy. A good metallurgical bonding exists between these layers. Faster cooling rates and lower temperatures may reduce the dissolution of aluminum bronze, and may result in establishing a good bonding between aluminum bronze and A354 alloy.

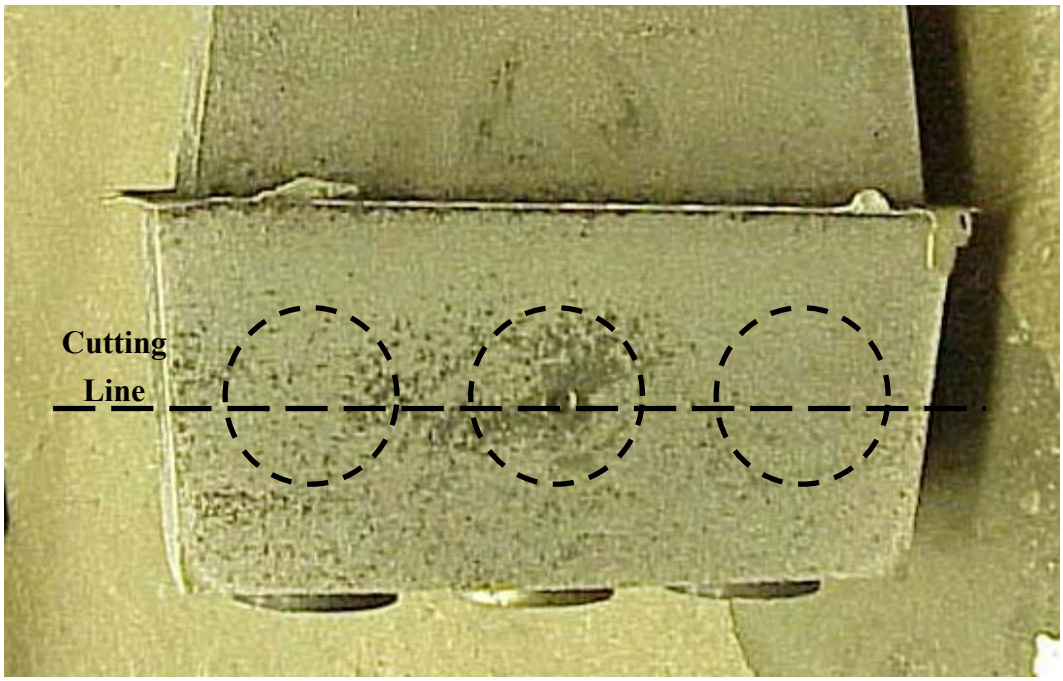


Figure 12: Casting with metallic inserts and cutting line

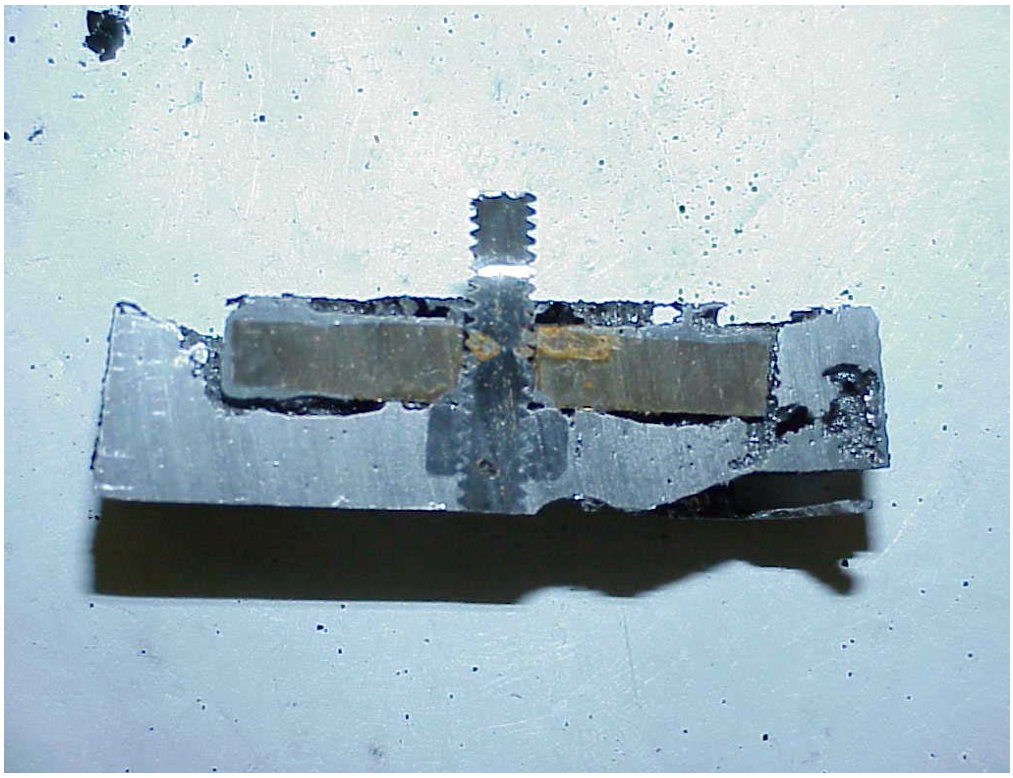


Figure 13(a:) Cross section of aluminum bronze insert

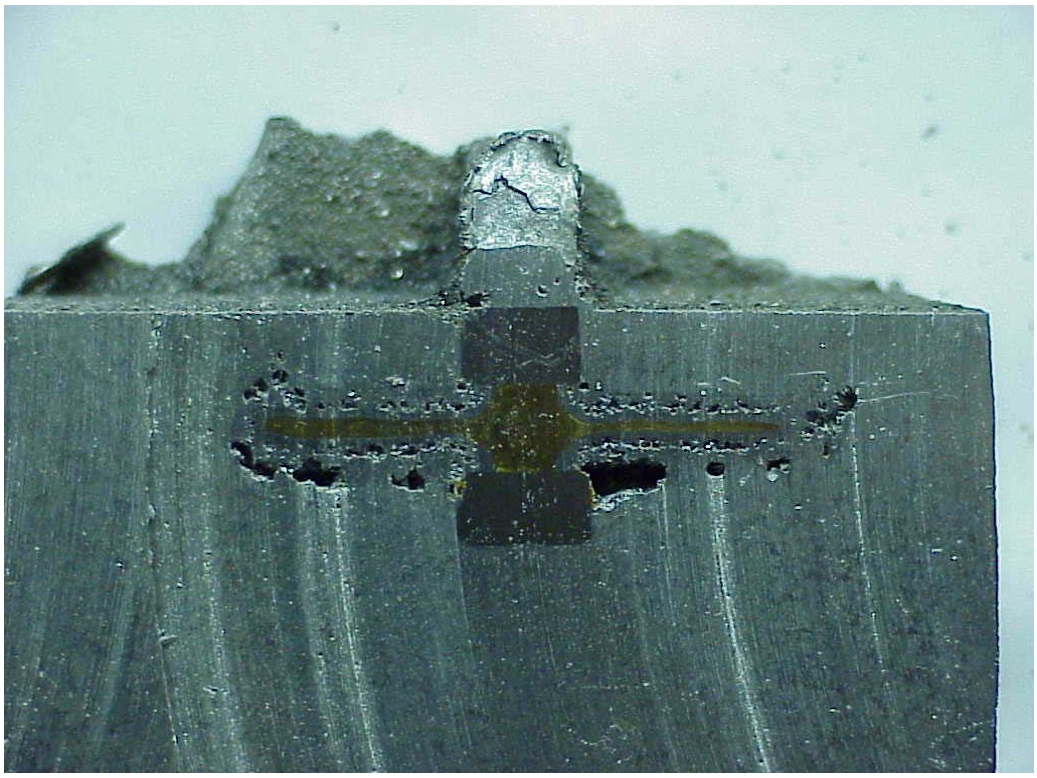


Figure 13(b): Cross section of an aluminum bronze insert with Cu Electroplating

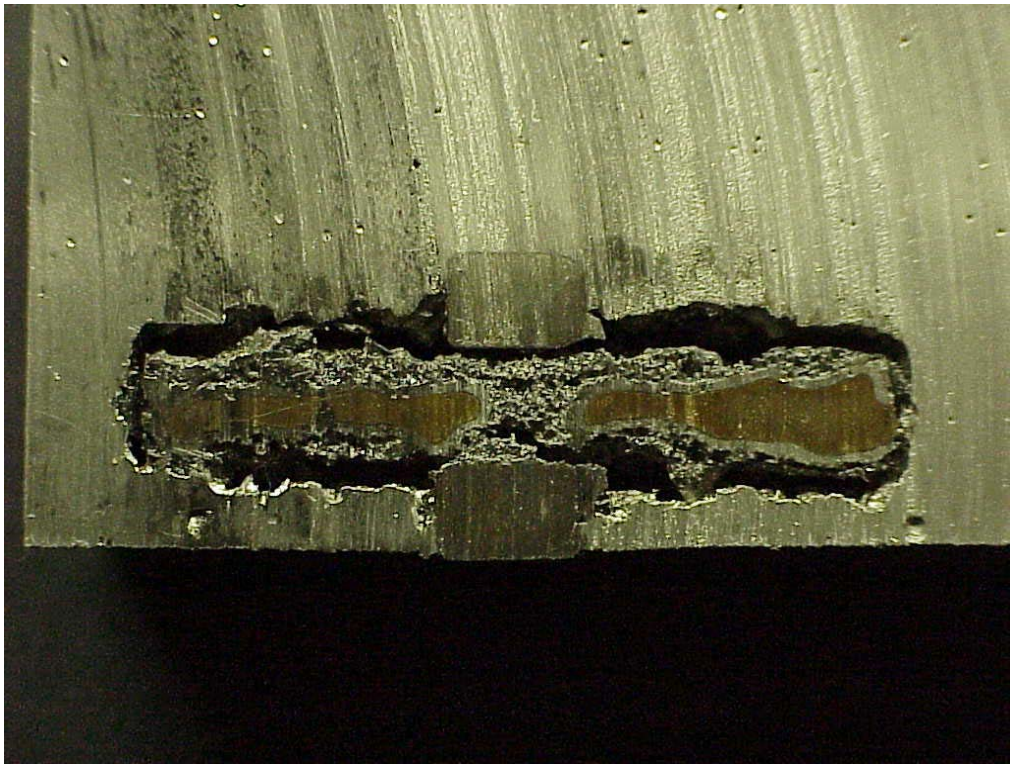


Figure 13(c): Cross section of an aluminum bronze insert with heavy Ni

Electroplating

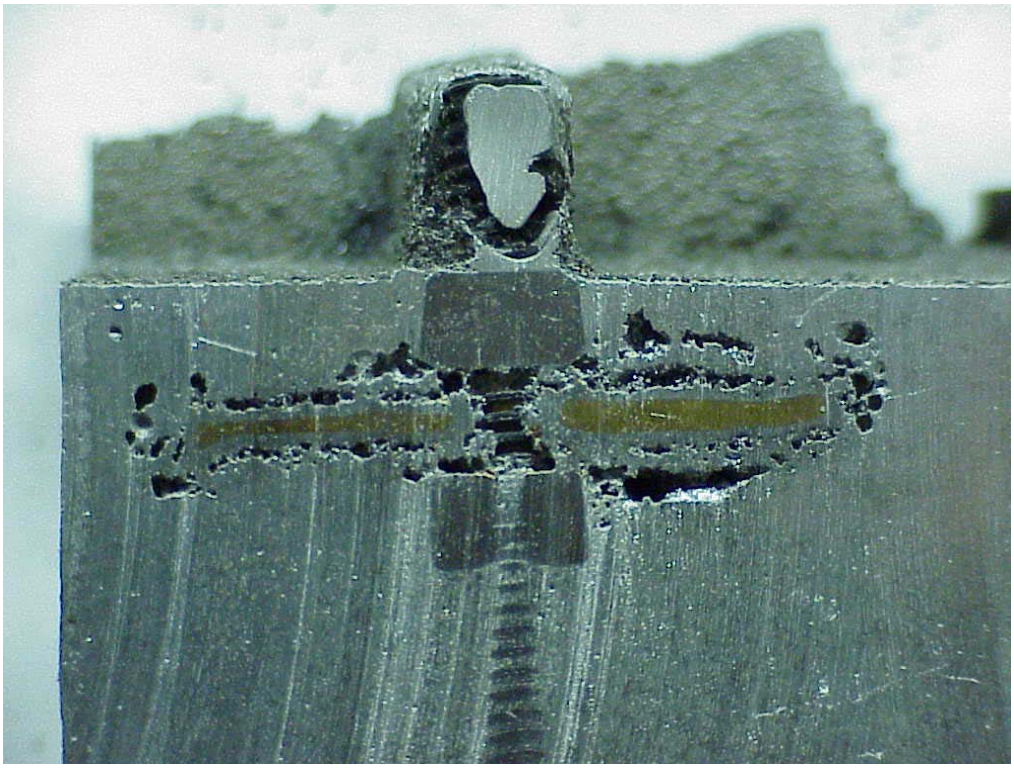


Figure 13(d): Cross section of an aluminum bronze insert with Cu/Ni Electroplating

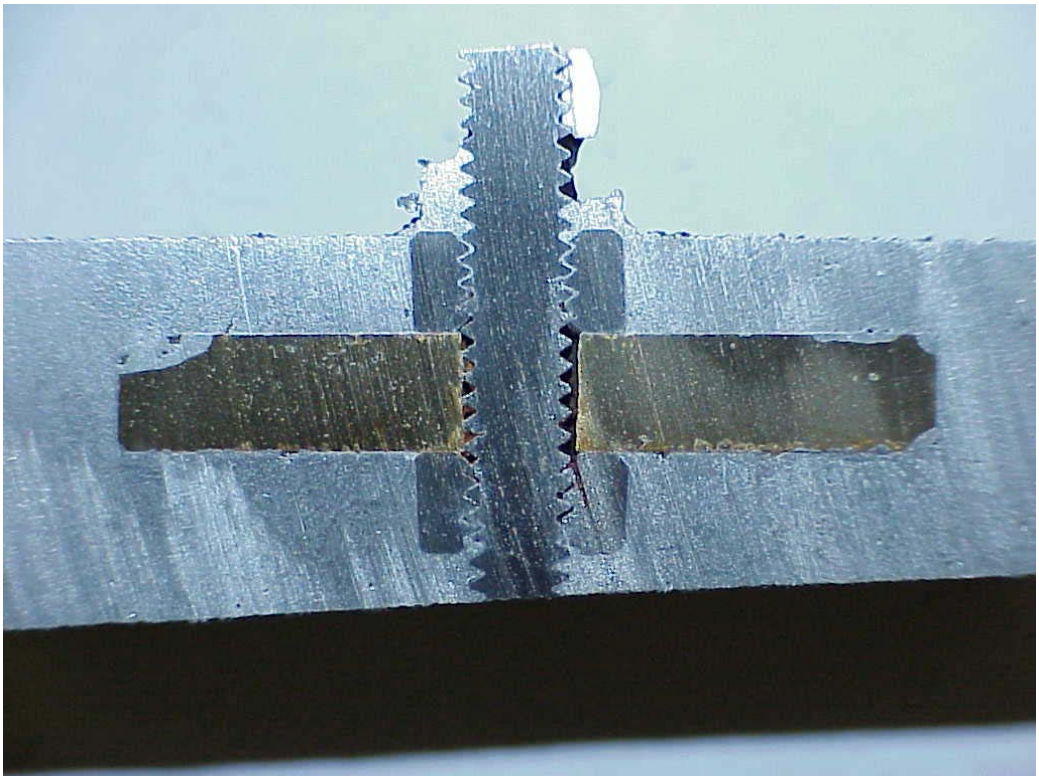


Figure 13(e): Cross section of an aluminum bronze insert with Zn Electroplating

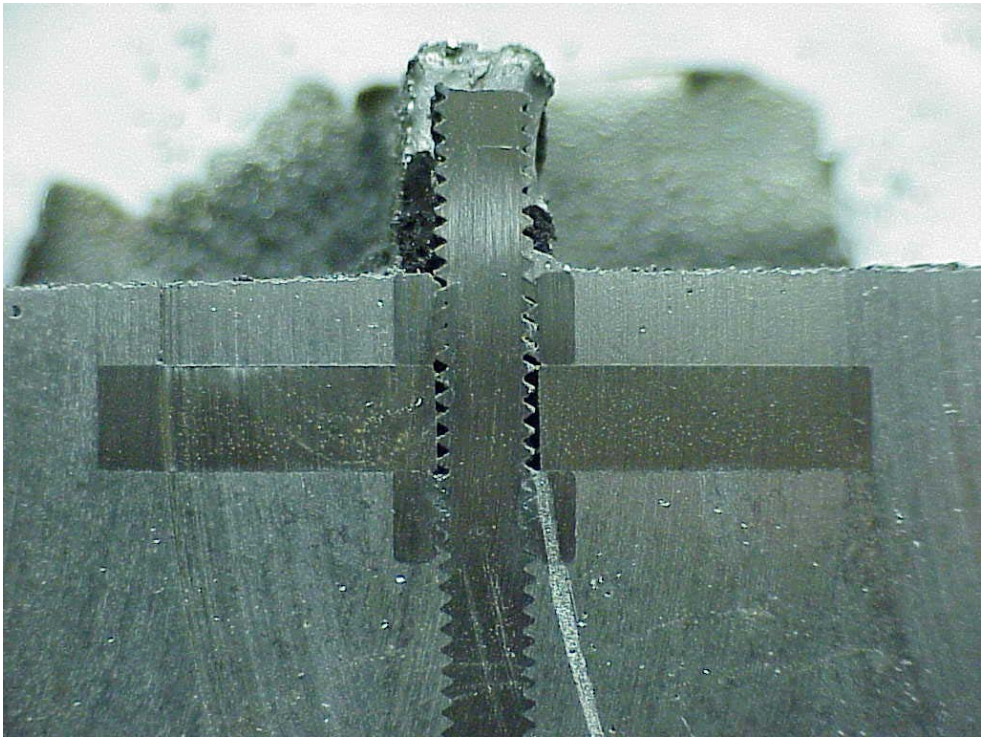


Figure 14: Cross section of a cast iron insert

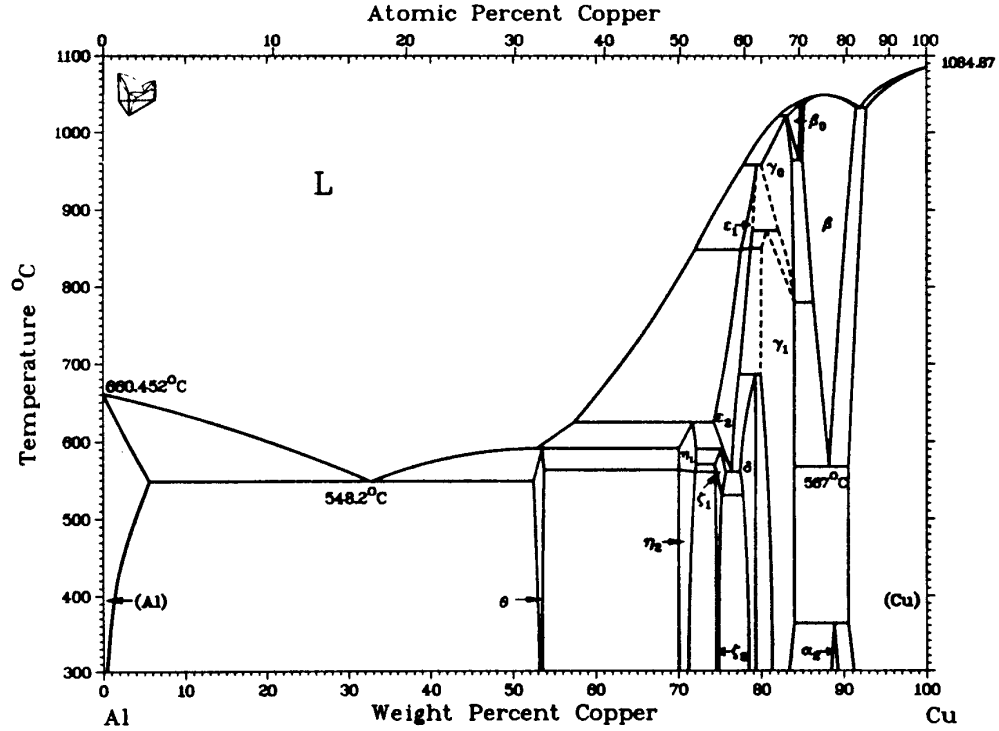


Figure 15(a) Phase diagram of Al-Cu binary system

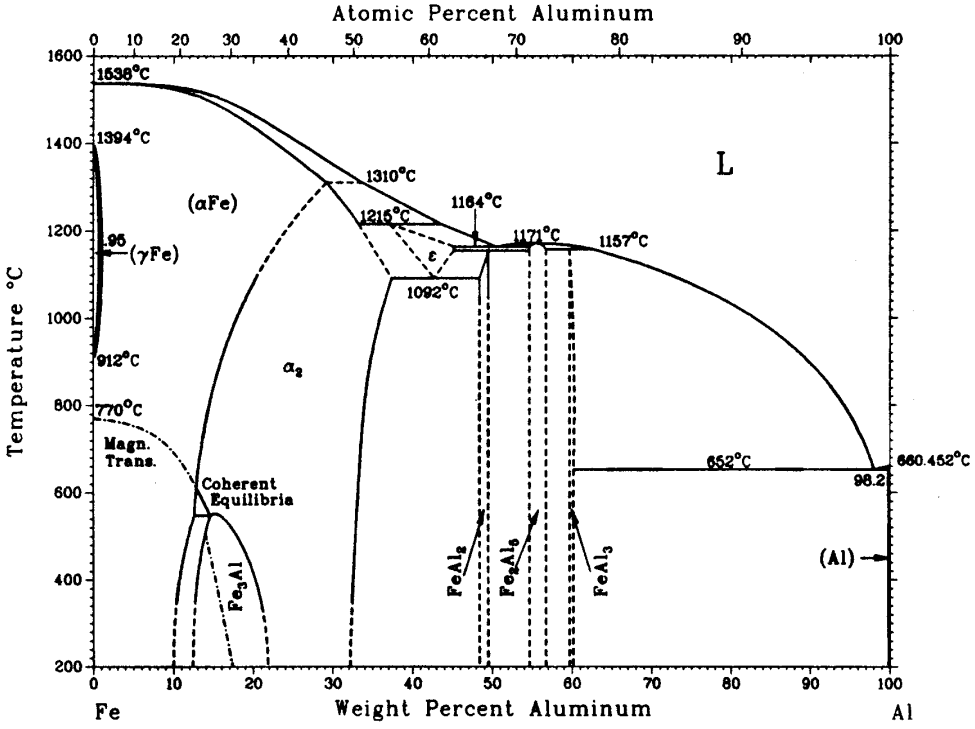


Figure 15(b) Phase diagram of Fe-Al binary system

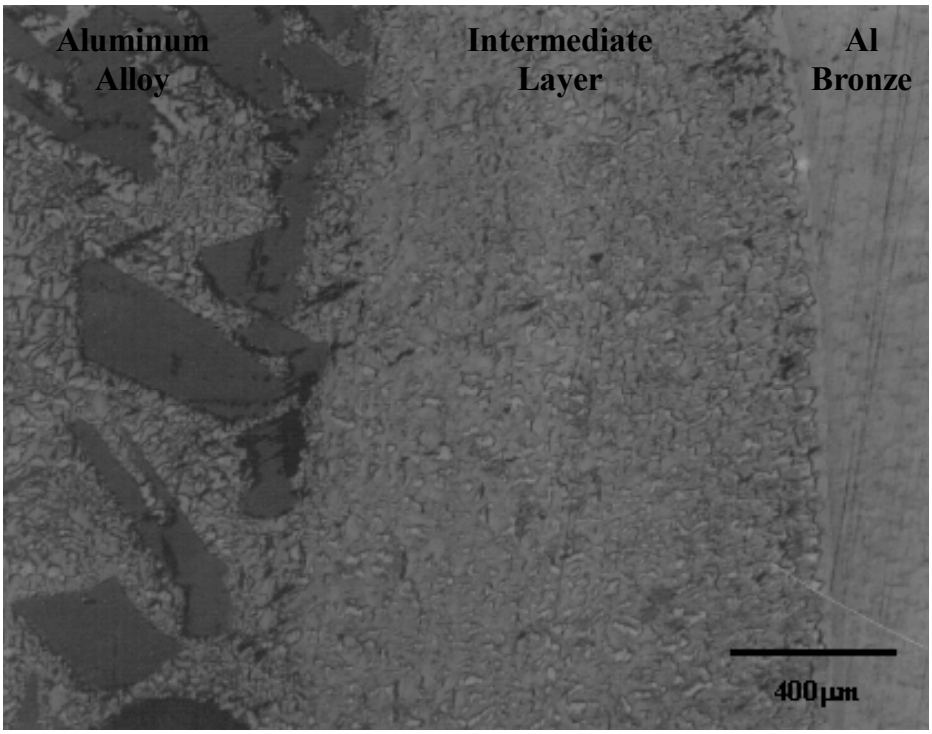


Figure 16(a): Optical microscope picture of the interface between Al bronze and aluminum alloy

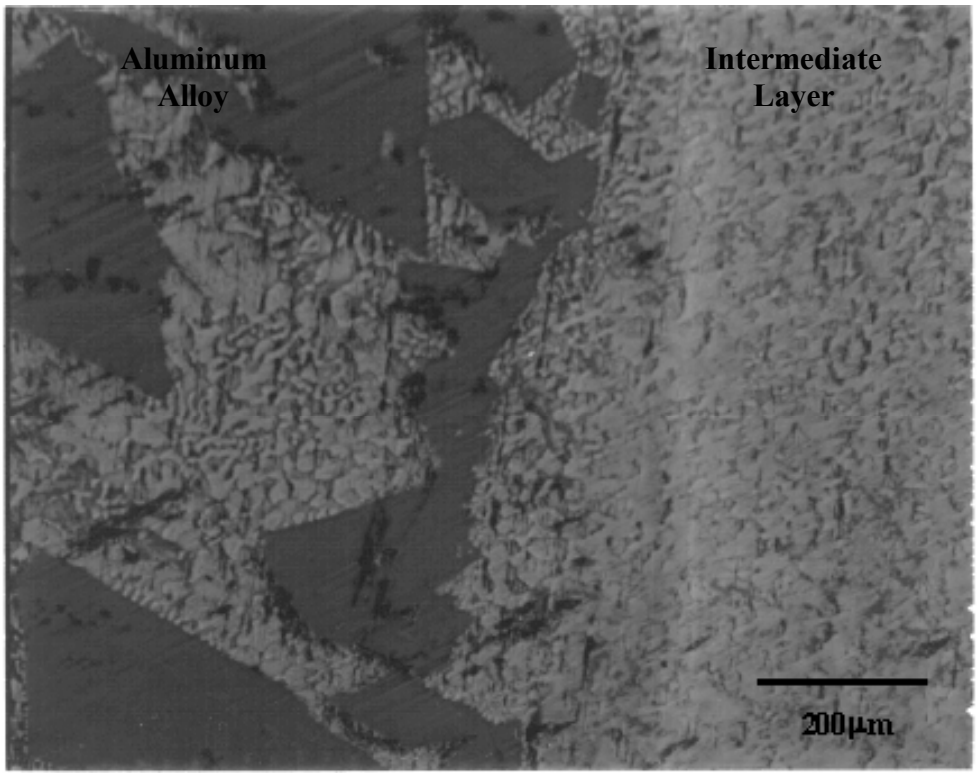


Figure 16(b): Optical microscope picture of the interface between the intermediate layer and the aluminum alloy

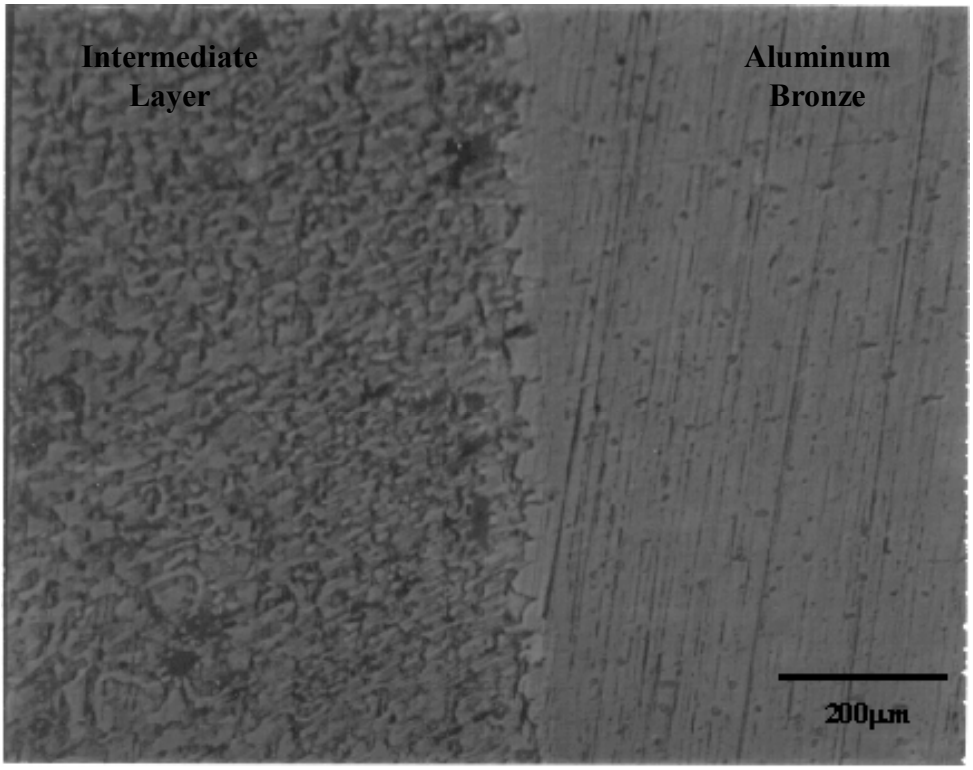


Figure 16(c): Optical microscope picture of the interface between the Al bronze and the intermediate layer

3.2 Analysis of Cast Iron Inserts in the Aluminum Casting

Figure 17 is the cross section of a cast iron insert. Dissolution of the cast iron insert is not as severe as that of aluminum bronze. The surface of insert may have dissolved but just slightly. A crack between the cast iron insert and A354 aluminum alloy is observed.

3.2.1 Metallurgical Analysis of Interface

Figure 18 is an optical micrograph of the interface between the cast iron insert and the A354 aluminum alloy. There is an intermediate layer between the cast iron insert and the A354 aluminum alloy. Micro hardness (Fig. 19) readings taken across the interface illustrate the hard and brittle characteristics of the intermediate layer. This brittle layer results in low ductility and increases crack sensitivity [1].

Figure 20(a) and (b) are SEM micrographs of the interface between cast iron with a Cu coating and the A354 aluminum cast alloy; also, compositional profiles across the interface obtained by EDS. The high-copper area indicates the original interface and shows diffusion of aluminum into the cast iron insert. There are solid solution and intermetallic compound layers at the interface. Moving from the cast iron insert (A in Fig. 20) into the A354 aluminum cast alloy (I in Fig. 20), there are Fe_3Al (B in Fig. 20), η-Fe_2Al_5 (D in Fig. 20), θ-$FeAl_3$ (E and F in Fig. 20), and β-$FeSiAl_5$ (G in Fig. 20) layers. A354 aluminum alloy shows very low silicon content (0.24%). Figure 21 is the phase

diagram of Al-Si binary system. Because silicon precipitates as silicon particles, the Si content in the aluminum solution is very low.

3.2.1.1 The Role of Surface Treatments and Coatings

The interface of the A354 aluminum alloy and a cast iron insert after a carbo-nitriding process is shown Figure 22. No bonding occurred between the cast iron and the Al alloy. The following facts may cause this poor bonding. First, the cast iron insert does not dissolve. No intermediate layer formed between the two metals. It is difficult to establish a good bond between an insert and aluminum alloy without some dissolution or reaction between them.

Figure 23(a) to (e) exhibit interfaces between A354 aluminum alloy and cast iron with Al, Cu, Cu/Ni, Ni/Cr and Zn coatings. Various kinds of electroplated coatings were employed. However the interface features are similar to each other. Figure 24 shows a thickness of the intermediate layer between 50 to 60 μm. The effect of electroplated coatings on the thickness of intermediate layer is not significant in this case.

Figure 25(a) and (b) are optical micrographs of the interface between A354 aluminum alloy and cast iron insert after a Kolene process with Cu and Cu/Ni coatings. Removing graphite from the surface of the cast iron inserts did not exert any significant differences from interface of cast iron.

3.2.2 Thermal Expansion Coefficient, Residual Stresses and Failure of Bonding

The thermal expansion coefficients of the alloys used are different from each other. The thermal expansion coefficient of A354 aluminum cast alloy is higher than that of cast iron. During the casting process, both cast iron and A354 aluminum cast alloy were cooled from high temperature. Because of differences in the thermal expansion of the cast iron insert and A354 aluminum cast alloy residual stresses form around the insert. When cast iron inserts are utilized in the aluminum casting, the residual stress does not degrade the interface seriously. Because of the higher thermal expansion coefficient of A354 aluminum cast alloy, there are compressive stresses around the cast iron insert (Fig. 26(a)). However, when the interface is opened, the residual stresses can degrade the bonding (Fig. 26(b)).

3.2.2.1 Effect of Electroplated Coatings

Failure of the bonding should occur at the weakest site across the interface. The failures of the interface between the cast iron inserts and the A354 aluminum cast alloy can be classified into two groups. The first group is failure at the intermetallic compound layer. In most cases, such as interfaces between A354 alloy and cast iron inserts with Ni, Cu/Ni, and Al coatings, these interfaces fail at the intermetallic compound layer (Fig. 27(a)). Another type of failure occurs in the A354 aluminum alloy, near the interface. Zinc and Copper coated inserts belong to this group (Fig. 27(b)).

3.2.3 Effect of Heat Treatment

Thermal energy supplied by heat treatment leads to the diffusion of elements across the interface and chemical reactions. These make the intermediate layer thicker. The thicker brittle intermediate layer causes higher crack sensitivity. Generally, the formation of intermetallic compounds results in negative volume change. Therefore heat treatment makes the intermediate layer weaker and the cracks wider.

$$Fe + 3Al = FeAl_3 \qquad \Delta V = -1.98\ cm^3/mol$$

$$2Fe + 5Al = Fe_2Al_5 \qquad \Delta V = -4.19\ cm^3/mol$$

$$2Fe + Si + 8Al = Fe_2SiAl_8 \qquad \Delta V = -8.01\ cm^3/mol$$

Figure 28(a) and (b) ilustrate the interface after heat treatment (T6). Heat treatment degrades bonding between A354 aluminum alloy and cast iron severely. Heat treatment leads to diffusion of elements and chemical reactions that make the intermediate layer weaker or more brittle.

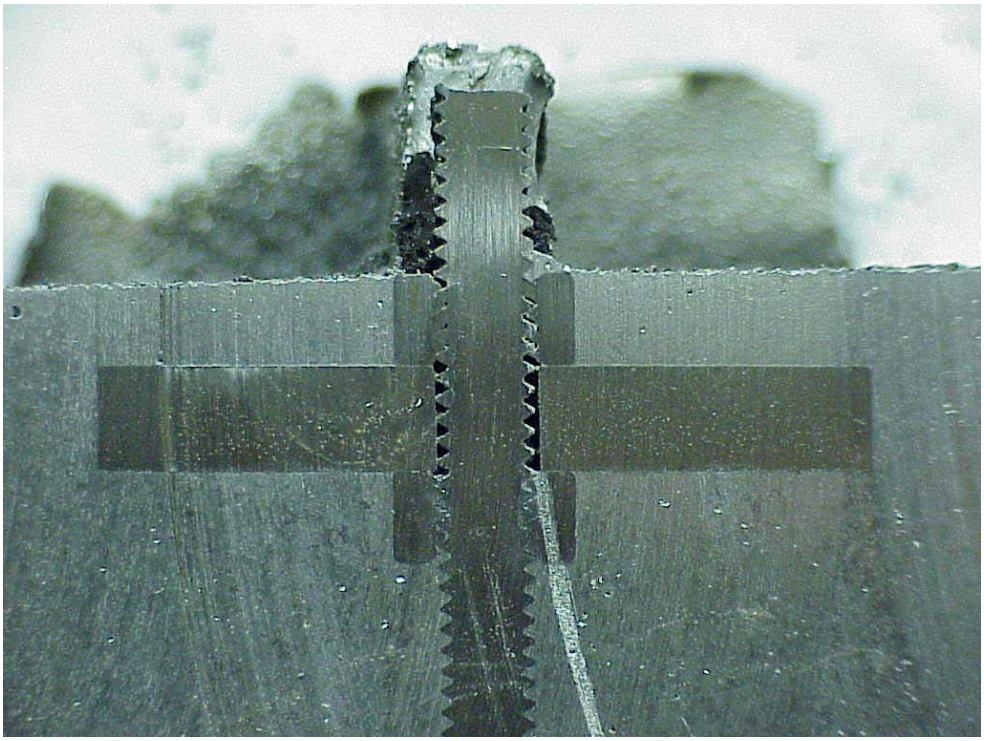


Figure 17: Cross section of cast iron insert

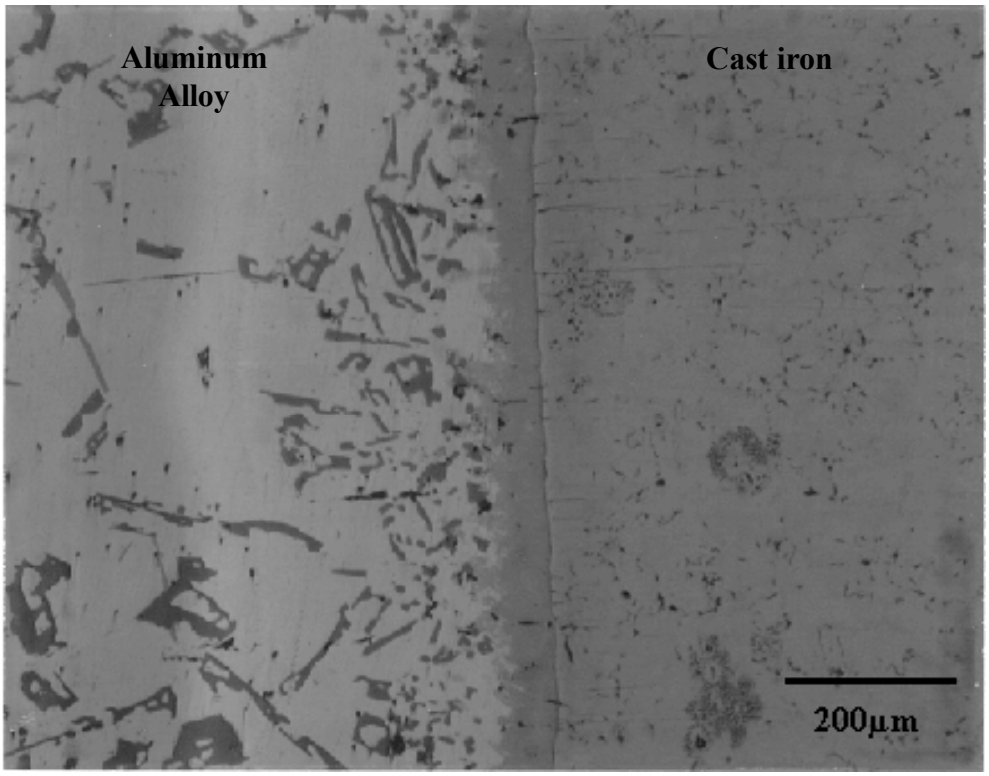


Figure 18: Optical microscope picture of the interface between cast iron and Al alloy

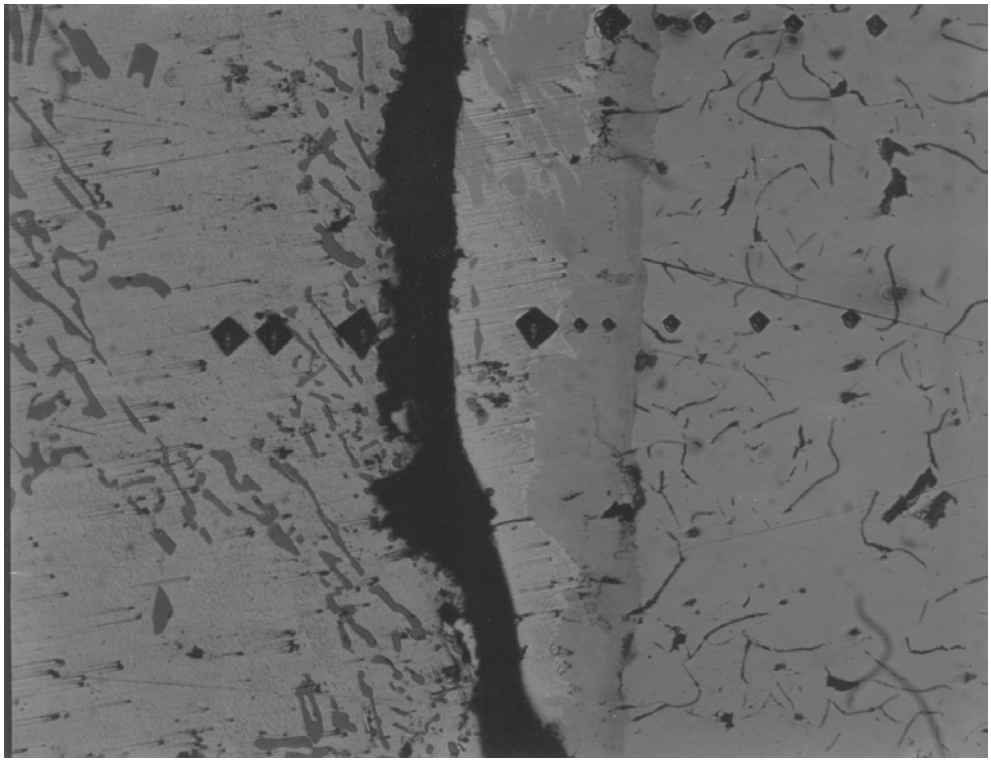


Figure 19(a): Result of micro hardness test across the interface between Al alloy and cast iron insert with Zn coating

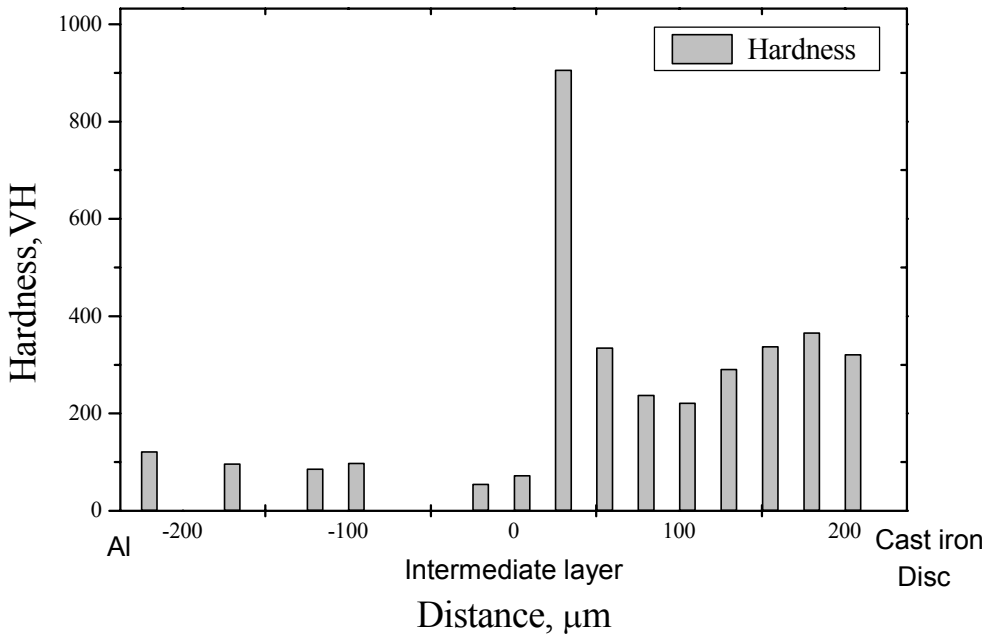


Figure 19(b): Micro hardness across the interface between Al alloy and cast iron insert

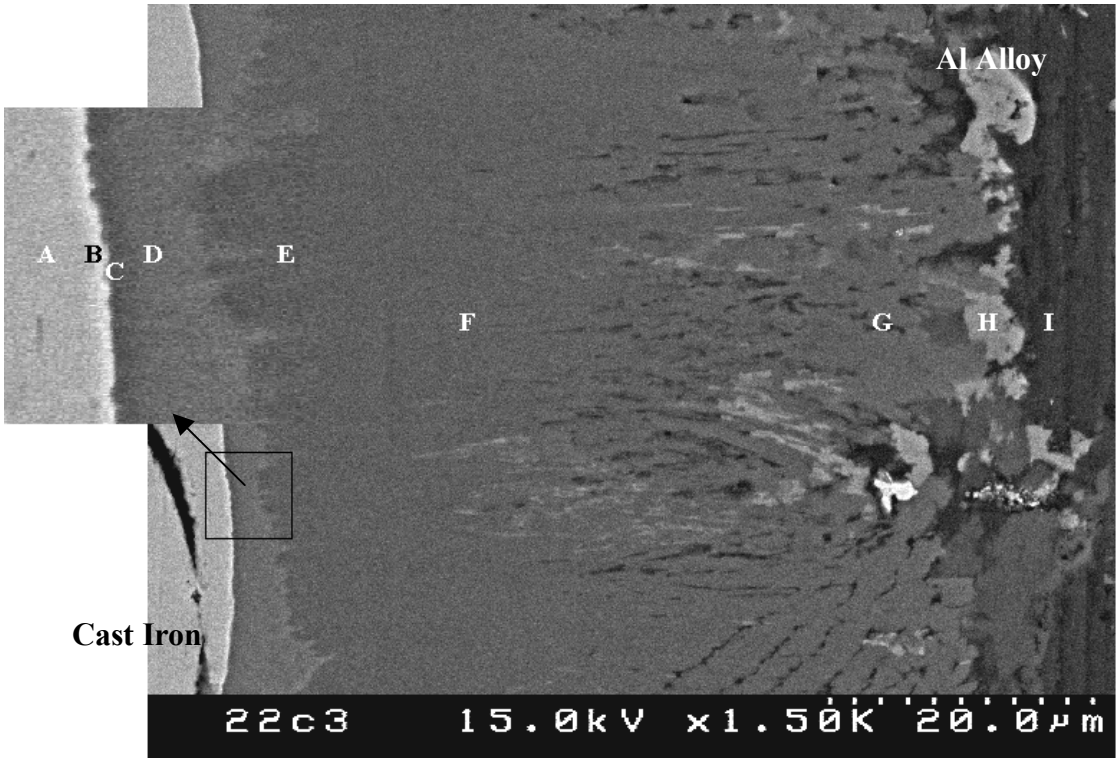


Figure 20(a): SEM picture of interface between A354 Al alloy and cast iron with Cu coating

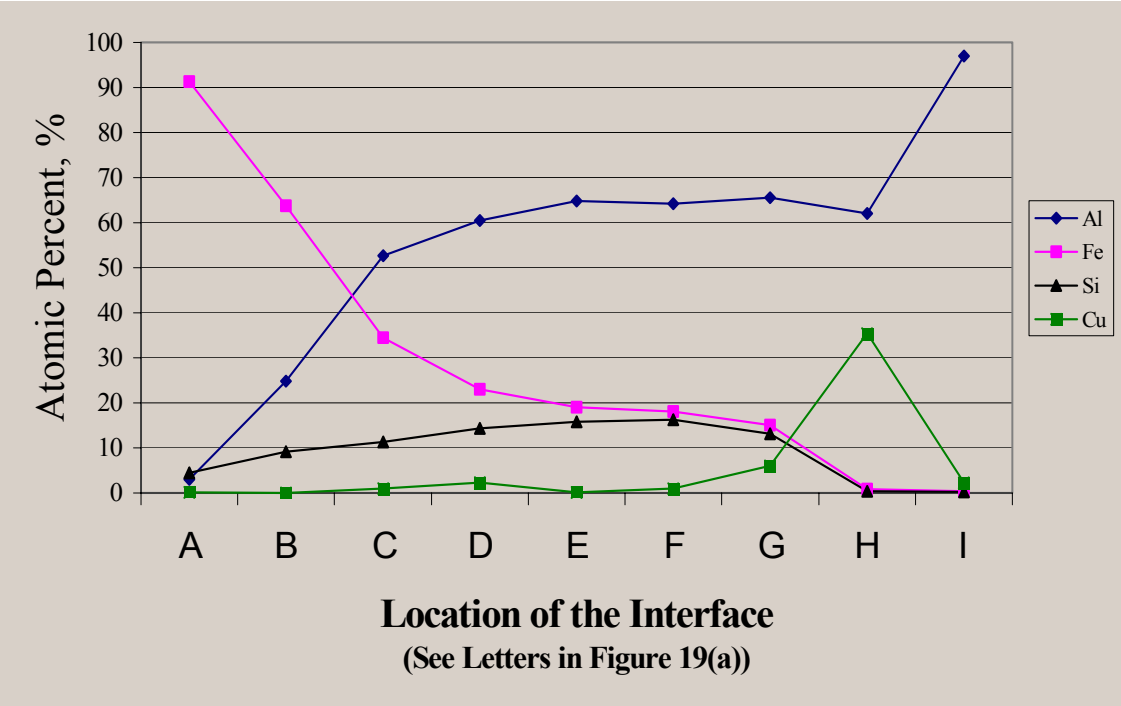


Figure 20(b): Compositional profile across the interface between A354 Al alloy and cast iron with Cu coating

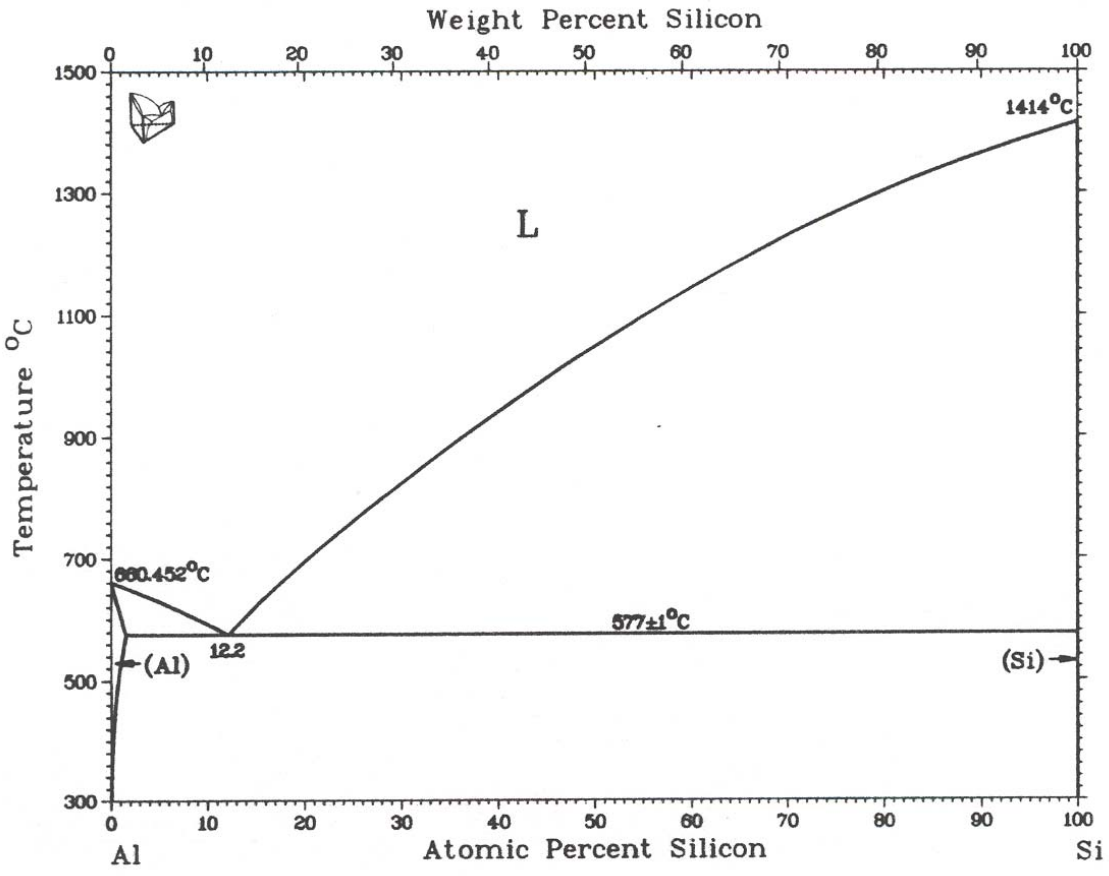


Figure 21: Phase diagram of Al-Si binary system

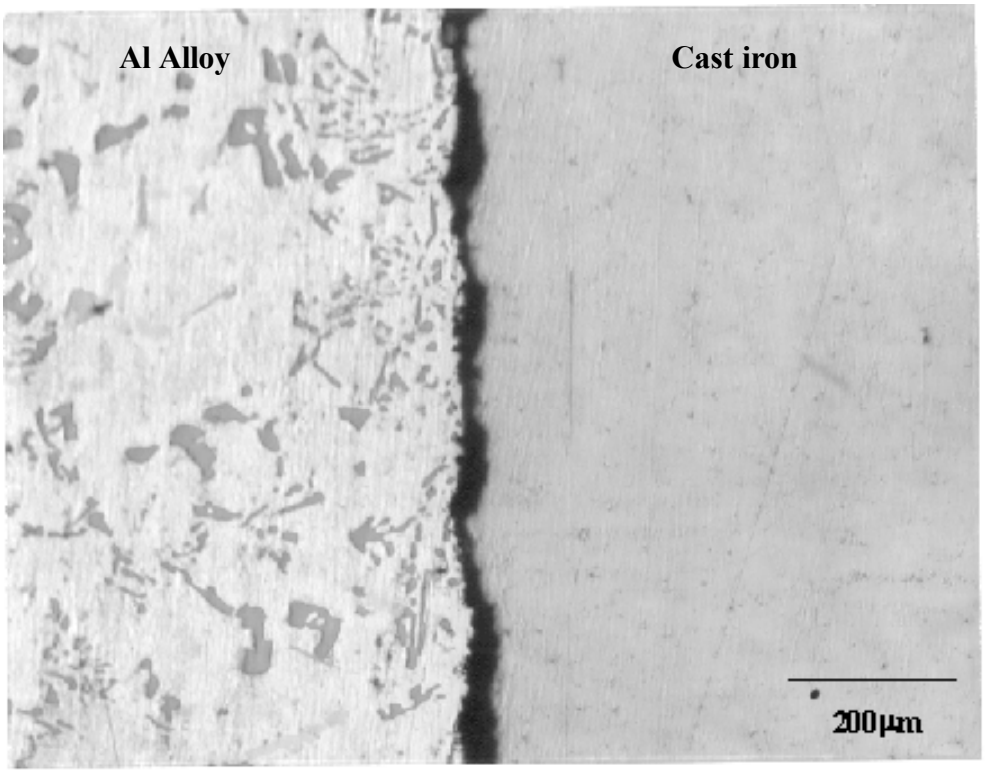


Figure 22: Interface of A354 aluminum cast alloy and cast iron with carbo nitriding

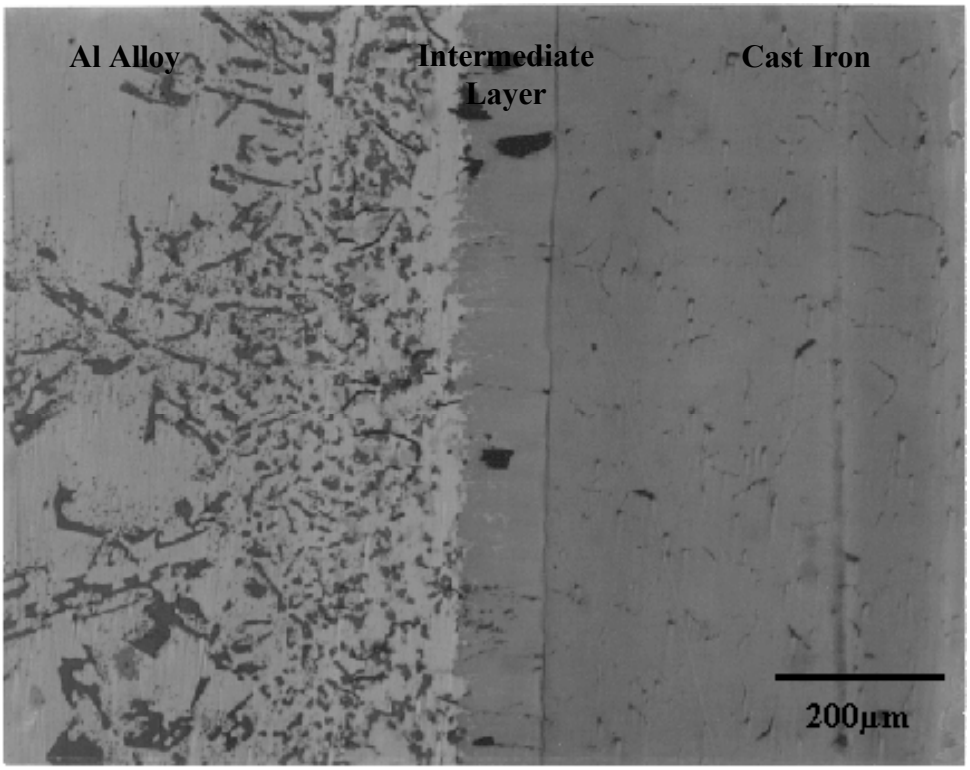


Figure 23(a) Interface of A354 Al alloy and cast iron after aluminizing

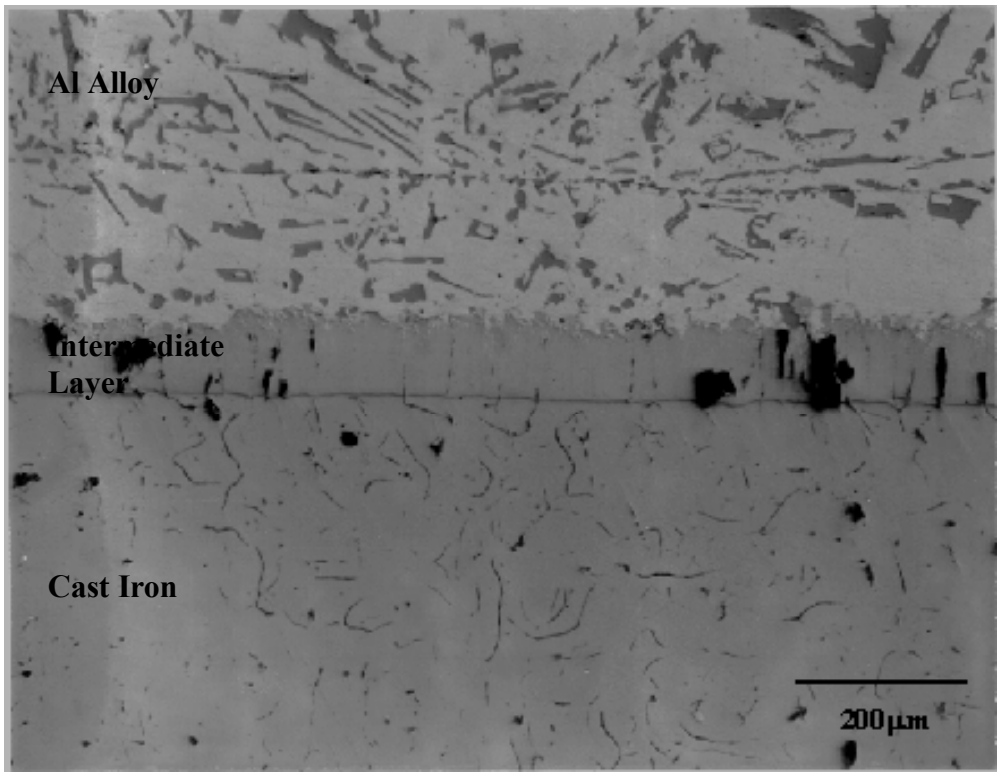


Figure 23(b) Interface of A354 Al alloy and cast iron with electroplated Cu Coating

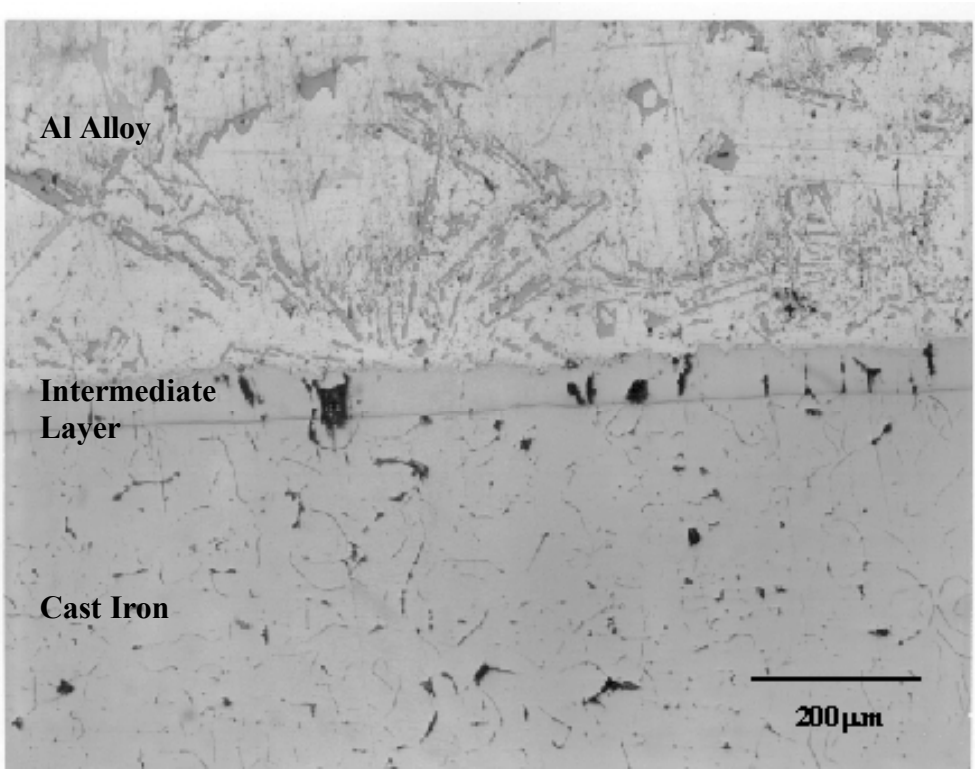


Figure 23(c): Interface of A354 Al alloy and cast iron with electroplated Cu/Ni Coating

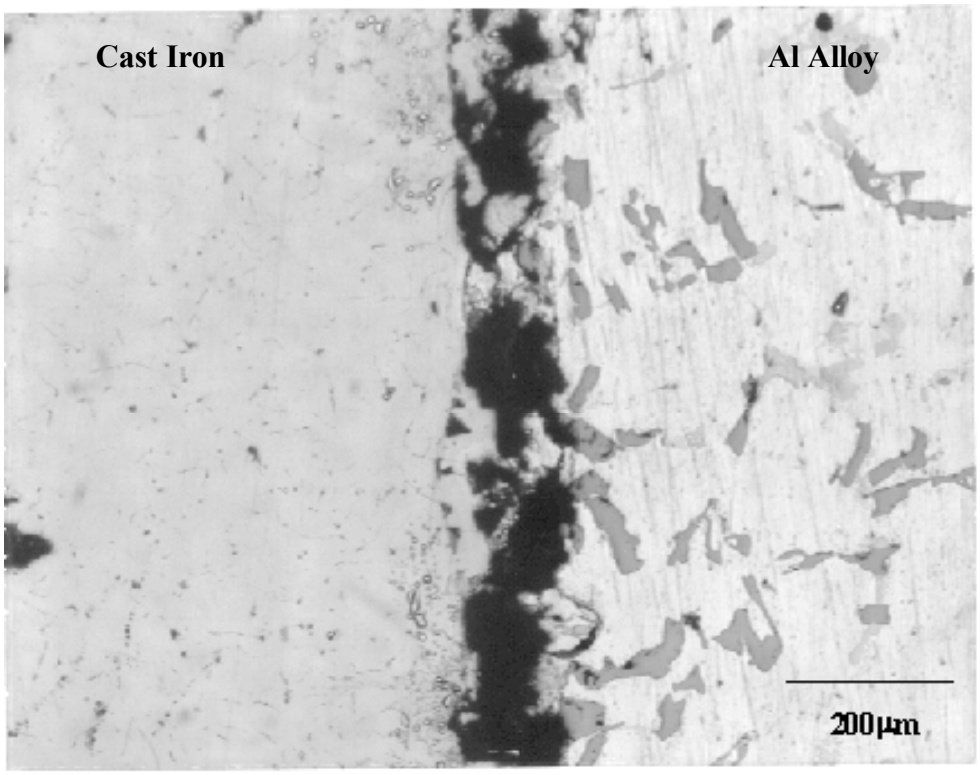


Figure 23(d): Interface of A354 Al alloy and cast iron with electroplated Ni/Cr Coating

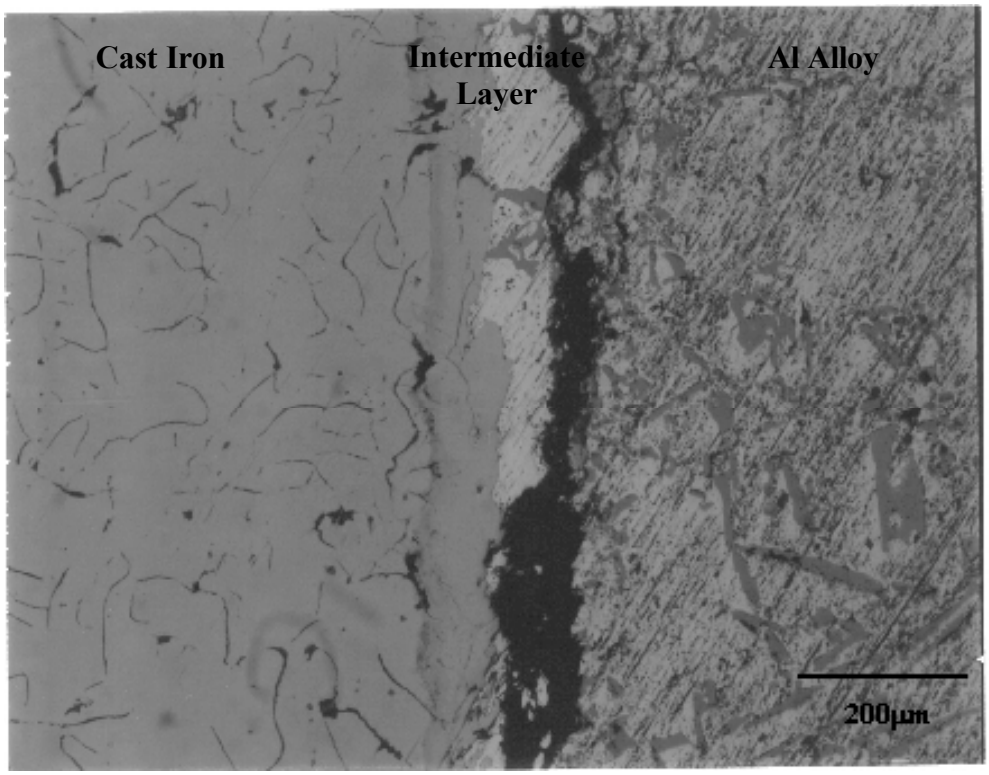


Figure 23(e) Interface of A354 Al alloy and cast iron with electroplated Zn Coating

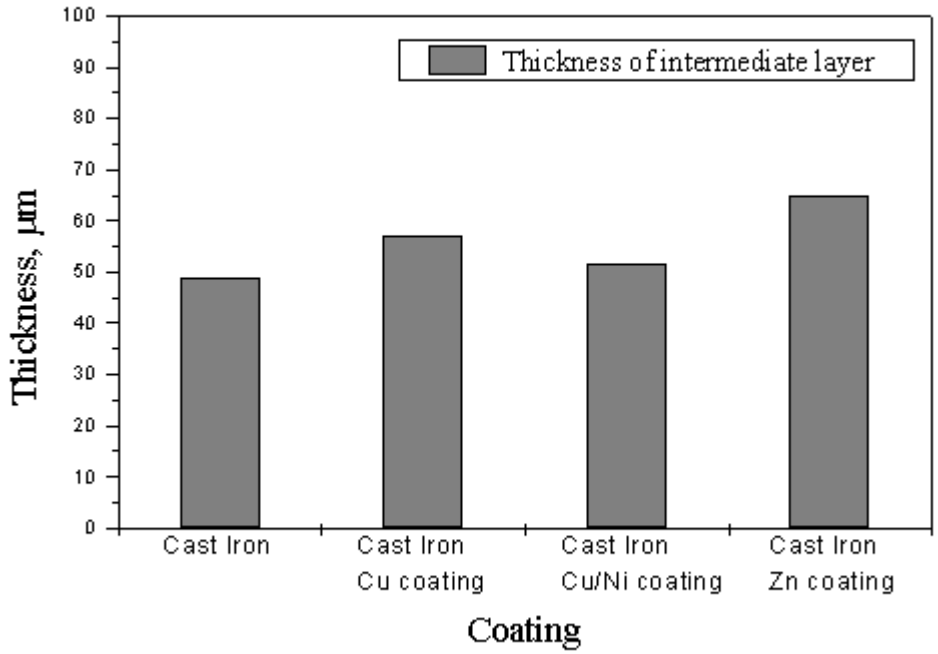


Figure 24 The thickness of intermediate layer of aluminum alloy and cast iron interface

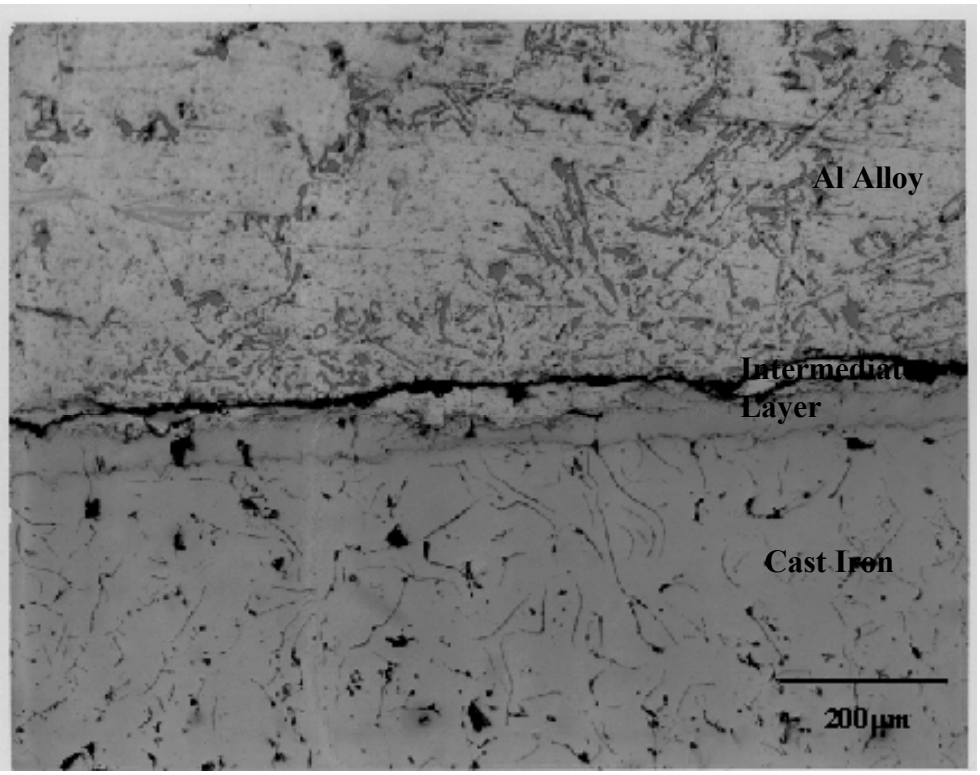


Figure 25(a): Interface between A354 Al alloy and cast iron after Kolene process with Cu coating

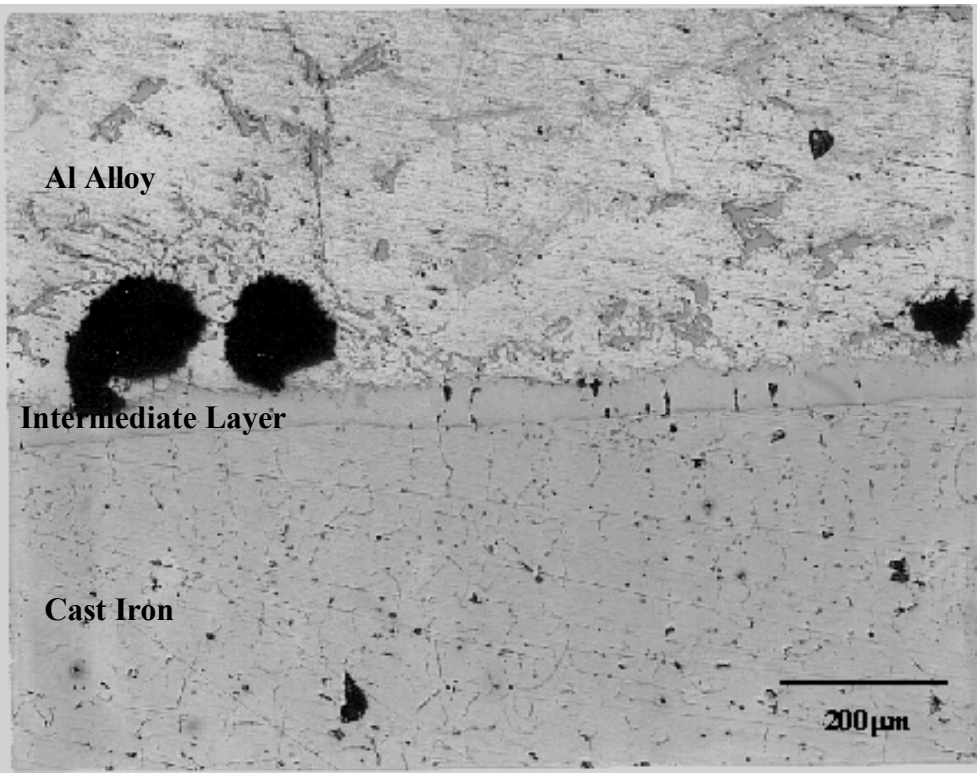


Figure 25(b): Interface between A354 Al alloy and cast iron after Kolene process with Cu/Ni coating

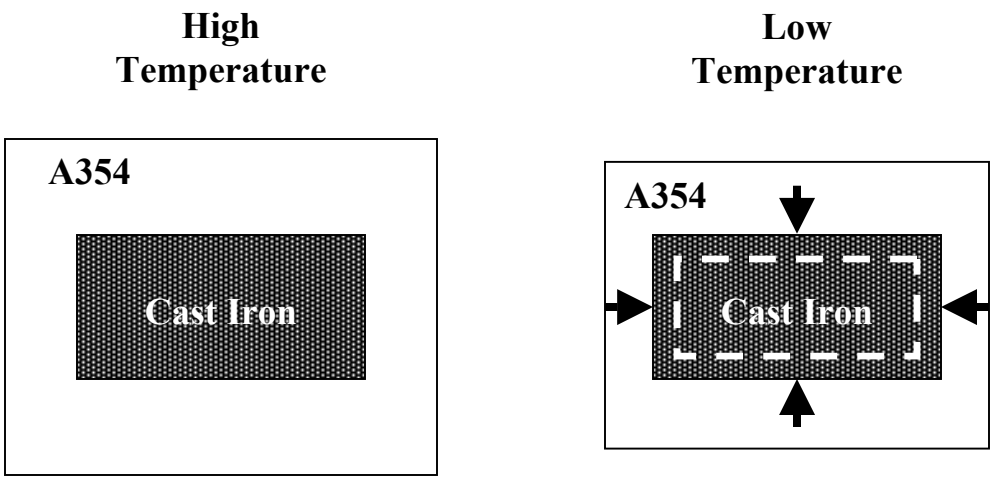


Figure 26(a): Cast iron insert utilized in the aluminum casting

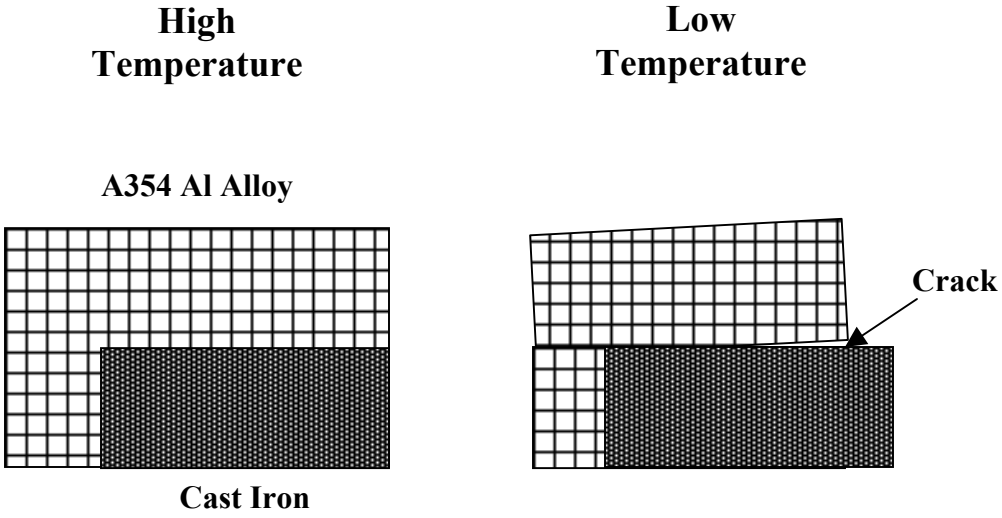


Figure 26(b): Degrading of the interface by different thermal contraction of A354 Al alloy and cast iron insert

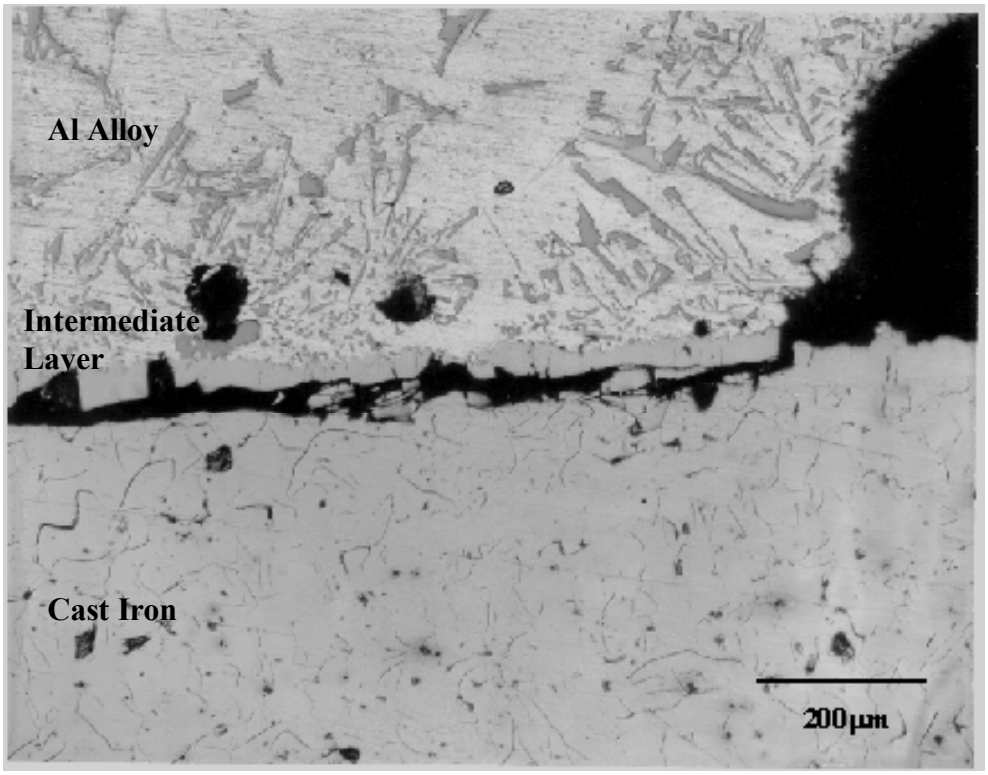


Figure 27(a): Crack in the intermediate layer

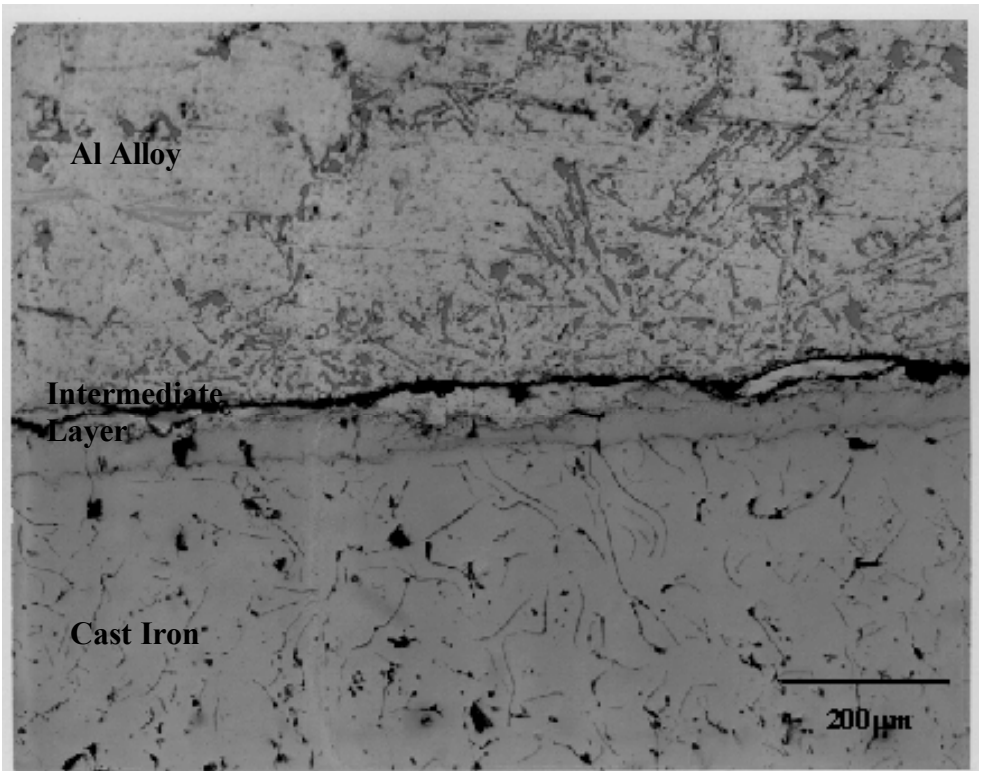


Figure 27(b): Crack in the Al alloy

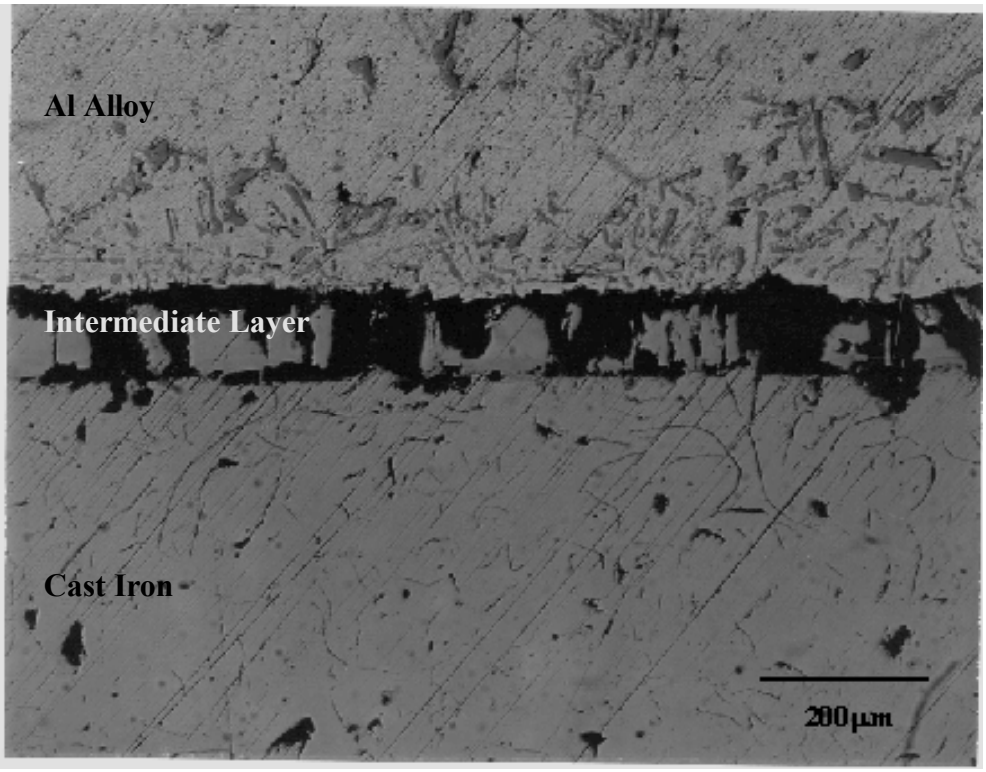


Figure 28(a): Interface between A354 and cast iron with Cu/Ni coating after heat treatment

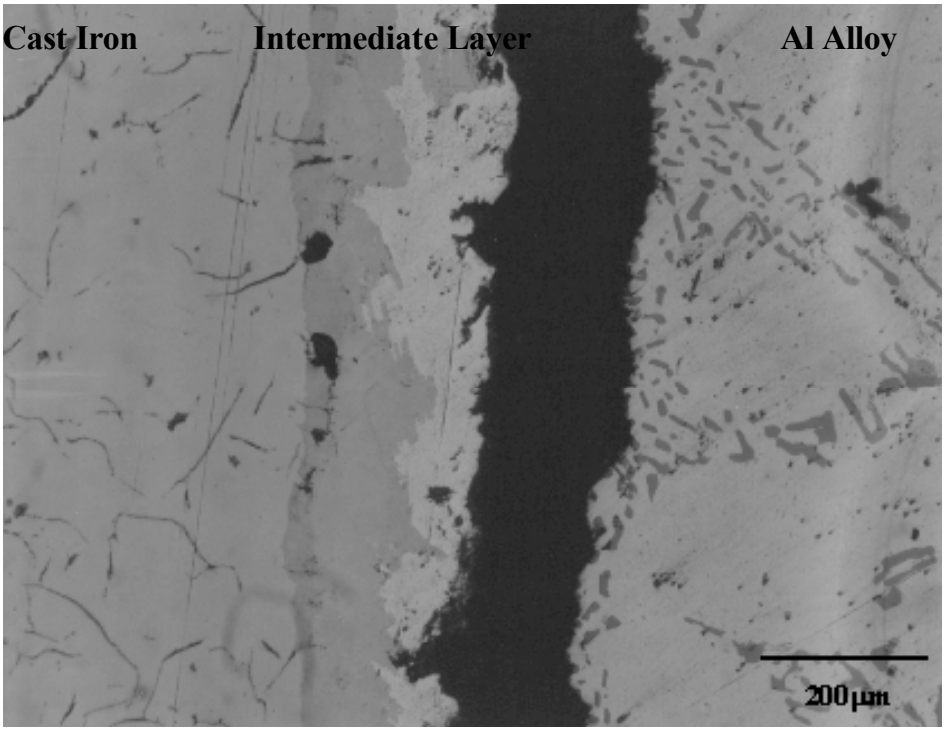


Figure 28(b): Interface between A354 and cast iron with Zn coating after heat treatment

3.3 Analysis of Ni-Resist Inserts in the Aluminum Casting

3.3.1 Metallurgical Analysis of Interface

Figures 29 and 30 show the interface between the A354 aluminum cast alloy and a Ni-resist insert. The structure of this interface is similar to that observed for cast iron inserts. However the graphite of the Ni-resist remains at the interface with the aluminum alloy after casting. The thermal expansion coefficient of the Ni-resist is close to the A354 aluminum alloy.

3.3.2 Effect of Heat Treatment on Bonding Strength

The bonding strength of A354 alloy to Ni-Resist is affected by heat treatment. Figure 31(a) is the small casting with Ni-resist insert and Figure 31(b) shows some shear test specimens and how the shear test specimens were made. The shear test results are listed in Table 9. The average shear strength of the bond in the as cast and T5 heat-treated specimens shows better results than the T6 heat-treated specimens. The scatter in these results is wide, indicating the variation in the properties of the bond. These results suggest the diffusion of elements and subsequent chemical reactions occurring during the T6 heat treatment degrades the strength of the bond between A354 and Ni-Resist. The T5 heat treatment somewhat improves bonding and reduces residual stresses.

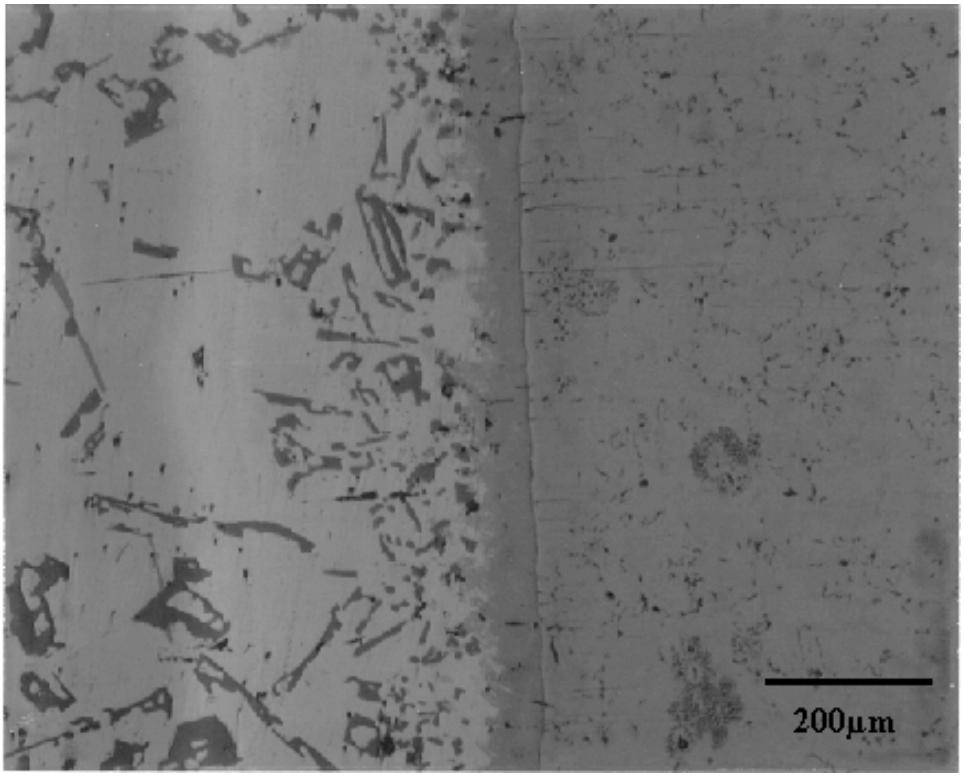


Figure 29: The interface between A354 Al alloy and Ni-Resist insert

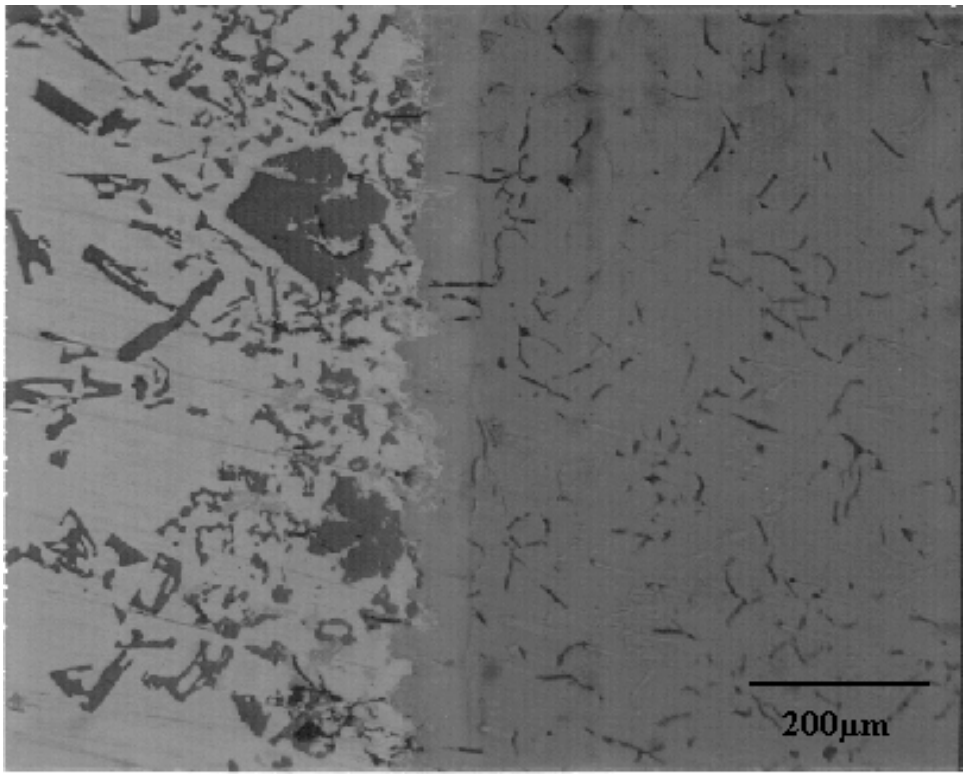


Figure 30: The interface between A354 Al alloy and Ni-Resist insert with Al coating

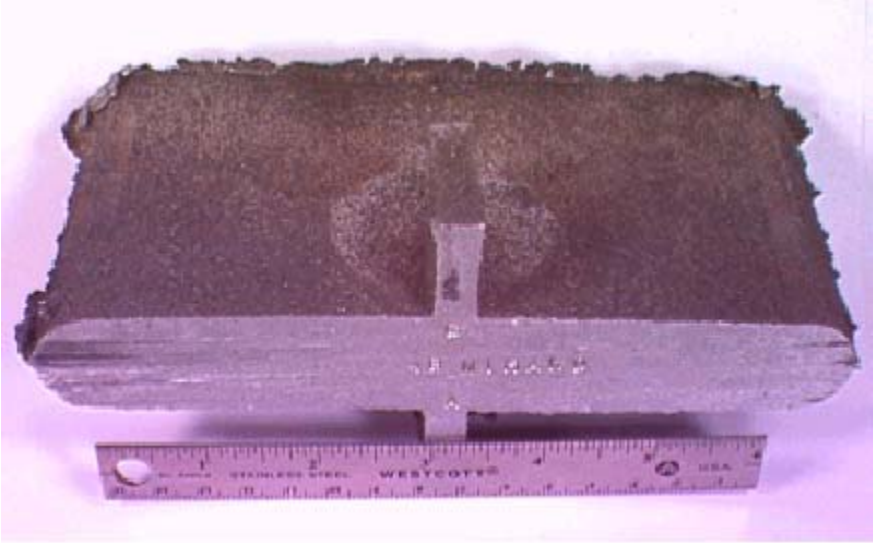


Figure 31(a): Small casting with Ni-resist insert

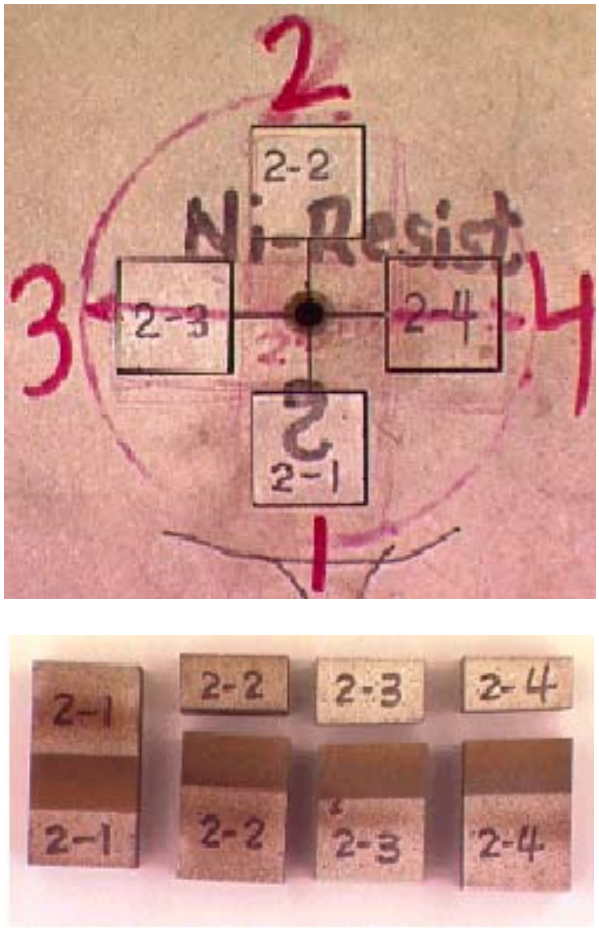


Figure 31(b) Shear test specimens

Table 9 Shear Test Results of Ni-Resist Insert in the Small Casting [Note the large scatter]

Heat Treatment.	Specimen No.	Thickness In	Width In	Area In^2	Peak Load Lbf	Peak Stress ksi
As cast	1	0.5	0.5	0.25	643.787	2.5
	2				378.573	1.5
	3				613.554	2.4
	4				814.242	3.2
	Average				612.539	**2.4**
T6	1	0.5	0.5	0.25	272.633	1.1
	2				92.366	0.4
	3				911.865	3.6
	4				446.757	1.8
	5				676.715	2.7
	Average				480.067	**1.92**
T5	1	0.5	0.5	0.25	953.447	3.8
	2				167.968	0.7
	3				584.375	2.3
	4				221.615	0.9
	5				997.958	4.0
	6				411.995	1.6
	7				657.661	2.6
	Average				570.717	**2.27**

3.4 Analysis of Mesh Reinforced Aluminum Castings

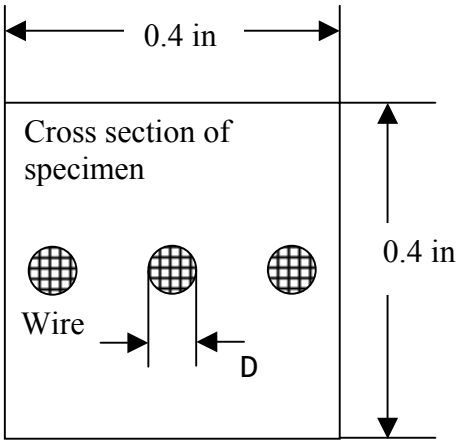
3.4.1 Metallurgical Analysis of Interface

Figure 32 (a) and (b) show optical micrographs of the cross section of zinc-coated stainless steel wire. The intermediate layer between the stainless steel wire and aluminum alloy has a thickness of 20μm. Some cold-shut defects are present near the wire. Bonding between the stainless steel wire and intermediate layer is good but poor bonding occurs between the aluminum alloy and intermediate layer. Figure 33(a) and (b) are SEM micrographs of the intermediate layer between the stainless steel wire and A354 aluminum cast alloy and EDS result of the intermediate layer. The intermediate layer is an Fe-Si-Al intermetallic compound with Cr and Ni from the stainless steel wire. Figures 34(a) and (b) illustrate the structure of the stainless steel wire with and without a Zn coating after heat treatment. Heat treatment degrades the interfacial bonding between stainless steel and A354 alloy because of the diffusion and subsequent chemical reactions.

3.4.2 Results of Charpy Impact Test

Figure 35 shows the Charpy V-notch impact energy of A354 aluminum cast alloy and a galvanized steel wire mesh reinforced aluminum alloy. These results indicate that the lower fracture strength galvanized steel wire mesh do not improve the toughness of aluminum casting. Because the ductile-brittle transition temperature of steel occurs at higher than room temperature, the steel wire fails in a brittle manner.

Data on stainless steel meshes with Zn coating and the impact test results are listed in Table 10. The mesh count is the number of squares per square inch. As mesh count is increased, the wire diameter of mesh is decreased and the number of wires in the cross section of the impact specimen is increased. Generally, as the mesh count is increased, the area fraction of wire is decreased (Fig. 36). Figure 37 shows impact test results with varying mesh count. A354 aluminum alloy reinforced by 14X14 mesh exhibits the best results. Figure 38 demonstrates how the impact test results vary with the area fraction of the wire. Generally, as area fraction of wire is increased, the impact strength also is increased. Consequently, the 14x14 mesh wire has the highest fracture energy in Figure 38.



$$\text{Area Fraction } A_f = \frac{(Number\ of\ wire) \times \pi (D/2)^2}{0.4 \times 0.4}$$

Impact test results with multiple mesh layers, coatings and heat treatment are listed in Table 11. Figure 39 shows improvement in toughness of casting reinforced by two mesh layers. As the number of mesh layer increases the toughness of the casting should increase. The lower toughness of the casting reinforced with a Zn coated stainless steel wire mesh can be explained by poor aluminum casting quality.

Since the interface properties affect the toughness of reinforced materials, toughness of reinforced aluminum casting should vary with heat treatment. Figure 40

illustrates the effect of heat treatment on impact test result. These results are the average of five tests with minimum scatter. Overall, heat treatment improves the toughness of mesh-reinforced aluminum castings. Toughening can be achieved by improving the toughness of the aluminum alloy and the bonding strength of the interface. Optimized interface bonding strength improves the toughness of reinforced materials. However, since the interface between aluminum and stainless steel is degraded by heat treatment (Fig.34), the improvement of toughness is mainly due to that of aluminum casting itself.

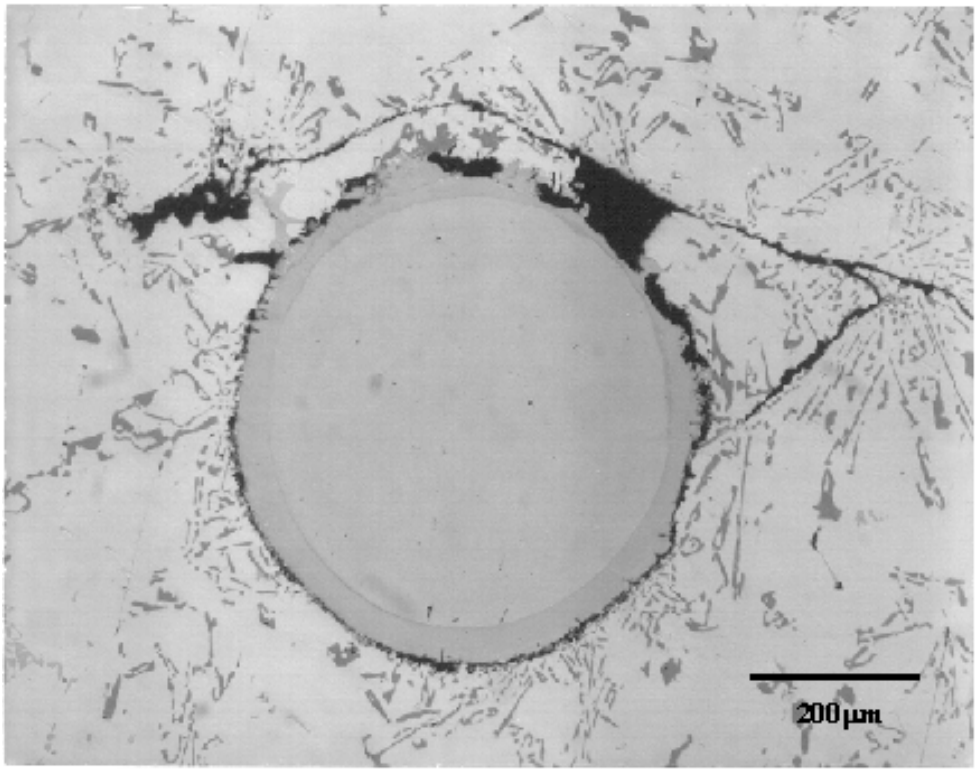


Figure 32(a): Optical microscope picture of stainless steel wire

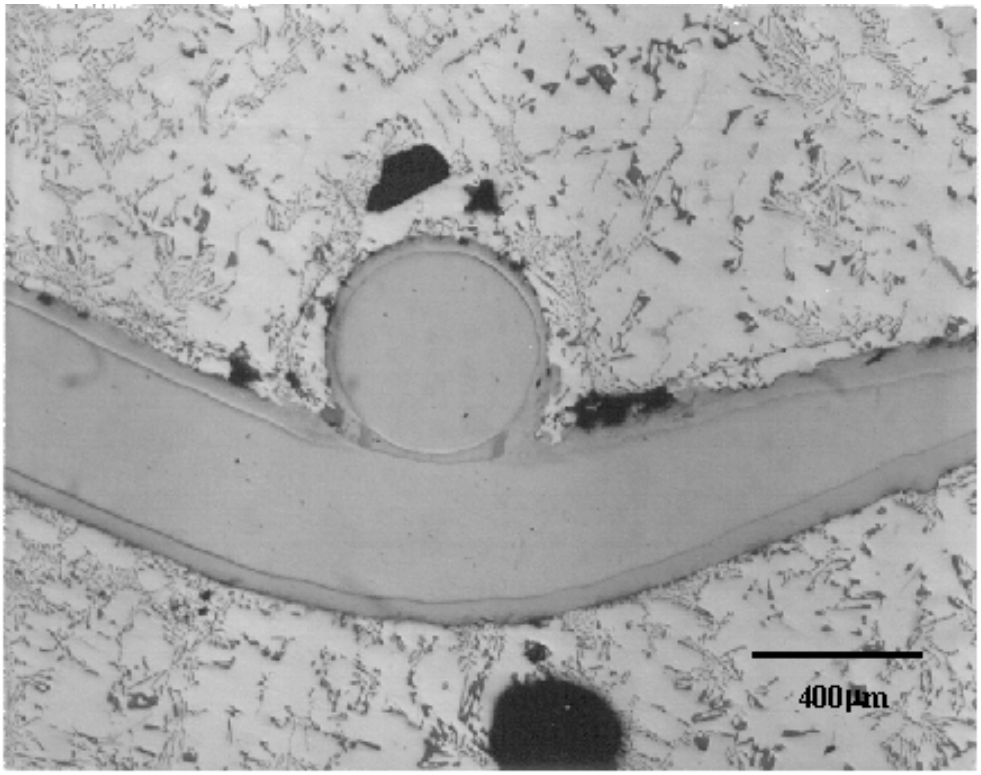


Figure 32(b): Optical microscope picture of stainless steel wire mesh

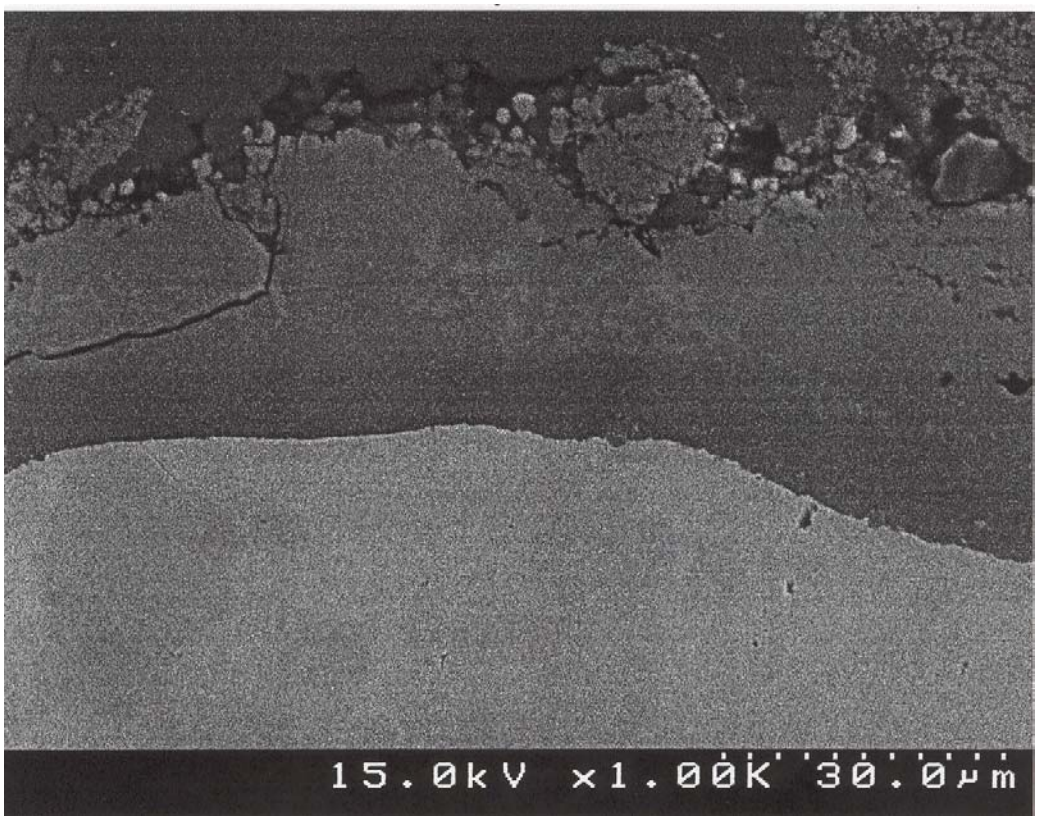


Figure 33(a): SEM micrograph of intermediate layer

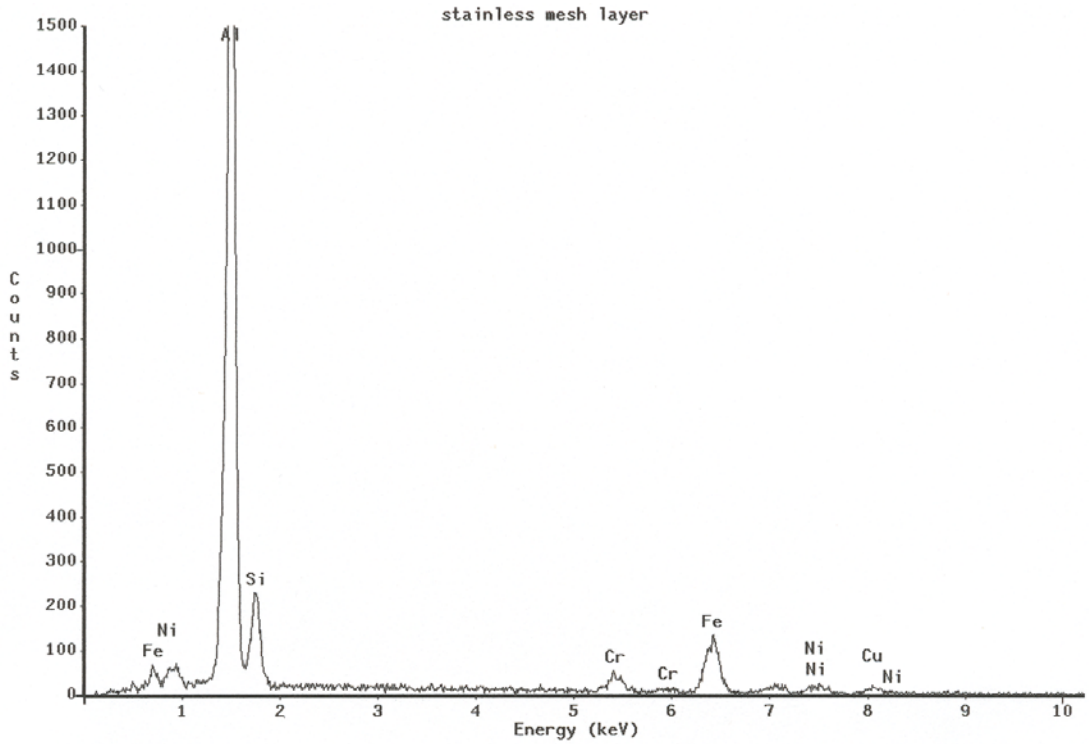


Figure 33(b:) EDS result of the intermediate layer

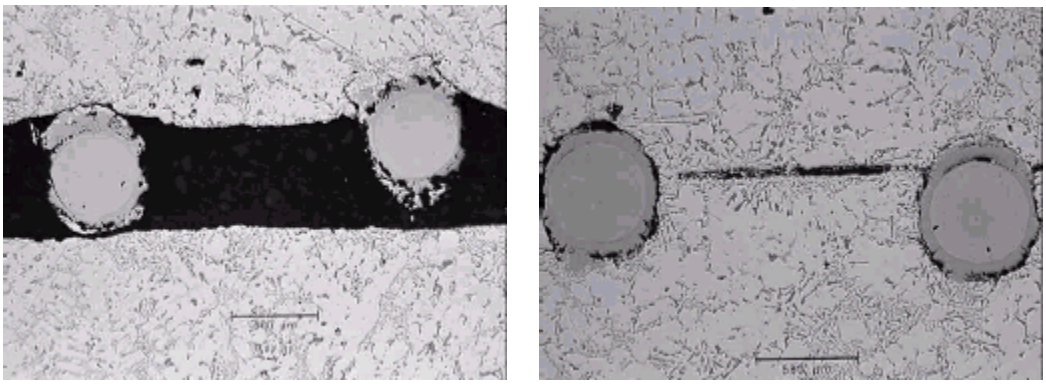


Figure 34(a:) Stainless wire with Zn coating after heat treatment

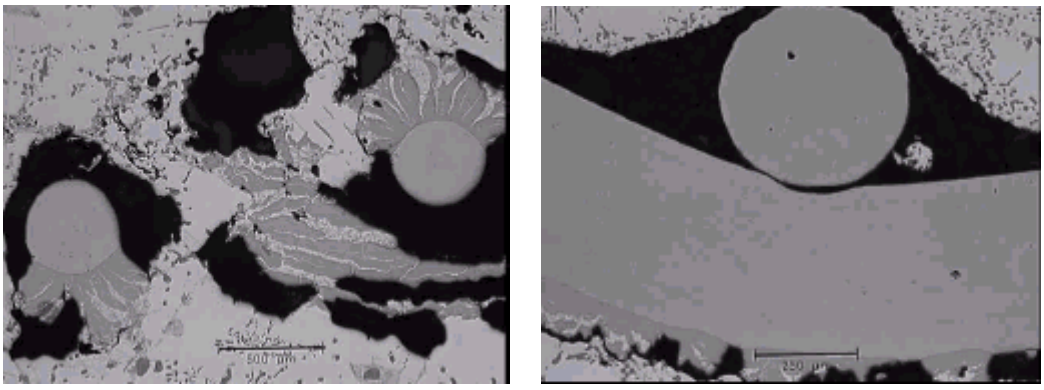


Figure 34(b:) Stainless steel wire without coating after heat treatment

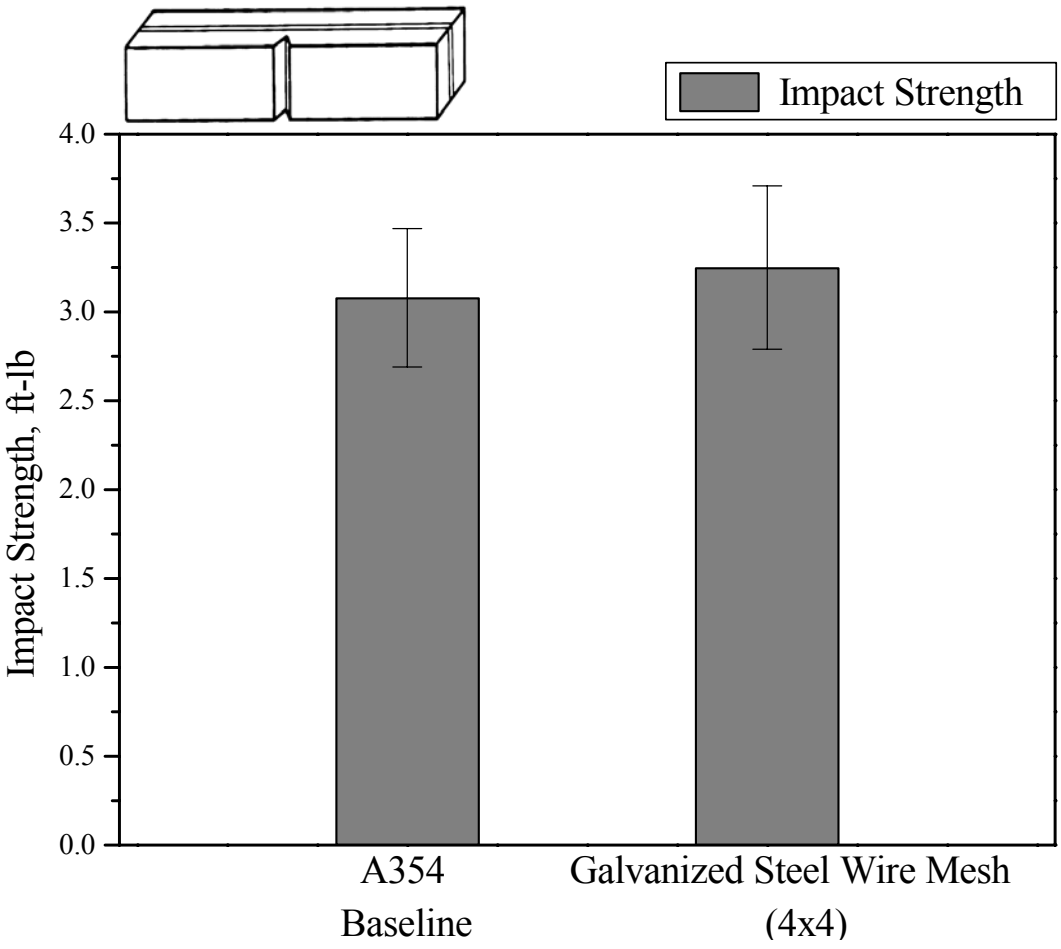


Figure 35: Impact Energy of A354 Aluminum alloy and casting reinforced by galvanized steel wire mesh

Table 10 Data on Meshes and Impact Energy

Mesh Count [No. of Sq./in^2]	Wire Diameter [in]	No of Wire per 0.16 in^2	Area Fraction of Wire	Impact Energy [ft-lb]
0x0	0	0	0	3.08
4x4	0.047	1.6	0.017349	
5x5	0.041	2	0.016503	
6x6	0.035	2.4	0.014432	
10x10	0.025	4	0.012272	4.83
12x12	0.023	4.8	0.012464	5
14x14	0.02	5.6	0.010996	5.4
16x16	0.018	6.4	0.010179	4.6
18x18	0.017	7.2	0.010214	4.67
20x20	0.016	8	0.010053	4
24x24	0.014	9.6	0.009236	4.17
30x30	0.01	12	0.00589	3.4

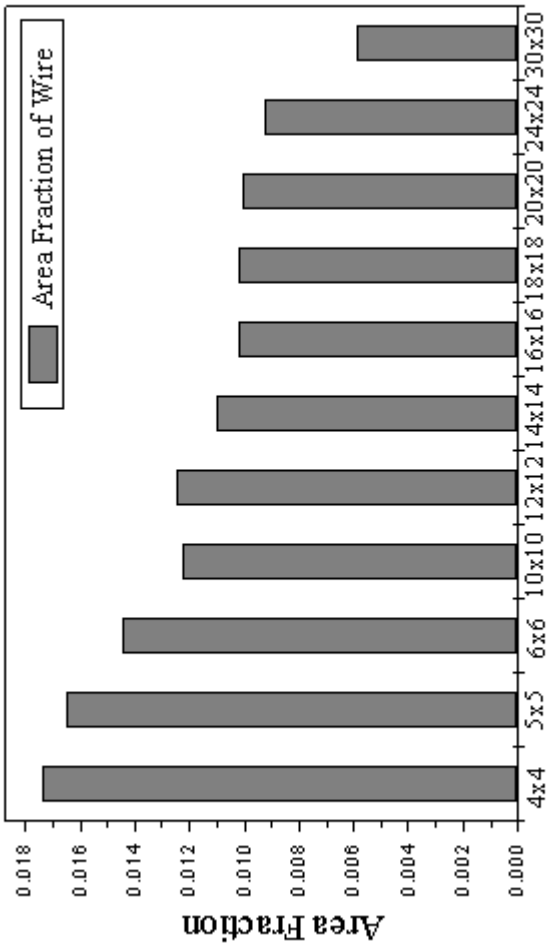


Figure 36 Area fraction with varying mesh count

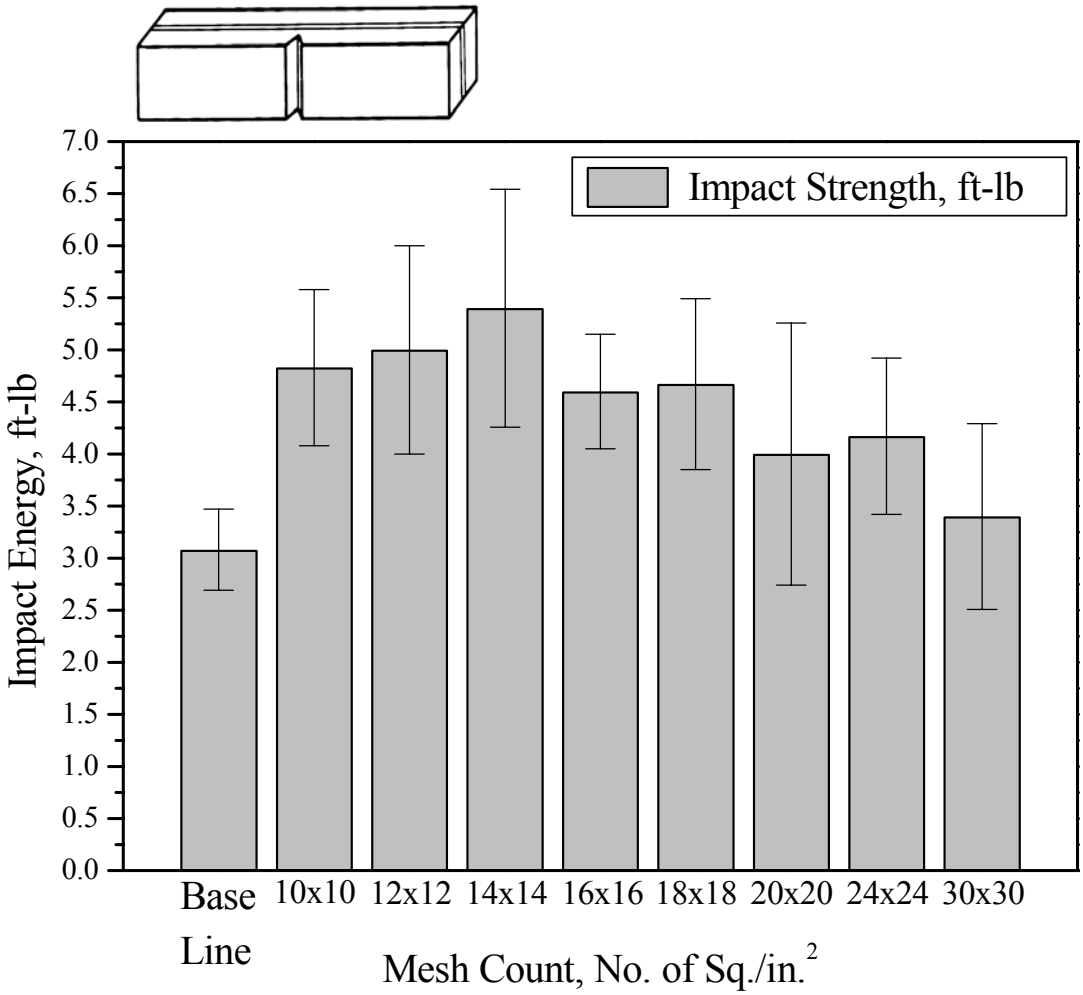


Figure 37: Impact energy with varying mesh count

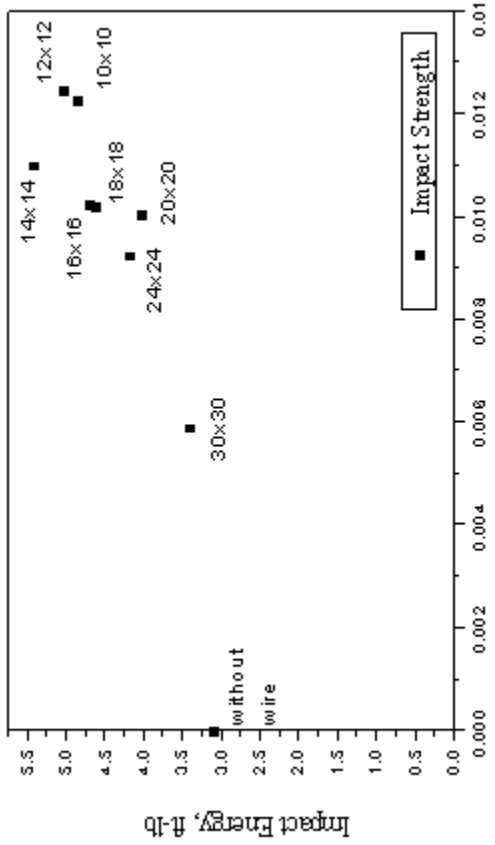


Figure 38 Effect of area fraction of wire on Impact Energy

Table 11 Impact Test Results

Number of Layer	Coating	Heat Treatment	Impact Strength Ft-lb	Standard Deviation
1	No	As-cast	3.25	0.68
1	No	T6	2.73	0.35
1	Zn	As-cast	3.62	0.61
1	Zn	T6	3.91	0.54
2	No	As-cast	4.14	0.62
2	No	T6	5.70	1.10
2	Zn	As-cast	3.25	0.63
2	Zn	T6	5.50	0.40

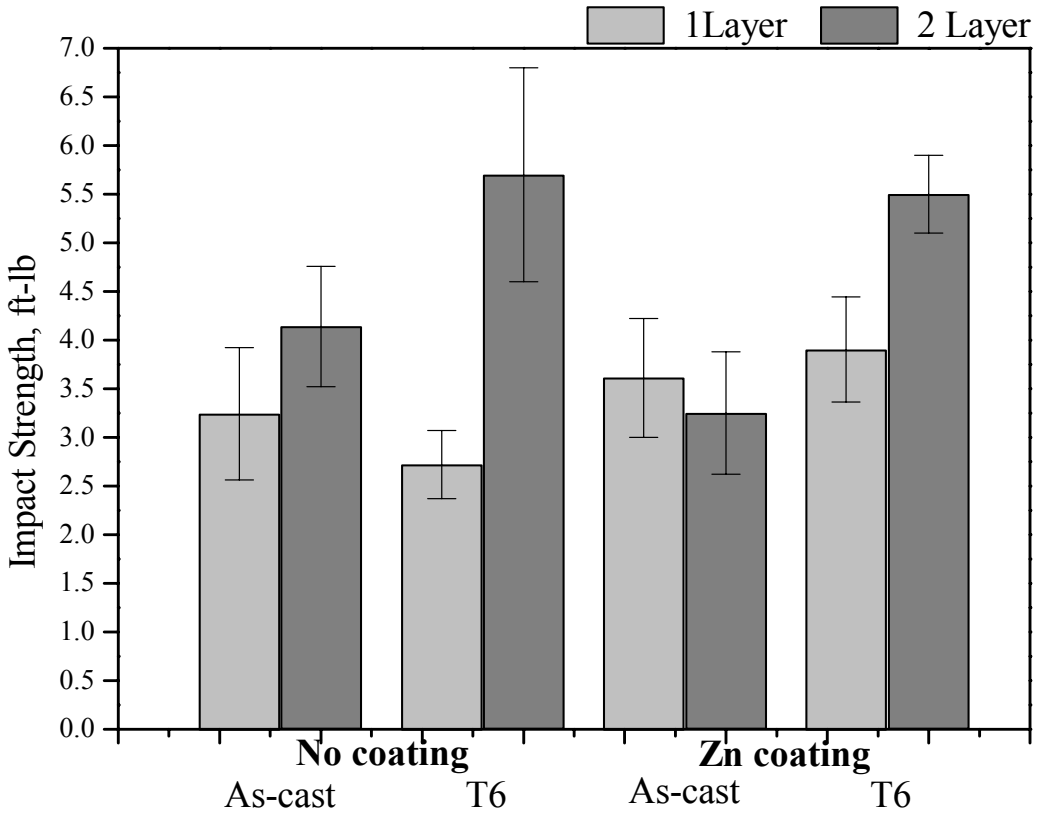


Figure 39: Effect of number of layer

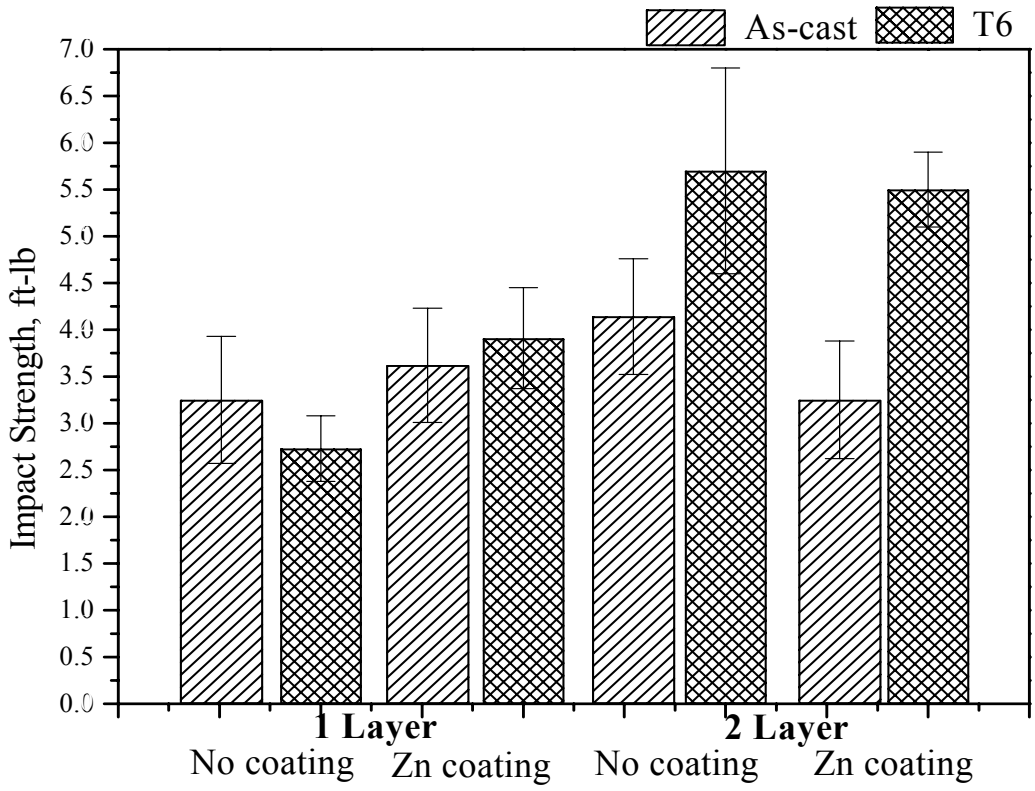


Figure 40: Effect of Heat Treatment

4.0 CONCLUSIONS

- Aluminum bronze inserts
    - Aluminum bronze inserts dissolved severely in A354 aluminum cast alloy.
    - None of electroplated coating could protect aluminum bronze inserts from dissolving.

- Ferrous metal inserts
    - A Fe-Si-Al intermetallic compound layer forms between ferrous inserts and the Al-Si alloy. This intermetallic compound layer decreases ductility and increases crack-sensitivity of the bond.
    - None of electroplated coating could avoid the formation and growth of the intermetallic compound layer.
    - Because the thermal expansion coefficient of Ni-resist is similar to that of A354 Al alloy, the interface of Ni-resist and A354 shows better bonding than the interface of cast iron and A354.
    - The difference in the thermal expansion coefficients between the reinforcements and the aluminum alloy matrix cause degradation of the bond during heat treatment .

- Wire mesh reinforced castings
    - The toughness of mesh- reinforced casting can be improved by optimizing the interfacial bonding strength.
    - A higher area fraction of stainless steel wire improves toughness.

PART 2: REINFORCEMENT OF SQUEEZE CAST ALUMINUM

5. 1 PROCEDURE AND EXPERIMENTS

A practical approach to reinforcement of die cast aluminum components is to use a reinforcing steel preform. Such performs can be fabricated from steel wire mesh or perforated metal sheet by stamping or deep drawing. A hemispherical, dome shaped casting was selected in this investigation. A deep drawing die was used to fabricate the reinforcing performs. The dimensions of the dies that were used to produce the 6 inches diameter hemispherical casting are shown in Figures 41 A and B. This shape was cast in 356 aluminum that was injected into the die as shown in Figure 42. These castings were all tested in the as cast condition without heat treatment. The squeeze casting was performed under two pressures at 7,600 psi and 17,000 psi, both with and without reinforcement. The appearances of the three types of reinforcement used in this investigation are shown in Figures 43 A and B. These steel meshes were formed into a dome shape to fit within the aluminum casting. Figure 44 illustrates the shape of these steels performs as they were prepared. The stainless steel wire mesh could be formed to the dome shape without any annealing process whereas some of the punched stainless steel sheets had to be annealed before deformed to the final shape or else the wires would break. The 1020 low carbon steel had to be annealed in all cases to avoid fracture during its deformation.

The reinforcement of the castings was accomplished by using either a 304 stainless steel wire mesh with a 0.075 inch diameter, a 1020 ferritic steel wire mesh with a 0.094 inch diameter or a 304 stainless steel punched sheet. Both the stainless steel and the 1020 ferritic steel wire mesh were made with 4 wires by 4 wires per inch square. The punched stainless steel sheet has a thickness of 0.055inch and 0.15inch diameter of punched holes with a connection space of 0.032 inch. The relative weights of the punched 304 stainless steel sheet, wire mesh of 304 stainless steel and 1020 unalloyed steels are shown in Figure 45. The different weights of materials influenced the weight of the casting as shown in Figure 46. The parts were radiographically examined before testing as shown in Figure 47. This method was used to determine the soundness of the casting both with and without the reinforcing steel.

The dome castings were then tested with internal water pressure in a special device shown in Figure 48 to determine their internal pressure tightness. The pressure testing rig includes an "O" ring, clamps and bolts that clamp the flange of the hemispherical casting to a steel plate during application of the internal water pressure. As shown in Figure 8, five of the reinforcing bolts around the outside diameter are missing. These bolts are installed when the actual tests are taken. The sketch at the left shows the 12 holes used for holding the rim of the hemisphere in place. A significant load was needed to fracture these castings through this area as shown in Figure 49 for non-reinforced and reinforced castings. This type of testing was not employed for the parts made with annealed unalloyed steel mesh and punched stainless steel sheet.

Numerous castings of each type were tested by holding these castings in a large Instron testing machine with a matching hemispherical rim and head that fitted inside of the hemisphere. Figure 50 shows the equipment, and parts used in this testing. These tests were conducted by mechanical loading of the hemisphere so that the testing and fracture of the material could be monitored and recorded with a computerized data acquisition system. This set-up is shown in Figure 50, with the actual machine shown on the right side. The left hand top figure shows the set up in the machine and the die and hemispheric head are shown at the bottom left.

Some work was also conducted to test the impact resistance of 354 aluminum casting. This work involved various meshes of stainless steel from small to large including a 0.25" diameter stainless steel bar inside of the bar with the dimension shown in Figure 51.

5.2 RESULTS AND DISCUSSION

The results of the internal pressure testing indicated that sound castings fractured under a internal pressure of about 700-800psi whether they were reinforced or un-reinforced. Once this fracture started, the water leaked out and the test was terminated. Hemispheres of 356 aluminum with internal ferritic wire and punched stainless steel sheet were not used in this internal pressure testing. This test measures the strength of the

material in its ability to withstand internal liquid pressure rather than testing the ability of the castings to absorb impact and contain flying objects inside the casting as required from an enclosure.

Applying a load with a hemispherical plunger head inside of the casting provided a more realistic test of the ability of the casting to resist applied forces without completely fracturing. This behavior is more significant for utilization in service. It became apparent that the fracture of the part with the wire mesh and with a punched stainless steel material required either a higher fracture energy or a higher fracture load. The relative load maxima shown in Figures 52 and 53 show the effect of the reinforcement. Figure 52 shows the load at lower pressure of 7,600 psi. It is noted that the area under the load-displacement curve of the reinforced castings is significantly higher than that the area under the nonreinforced casting. A similar behavior is noted in Figure 53 where the material has been produced with a higher pressure at 17,000 psi. In this case, a higher pressure was employed during squeeze casting. The best results were obtained with the reinforced stainless steel punched sheet The areas under the load-dispacement curve are shown in Figure 54 for the lower pressure (7,600 psi) and in Figure 55 for the average results at the higher pressure at 17,000 psi. It is noted that the higher strength and energy obtained with the increased pressure is apparent in these results.

The reason reinforced castings could withstand higher loads is illustrated in Figure 56. In the case of the reinforced castings even after a crack is initiated, significant deformation of

the reinforcement takes place before separation of the broken casting. The unreinforced castings usually break at the radius of the hemispherical edge. The broken parts of the casting could be readily separated. However, the stainless steel wire reinforced castings held together better and the parts remained attached. Some reinforcement effect was also provided by the austenitic stainless steel mesh. However, he relative strength of these parts before fracture was less than shown for the punched sheet. This behavior is illustrated in Figures 53 and 56 where the wire maintains the casting in one piece.

Utilizing meshes to reinforce the hemispherical dome provided the maximum area under the load-displacement curve as shown in Figures 54 and 55. In the case of Figure 55, the maximum fracture energy was higher for the stainless steel wire mesh reinforcement, followed by the hard punched stainless sheet. The non-reinforced materials and the soft punched stainless sheet were definitely inferior. The difference between the soft and hard punched stainless sheet arose from the processing of this material. Some of the punched stainless steel sheets fractured during forming into the dome shape. For this reason, some of these had to be annealed to obtain the final shape. It is apparent that the residual compressive stress in the stainless steel sheet tested before annealing increased the strength of these parts, as shown in Figures 53 and 55.

The stainless steel wire mesh reinforcement maintained the casting in one piece even after cracking was initiated, and the wire mesh stretched over a considerable period. This behavior was demonstrated in several tests. It is also apparent that the slope of the load

application is much steeper with the wire reinforcement. Even when the reinforced casting breaks, the wire reinforcement maintains the casting in one piece, making it an effective enclosure for confining parts that are moving inside. This arrangement will prevent internal components from escaping.

The greater fracture strength and impact resistance of the stainless steel reinforced material is also shown by means of the regular Charpy impact test which has been prepared with and without the use of wires for reinforcement. The test without the reinforcement in 354 alloy fractures at about 3-foot pounds, whereas the presence of a large diameter wire of 0.250 inch diameter greatly increases the impact strength to 120 foot pounds for each unit as shown by the attached Figure 57.

5.3 CONLUSIONS

1. Aluminum castings were reinforced with hard stainless steel punched sheet or wire mesh of 0.075 inch 304 stainless steel with a high hardness and a 4 x 4 mesh per square inch. The mesh wire reinforced castings are superior in maintaining the integrity of the casting after fracture initiation relative to un-reinforced castings.

2. The reinforcement with soft stainless steel punched sheet produced a smaller increase in strength.

3. When casting with an austenitic stainless steel mesh reinforcement fracture, the broken parts of the casting still remain together. The reinforcement provides a definite resistance to the escape of any parts that are loose or flying apart inside of the casting.

Figure 41a: Ejector insert for metal reinforced aluminum dome casting

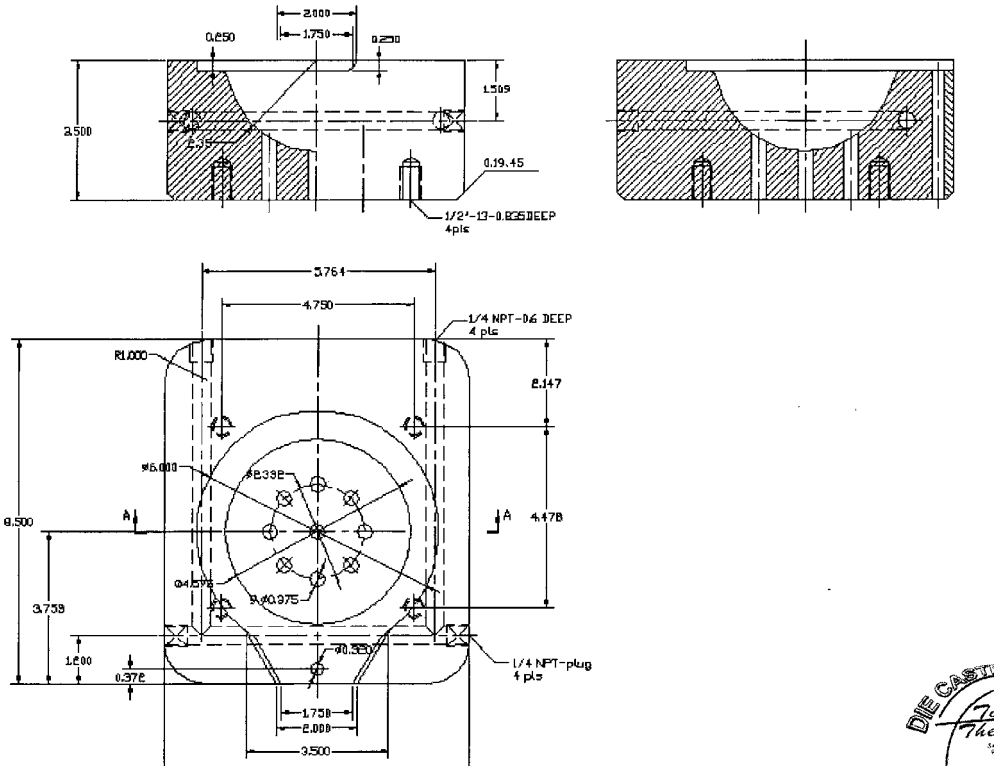


Figure 41b: Cover insert for metal reinforced aluminum dome casting

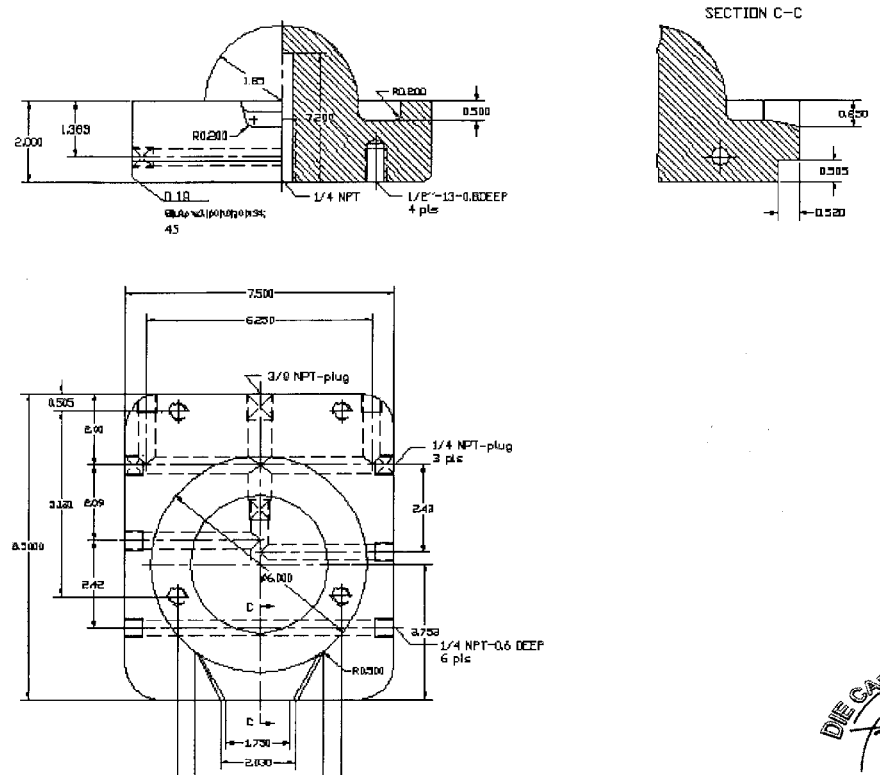
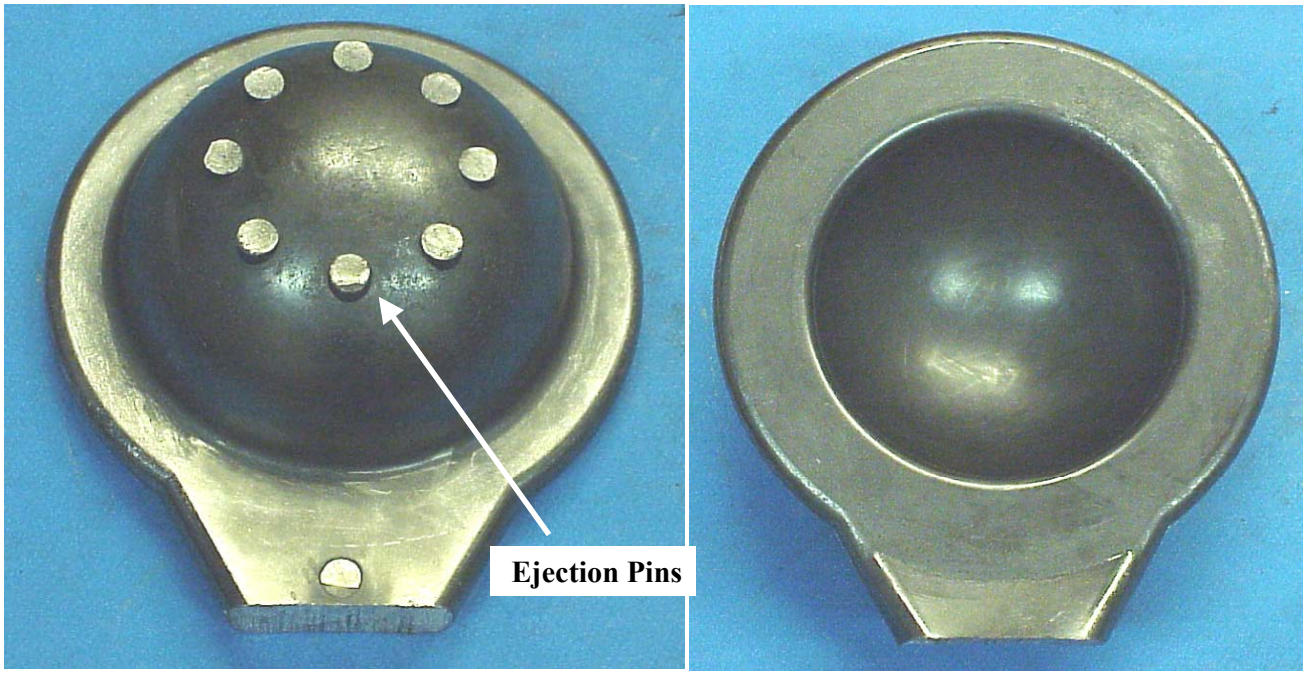
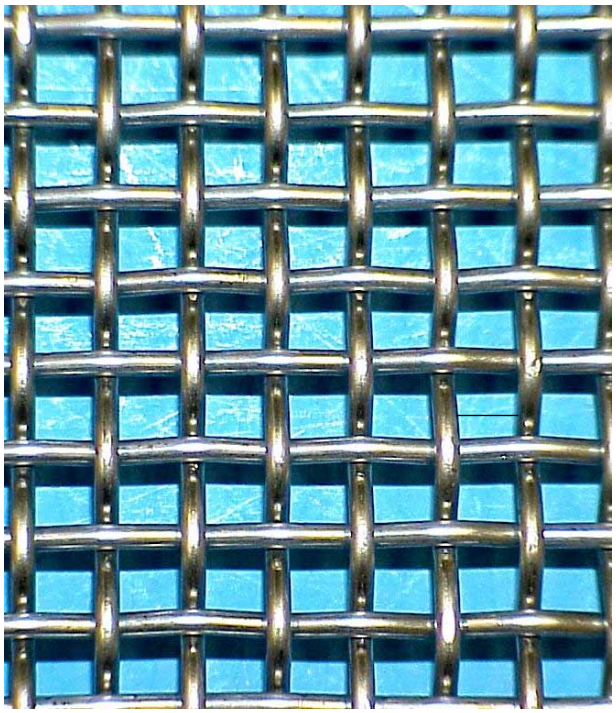


Figure 42: Design of 6” diameter hemispheric casting

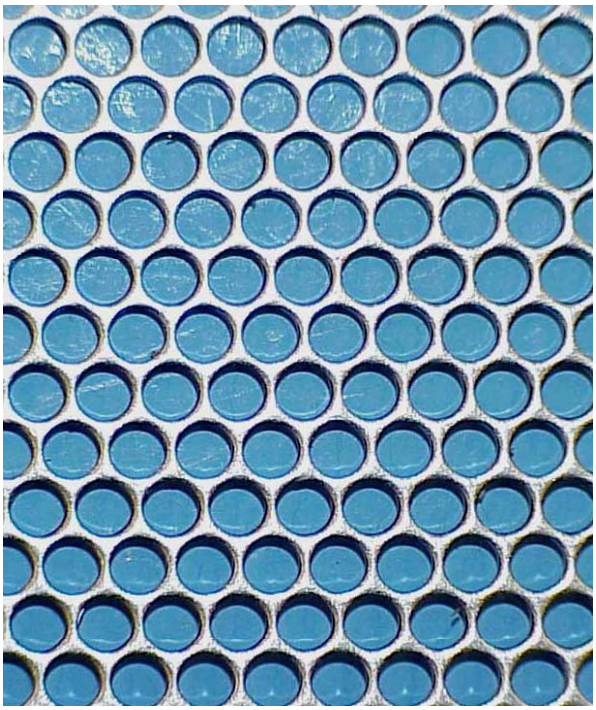


(a) Top View with the Ejection Pin **(b) Bottom View**

Figure 43a: AISI 304 Stainless wire mesh and punched sheet

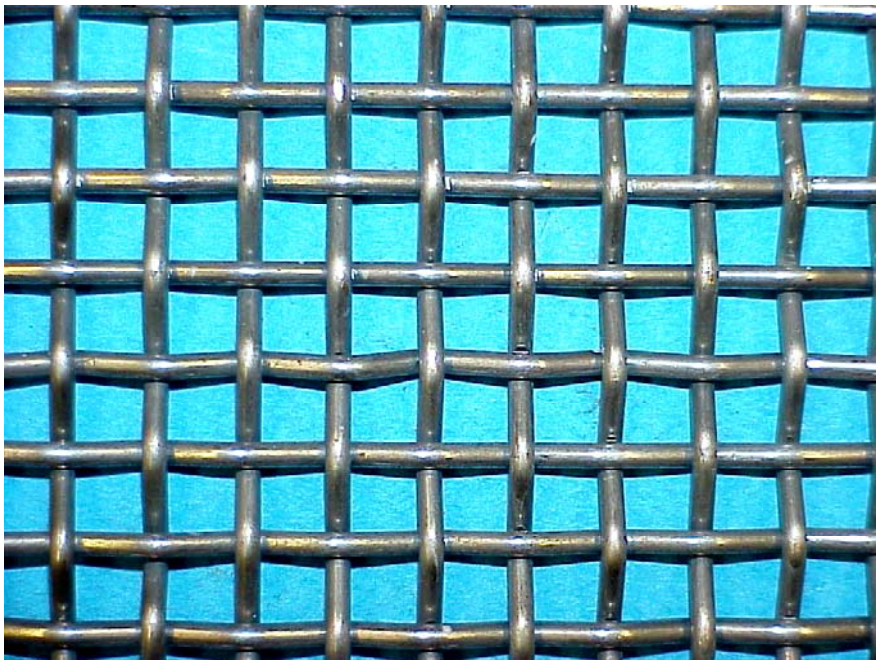


The wires are a 4 X 4 Mesh Per Square Inch With a 0.075 in. Diameter of the Wire



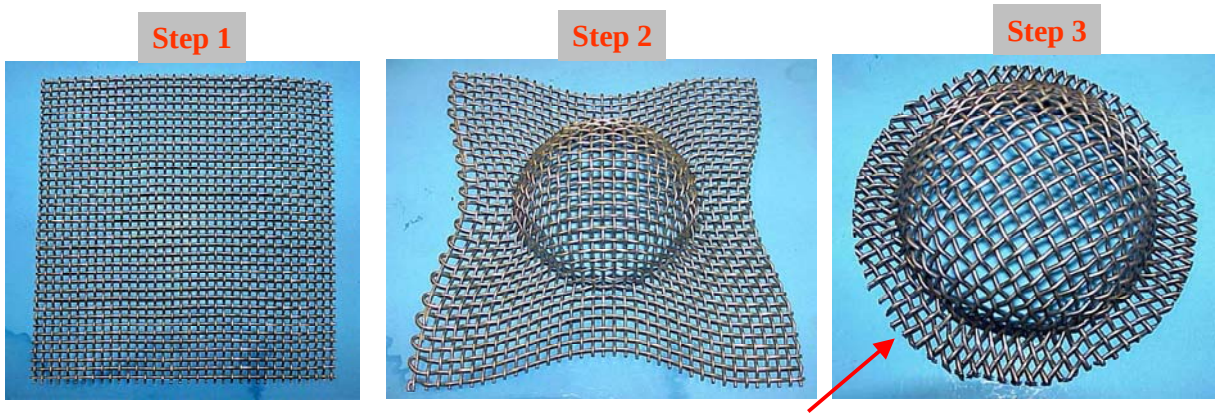
The diameter of the punched hole is 0.15 in. with a Thickness of 0.055 in. and 0.032 in. between holes

Figure 43b: Unalloyed 1020 steel wire mesh

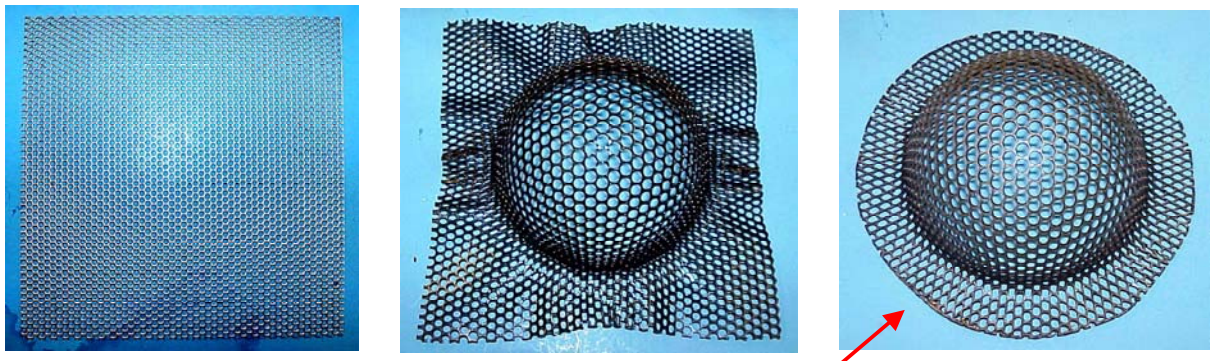


The wires are a 4 X 4 Mesh Per Square Inch with a 0.094 in. Diameter of the Wire

Figure 44: Dome preforms of 304 stainless, 1020 unalloyed wire mesh and punched 304 stainless steel sheet



304 stainless steel wire mesh Dome 0.43Lb and 1020 unalloyed wire mesh Dome 0.49Lb



304 stainless steel punched Sheet Dome 0.20Lb

Fig.45: Weight of the reinforcement material in aluminum dome casting

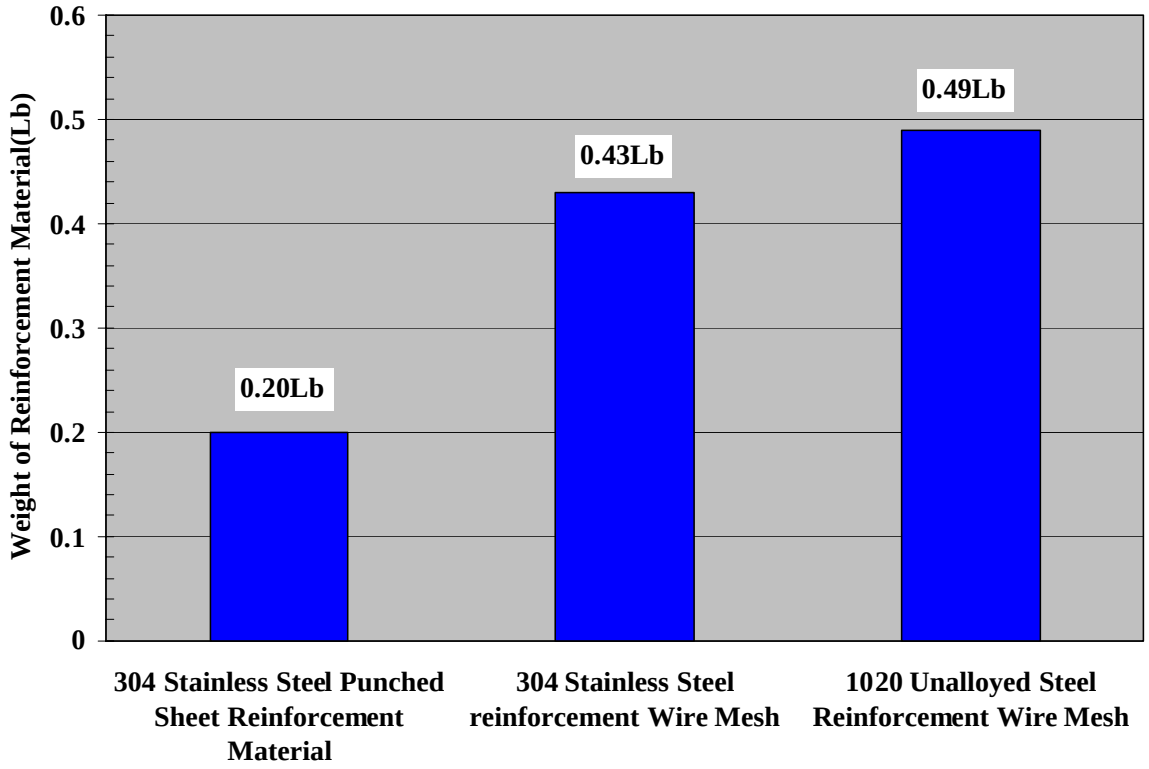


Fig.46: Weight of castings made of aluminum with/without reinforcement

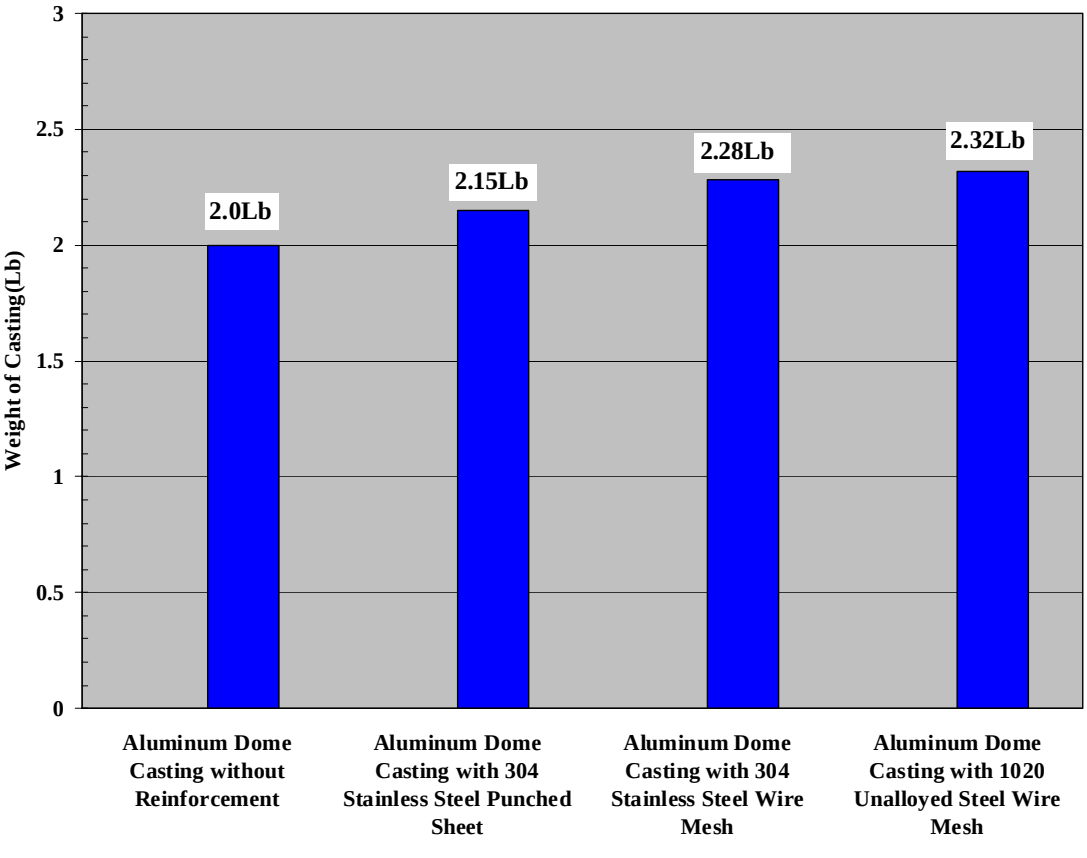
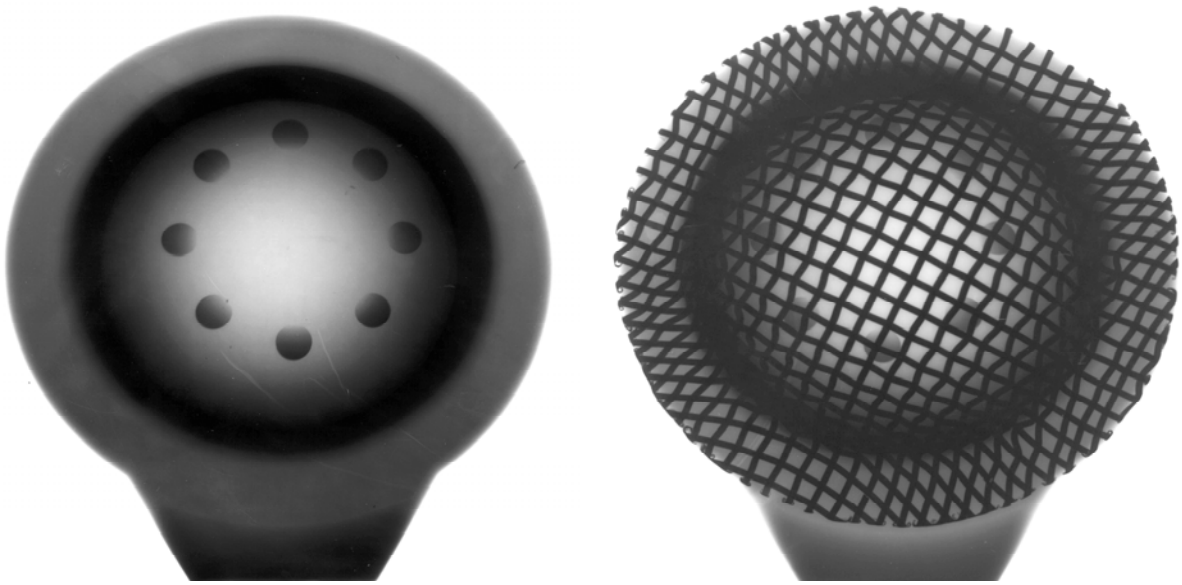


Figure 47: X-Ray Picture of castings with & w/o reinforcing wire



(a) Without wire **(b) With wire**

Fig.48: Setup for water pressure testing

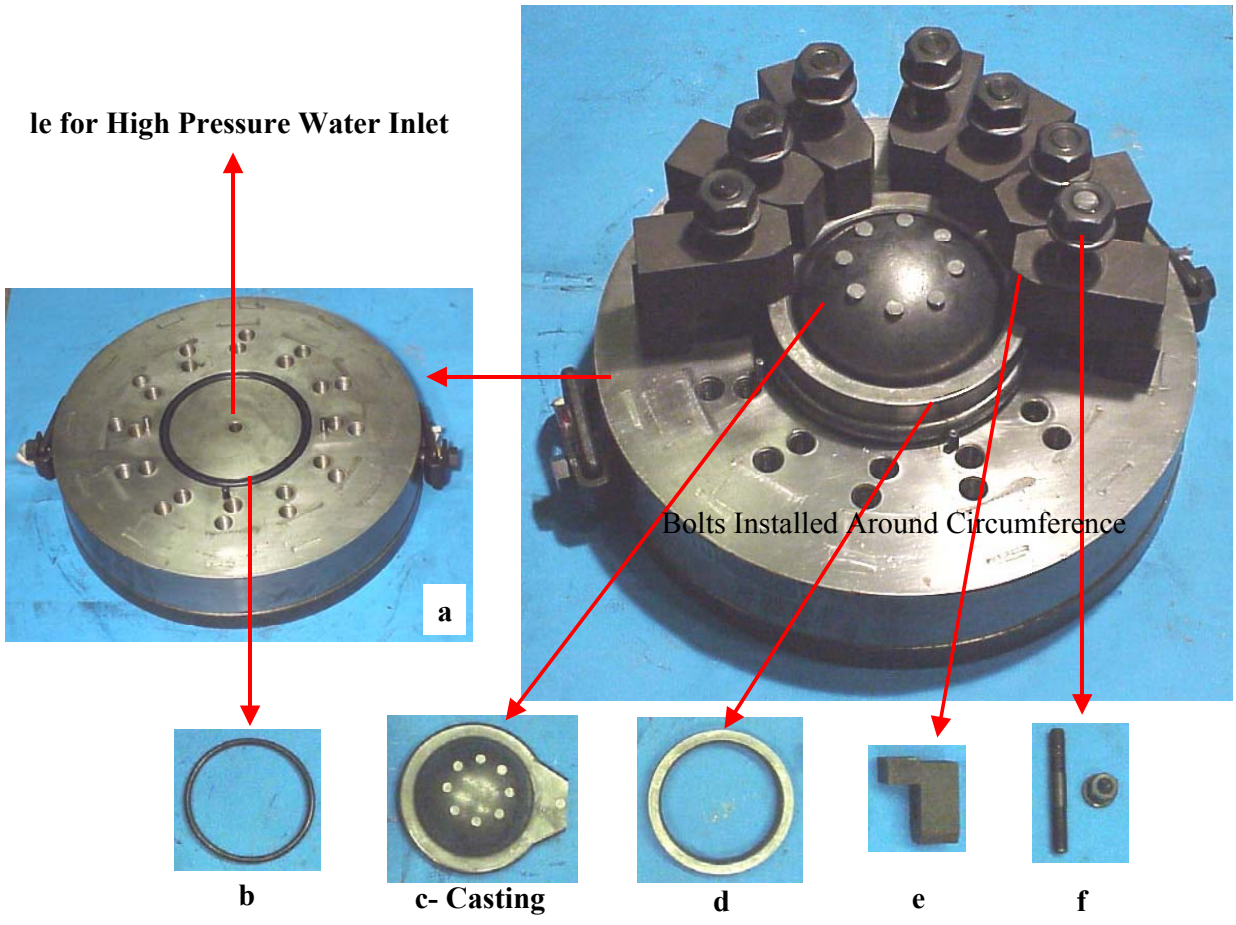
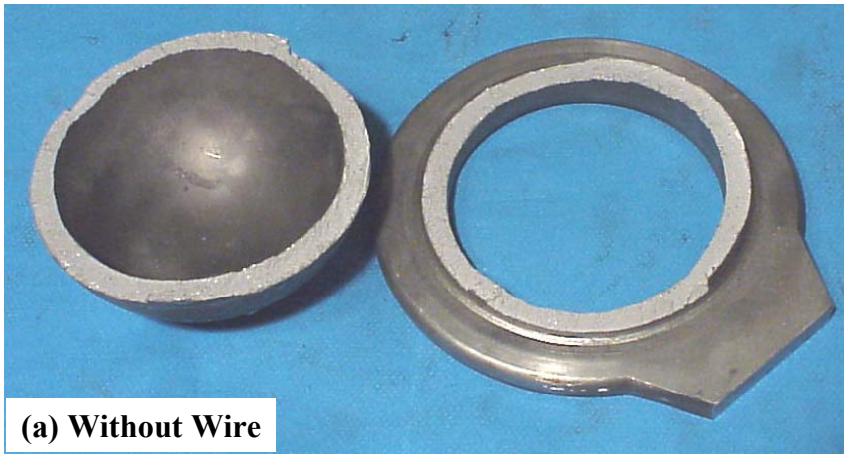
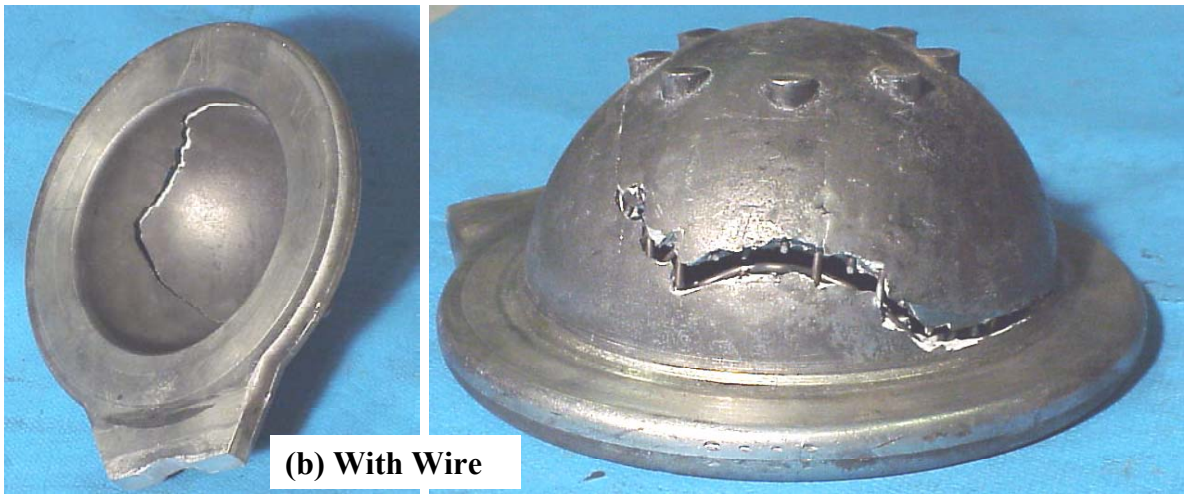


Fig.49: Failure mode of castings in water pressure testing



(a) Without Wire

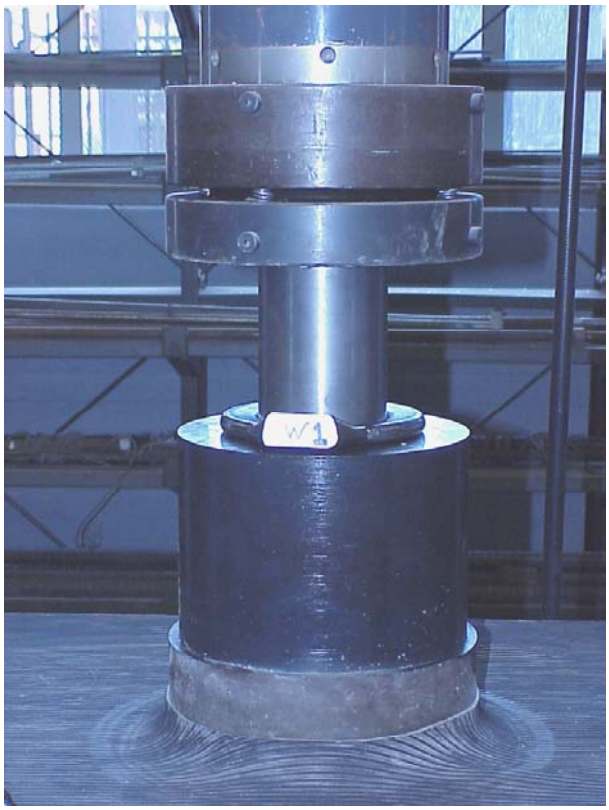


(b) With Wire

Fig.50: Setup for piston pressure testing of the hemispheric castings

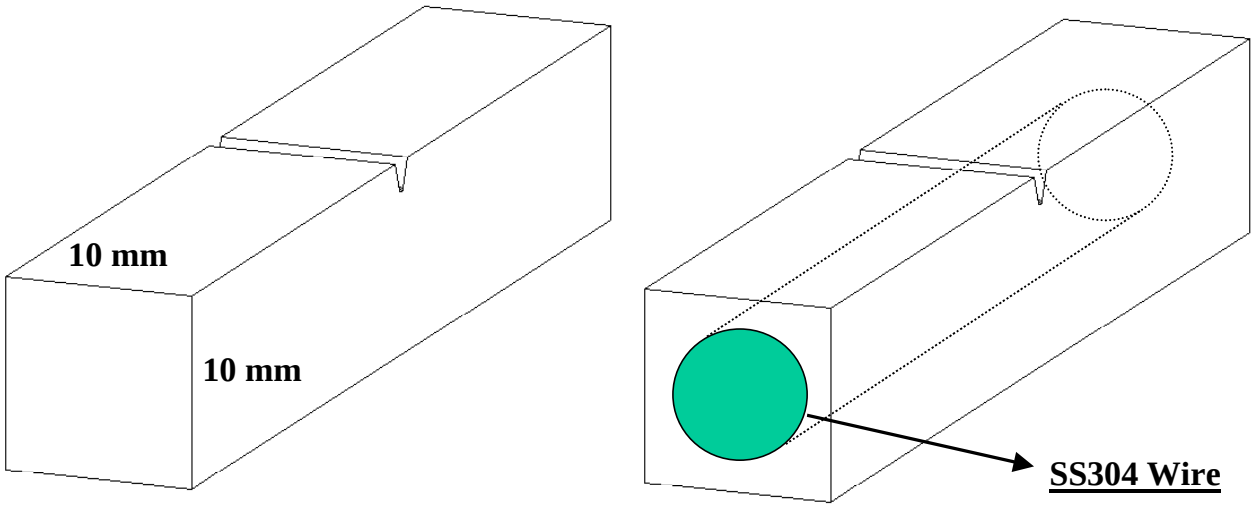






Rounded plunger head fits inside of the hemispheric casting during testing

Fig.51: Effect of reinforcement on impact resistance



A354-Base

3 ft *lb

A354 + 0.25 in. Dia. SS304

120 ft *lb

A very large increase in Charpy V-notch was obtained by selective reinforcement of cast A354 with SS304 Bar

Figure 52: Effect of SS304 wire reinforcement (casting produced at 7,600psi

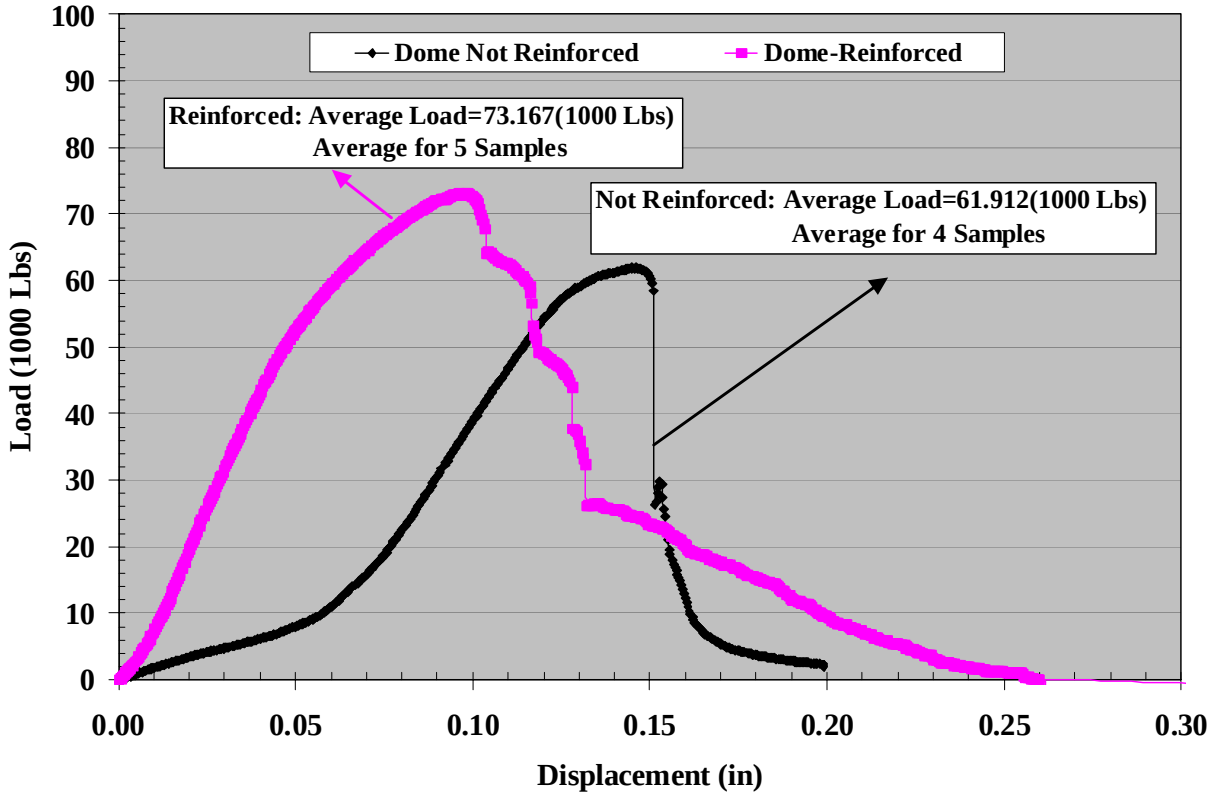


Fig.53: Typical load-deformation plot of castings made with 17,000 psi pressure with/without Reinforcement (As Cast)

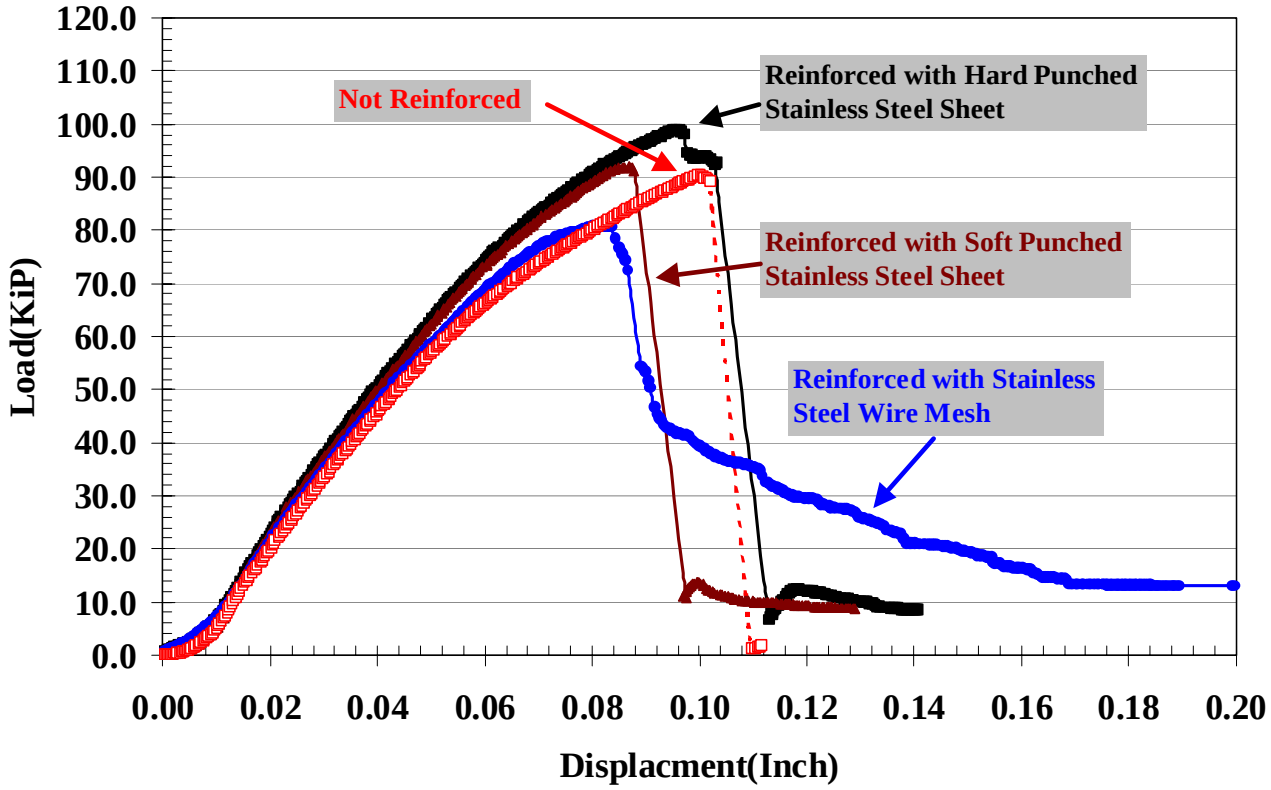


Fig.54: Effect of SS304 wire reinforcement on failure energy (Load * Displacement) produced at 7,600 psi (as-cast)

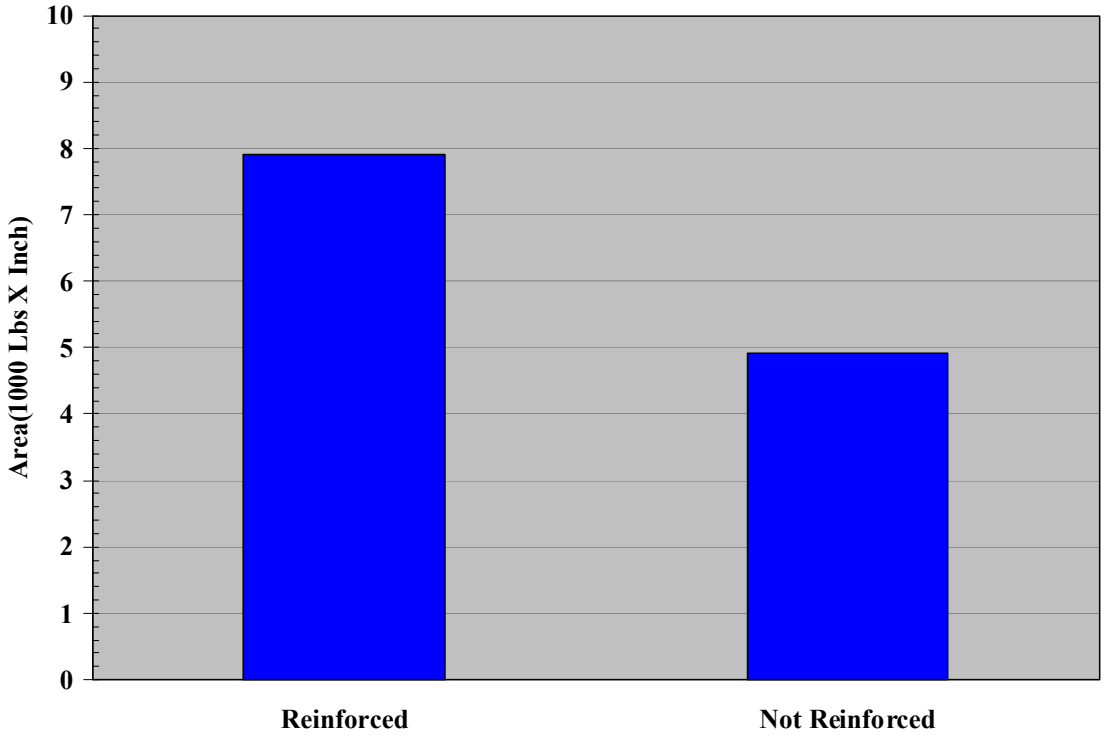


Figure 55: Effect of reinforcement on energy(area) of dome-shaped squeeze casting produced with 17,000 psi pressure (as-cast)

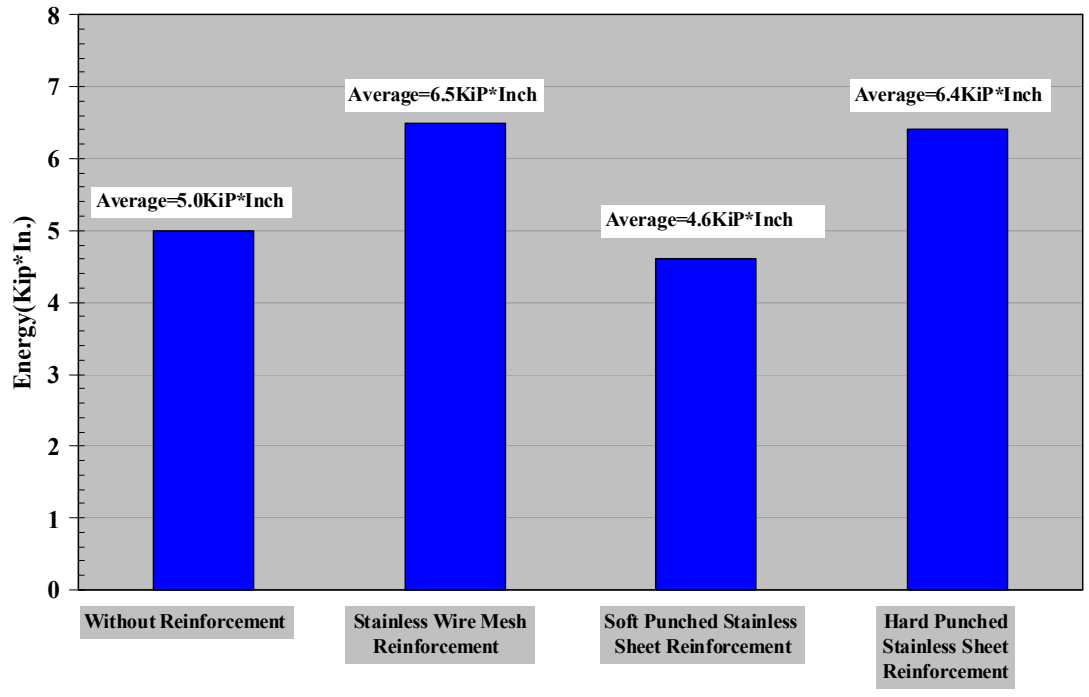


Fig.56: Failure mode of casting produced with 7600 psi pressure tested with piston pressure





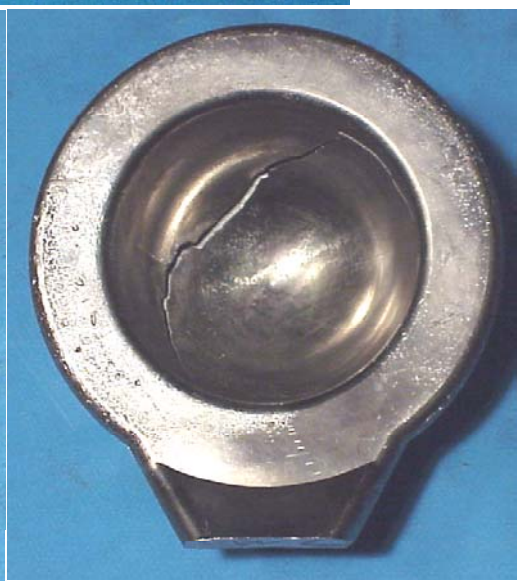
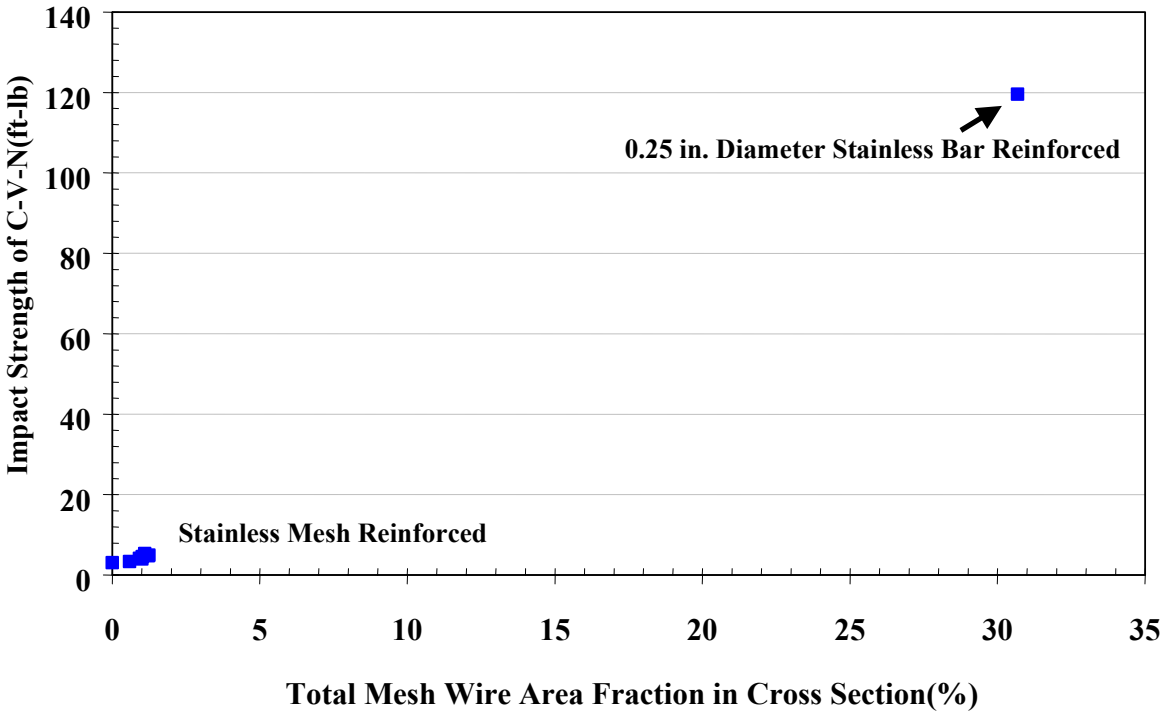


Fig.57: Effect of mesh area fraction in cross sections of stainless mesh reinforced A354 on CVN impact strength



BIBLIOGRAPHY

Akdeniz, M.V.; Mekhrabov, A.O. "The effect of substitutional impurities on the evolution of Fe-Al diffusion layer," *Acta mater*., **46 [4]** (1998) 1185-1192. **30**

Akdeniz, M.V.; Mekhrabov, A.O., in The 4th European Conference on Advanced Materials and Processes: EUROMAT 95, Padua/Venice, Conf, Proc., Vol. 4. Associatione Italiana Di Metallurgica, Italy, 1995, p. 487 **20**

Akdeniz, M.V.; Mekhrabov, A.O.; Yilmaz, T. "Interfacial interaction in Fe-Al diffusion layer," *Scripta Metallurgica et Materialia*, **31 [12]** (1994) 1723-1728. **21**

Almond, E.A.; Embury, J.D.; Wright, E.S. "Fracture in Laminated Materials," *Interfaces in Composites*, ASTM STP 452, American Society for Testing and Materials, 1969, 107-129.

Anik, S.; Dorn, L. "Metallo-Physical Processes Involved in Welding Different Materials--Materials Fundamentals and Joints Between Heterogeneous Steels," *Schweissen und Schneiden*, **44 [3]** (1992) 148-152. **2**

Arkharov, V.I., *Okisleniye Metallov pri Visokikh Temperaturakh*, Sverdlivsk, Metallurgizdat, 1945. **13**

Arkharov, V.I.; Balaneeva, N.A.; Bogoslovskii, V.N.; Stafeva, N.M. "Mechanism of chemical diffusion in solids and its application to oxidation," *Oxid. Metals*, **3** (1971) 251. **14**

Bahadur, A. "Aluminum coatings for steel," *Materials and Manufacturing Processes*, **11 [2]** (1996) 225-232. **36**

Bedford, G.M.; Boustead, J. "The Influence of Oxygen and Nitrogen on the Growth of Intermediate Phases During the Bonding of Iron to Aluminum," *Journal of Materials Science*, **13** (1978) 253-260. **27**

Chawla, K.K. *Composite materials: science and engineering***,** Springer-Verlag, New York,

1987.

Cooper, G.A.; Kelly, A. “Role of the Interface in the Fracture of Fiber-Composite Materials,” *Interfaces in Composites*, ASTM STP 452, American Society for Testing and Materials, 1969, 90-106.

Dini, J.W. “The role of electroplated coatings in metal joining,” *Welding Journal*, **75 [5]** (1996) 47-49.

Dini, J.W. “Use of Electrodeposition to Provide Coatings for Solid-State Bonding,” *Welding Journal*, **61 [11]** (1982) 33-39.

Dunkerton, S.B. “Diffusion Bonding--Process and Applications,” *Welding and Metal Fabrication*, 59 [3] (1991) 100-104.

Dybkov, V.I. “Reaction diffusion in heterogeneous binary systems-Part 1 Growth of the chemical compound layers at the interface between two elementary substances: one compound layer,” *Journal of Materials Science*, **21** (1986) 3078-3084 **6**

Evans, U.R., *The corrosion and Oxidation of Metals*, Edward Arnold, London, 1960. **12**

Gopal, S.; Lakare, A.; Shivpuri, R. “Soldering in die casting: aluminum alloy and die steel interactions,” *Die Casting Engineer*, 44 [3] (2000) 70-81.

Guo, H.; Steinhauer, E.; Chene, J.J. “Solid state diffusion bonding for structural joining with similar and dissimilar materials,” *Welding in the World*, 37 [3] (1996) 107-113.

Gupta, V.; Argon, A.S.; Counie, J.A. “Interfaces With Controlled Toughness as Mechanical Fuses to Isolate Fibers From Damage,” *J. Mater. Sci*., **24 [6]** (1989) 2031-2040. **32**

Hauffe, K., *Reactionen in und an festen Stoffen,* Springer, Berlin, 1955. **7**

Hayhurst, D.R.; Lechie, F.A.; Evans, A. G. “Component Design-Based Model for Deformation and Rupture of Tough Fibre-Reinforced Ceramic Matrix Composites,” *Proc. R. Soc.*, **434 [1891]** (1991) 369-381. **33**

Hillert, M. “Diffusion and Interface Control of Reactions in Alloys,” *Metal. Trans*. *A*, **6A [1]** (1975) 5. **5**

Ip, S.W.; Sridhar, R.; Toguri, J.M.; Stephenson, T. F.; Warner, A. E. M. “Wettability of nickel coated graphite by aluminum,” *Materials Science and Engineering A* (Switzerland), **244 [1]** (1998) 31-38.

Jost, W., *Diffusion in Solids Liquids, Gases*, Academic Press, New York, 1960. **11**

Karlsson, L. “Welding of dissimilar metals,” *Welding in the World*, **36** (1995) 125-132.

Knibloe, R.; Wright, R. N.; Trybus, C. L.; Sikka, V. K. “Microstructure and Mechanical Properties of Fe sub 3 Al Alloys With Chromium,” *J. Mater. Sci*., **28 [8]** (1993) 2040 **18**

Kofstad, P., *High-Temperature Oxidation of Metals,* Wiley, New York, 1968. **8**

Kopylov, N.; Lantsmar., P. “Electron-Microscope Investigation of Cold-Welded Steel/Al Joints,” Russian *J. Svar. Proiz*, **20 [2]** (1973) 15. **29**

Kotani, K.; Ikeuchi, K.; Matsuda, F. “Behavior of interfacial oxide during diffusion bonding of aluminum alloys and its influence on joint strength,” Transactions of *JWRI*, **26 [2]** (1997) 13-22.

Kotani, K.; Jung, J.; Ikeuchi, K.; Matsuda, F. “Interfacial oxide in diffusion-bonded joints of Al-binary alloys by transmission electron microscopy,” Transactions of *JWRI*, **28 [2]** (1999) 27-37.

Layner, K.I.; Kurakin, A.K., Fiz. Metal. Metaloved., 1964, 18(1), 145 **25**

Lesuer, D.R.; Syn, C.K.; Sherby, O.D.; Wadsworth, J.; Lewandowski, J.J.; Hunt, Jr., W.H. “Mechanical behavior of laminated metal composites,” *International Materials Reviews* (USA), **41 [5]** (1996) 169-197.

Loehman, R.E. *Joining engineering ceramics,* Technical Report SAND-90-0966C, CA. USA. 1990. **4**

Mekhrabov, A.O.; Akdeniz, M. V.; Aktürk, I., in Stability of Material, ed. A Gonis, P. E. A. Turchi and J. Kudrnovsky. Plenum Press, New York, 1996, p. 681 **24**

Mekhrabov, A.O.; Akdeniz, M.V. "Effect of ternary alloying elements addition on atomic ordering characteristics of Fe-Al intermetallics," *Acta mater*., **47 [7]** (1999) 2067-2075.

Mondolfo, L.F., *Aluninum alloys, structure and properties*, London, Butterworths, 1976. **23**

Noone, M.J.; Feingold, E.; Sutton, W. H. "The Importance of Coatings in the Preparation of Al2O3 Filament/Metal-Matrix Composites," *Interfaces in composites*, ASTM STP 452, American Society for testing and Materials, 1969, 59-89.

Omar, A.A. "Effects of welding parameters on hard zone formation at dissimilar metal welds," *Welding Journal*, **77 [2]** (1998) 86s-93s.

Parker, R.H., *An Introduction to Chemical Metallurgy*, 2nd Edn, Pergamon Press, Oxford, 1978. **10**

Partridge, P.G.; Ward-Close, C.M. "Processing of Advanced Continuous Fibre Composites: Current Practice and Potential Developments," *International Materials Reviews* (USA), **38 [1]** (1993) 1-24.

Richards, R.W.; Jones, R.D.; Clements, P.D.; Clarke, H. "Metallurgy of continuous hot dip aluminizing," *International Materials Reviews* (UK), **39 [5]** (1994) 191-212.

Rivlin, V.G.; Raynor, G. V. "Phase Equilibria in Iron Ternary Alloys. Pt. 4. Critical Evaluation of Constitution of Aluminum -- Iron -- Silicon System," *Int. Met. Rev.*, **26 [3]** (1981) 133-152. **22**

Ryabov, R., *Protective Coating on Metals*, Vol. 3, Consultant Bureau, New York, 1971, 96. **15**

Ryabov, R.; Yumatova, V.I.; Grabin, V.F.; Butnik, A.P., *Protective Coating on Metals*, Vol. 4, Consultant Bureau, New York, 1971, 98. **17**

Savov, L.; Heller, H.P.; Janke, D. "Wettability of solids by molten metals and alloys," *Metallwissenschaft und Technik*, **51 [9]** (1997) 475-485. **3**

Shankar, S.; Apelian, D. "Effect of variation of aluminum-alloy chemistry (titanium and strontium additions) on die/molten metal interface interactions," 5th International AFS Conference on Molten Aluminium Processing Proceedings (USA), Nov. 1998, 211-230.

Shankar, S.; Apelian, D. "Role of aluminum alloy chemistry and die material on die soldering," *World of Die Casting*: 1999 Transactions (USA) 285-293.

Sibata, K.; Morodzani, S.; Koda, S., *J. Japan Inst. Metals*, **30** (1966) 382. **16**

Sun, Z.; Karppi, R., *Joining of Dissimilar Materials. A Review*, Technical Research Centre of Finland. Research Notes, 1994. **1**

Thouless, M.D.; Evans, A.G. "Effects of Pull-Out on the Mechanical Properties of Ceramic-Matrix Composites," Acta Metall., 36 [3] (1988) 517-522. **34**

Tretyakov, U.D., *Tverdofazniye Reactsii,* Khimiya, Moscow, 1978. **9**

Trutnev, V.; Sharsharov, M.K. "Diffusion welding of austenitic steel to aluminum and aluminum alloys," *Weld Produc*., **14 [10]** (1967) 18. **28**

Wagner C., *Thermodynamics of Alloys*, Reading, Mass., Addison-Wesley, 1952. **31**

Wright, J.K.; Wright, R.N.; Moore, G. A. "Combustion Synthesized Iron Aluminide Coatings and Joints," *Scripta Metallurgica et Materialia*, **28** (1993) 501 **19**

Yang, L.; Hosoda, N.; Suga, T. "Investigations on the interface microstructure of stainless steel /aluminum joints created by the surface activated bonding method," *Interface Science*, 5 [4] (1997) 279-286.

Yardy, J.W. *The Role of Protective Coatings in Metal Joining*, ASM International (United States), 1992, 607-615. **35**

Yilmaz, T.; Akdeniz, M. V., in EUROMAT 94: 15th Conference on Materials Testing in

Metallrugy, Conf. Proc., Vol. 4, ed. B. Vorsatz and E. Szöke). Federation of European Materials Societies (FEMS), Balantonszeplak, Jungary, 1994, p. 1192 **26**